Royal Netherlands
Meteorological Institute
Ministry of Infrastructure
and Water Management

Quality assurance and publication of the KNMI 1995-2013 induced seismicity data

B. Dost, W. Zhou and E. Ruigrok

De Bilt, 2023 | Technical report; TR 412

Quality assurance and publication of the KNMI 1995-2013 induced seismicity data

Bernard Dost, Wen Zhou and Elmer Ruigrok

May 2023

Preamble

Implementation of proposed data structure and KNMI response to NORSAR review

In the KNMI report we describe the conversion of an old triggered dataset, consisting of acceleration data and velocity data from borehole arrays, from a local data format to a standard data exchange format (SEED). The meta-data have been carefully evaluated and a proposal for storage in a FDSN StationXML structure is given. After conversion, the dataset was integrated in the KNMI data archive, which consists of a Seiscomp archive. Seiscomp, however, has its own implementation of the standard FDSN StationXML and this has impact on some of the proposed features. We will explain the impact in detail below. NORSAR reviewed the document and the implementation of the data into the KNMI archive, which was very helpful. We will also comment on their main findings.

Metadata

The *units* of the individual stages in the description of the instrument response are not always known. The acceleration data are recorded in the local format in cm/s2 or g, not in Counts. We do not have enough detailed information on the Vs/m or Counts/V for the individual stages and therefore we proposed an alternative formulation. The Seiscomp archive, however, requires the information on Counts/V. Therefore, this proposal could not be implemented. In the present implementation all stages combined yield the correct amplitude, but the units of the individual stages are incorrect.

At the end of chapter 3.1 (p16) we added text on the consequences of the small differences in gain settings we found with the settings used in standard analysis of the data.

The *uncertainties* in the *orientation* of the acceleration data channels are determined in the report and could be included into the FDSN Station XML string. However, this is unfortunately not the case in the Seiscomp archive structure. Therefore, we refer the user of the data to the values mentioned in the report (Table 8, p30).

Since the orientation angles of the horizontal borehole channels are not oriented N and E, the *channels* should be *named* HH1 and HH2 instead of HHN and HHE. However, the existing continuous data streams from the boreholes in the archive are named HHE and HHE. Therefore, it was decided to keep the *channel names* as HHN and HHE, to avoid confusion (see NORSAR report p29). This is not due to the Seiscomp implementation, but due to the present build-up of the archive.

The NORSAR review revealed four issues on the Station metadata:

1. FSW1 instrument response is wrong for the period 1996-05-05 to 2010-04. The response should have been similar to the response of the other levels (FSW2-5) and has been corrected. We do not see evidence of a switch between components for FSW1 as suggested in the NORSAR report.
2. A polarity flip at PPB2.HHZ between 1995-05 and 1998-05 was detected and reported, but not listed in the StationXML file in the Seiscomp archive. This has also been corrected.
3. ZL2 end time differences (see NORSAR report p67). The second string at the ZLV station (ZL2) was dismantled at an earlier date than the main string (ZLV). The date in the xml file is correct (2009-04-10). Please note that ZL2 did not deliver data beyond 2001.
4. ZLV0 start time differences (see NORSAR report p67). The correct start time is 2006-02-15, as listed in the present KNMI report and in the online xml data.

Waveform data

The NORSAR report revealed some issues in datafiles that will be corrected. Most important are:

1. Missing borehole data for event #500 (2009-02-26 01:22). Data is available, has been added.
2. DCF channel data for FSW for time period < 1996-05-05 are missing. We checked and indeed the time channels were absent in the online archive. They have been added.
3. Gaps in WDB records for event #512, 513 and 518. Although the data are available, there is a problem when requesting the data through obspy. We are working on a solution for these events.

Contents

1. Introduction

The KNMI is monitoring induced seismicity in the north of the Netherlands with an advanced geophone borehole network since 1995. Later this network was extended by surface accelerometers. Both types of seismic stations operated in an off-line and triggered mode. The borehole network was gradually converted to a real-time operation between 2010 and 2012, the accelerometer network in 2013/2014. All real-time data collected are directly accessible to users through the KNMI webpages and through a webservice.

The triggered data are not yet publicly available, although they were distributed to individual researchers on request. The aim of this project is to convert the off-line triggered dataset into standard exchange format and add up-to-date information on the meta-data, describing the measurement system in detail. We will describe the acceleration and borehole dataset separately, so information on both measurement systems can easily be found.

After the format conversion and evaluation of the meta-data, quality control will be carried out on both datasets. The possibilities for quality control on the acceleration data are limited. In their set-up the borehole arrays, consisting of multiple levels of sensors at depth, are more flexible and allow for more quality control tests. Important issues are timing quality, component malfunctioning, noise characteristics and stability of waveform amplitude measurements.

In this report, we will start with an overview of the network development and a description of the data. This is followed by a detailed description of the measurement systems, which is an update of Dost and Haak (2002). New insights are presented and previously unpublished material on the orientation of the borehole network is added to this report (Diephuis & Asmussen, 1995). The orientations of the channels of the acceleration network, operated between 1997 and 2013, are estimated and results are presented including their uncertainties. A similar operation is carried out for the borehole systems for the period 1995-2010, although most of the work was carried out in advance and parts were already published (Hofman et al., 2017; Ruigrok et al., 2019).

Information on the accuracy of the timing could be retrieved for a part of the accelerometer data. Based on this information, a flag was set in the converted data indicating timing quality. For the boreholes, the timing signal was recorded as a separate channel, which is also kept during data conversion.

Data are stored into miniSEED files together with the accompanying meta-data in FDSN Station XML format. Quality control procedures are developed and applied to the converted dataset. Finally, waveform amplitudes are evaluated through comparison with subsequent networks in the region for the accelerometers. The borehole data allowed for comparison between the individual depth levels and between similar levels at multiple borehole sites. We used teleseismic events, manually triggered over the period 1995-2010 for this comparison.

2. Network development

Different network configurations were deployed over the years. In this chapter, we will give an overview of these developments in time for the period 1986-2014. In 1986, the first induced earthquake was recorded. After 2014 all data were recorded in real-time, except for a few remaining off-line stations that did not record any triggered data after 2014 (see Table 5). Data for the pre-1995 network are not part of the current dataset. However, a description is given for future reference.

2.1 Pre-1995

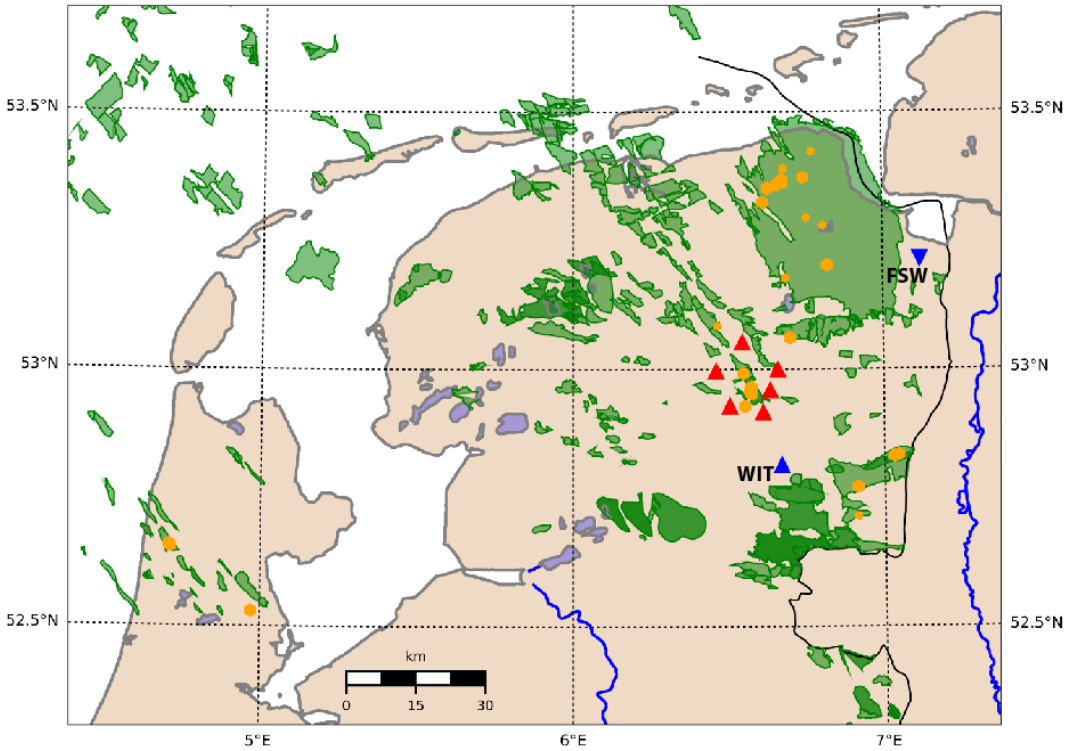

Figure 1. Overview of seismic networks operational before 1995. Surface sensors are indicated by triangles, the Assen array is marked in red. Inverted triangles indicate borehole systems. Green polygons denote gas fields, orange dots are induced earthquakes <1995.

At the time of the first induced earthquakes in the North of the Netherlands in 1986, only one analogue station was operational in the region. Station WIT (Witteveen, Drenthe) was in operation since 1951 with different instrumentation over the years. The station recorded in digital form since November 1993 and stopped recording in December 2013. At larger distances, two more stations were present: station WTS (Winterswijk) and Epen (ENN). The first three induced events were recorded on these three stations (Haak, 1993).

In 1989, a vertical component short period seismometer network was installed near Assen and a first prototype borehole array near Finsterwolde (FSW) in 1991 (Figure 1). FSW was designed as a vertical array of 4 3-component geophones with 75 m vertical spacing and a total depth of 300 m with the aim to analyze noise reduction with depth. It was found that within the first 75 m most noise reduction is achieved with a further smaller improvement at larger depths. Based on these results it was decided to limit the depth of future boreholes to a maximum of 200 m. Table 1 lists the surface stations in operation in this period. Further information on FSW can be found in Table 2. Data for this time period will not be part of this project, but will be processed later.

Station	Name	Open since	Closed at	Latitude	Longitude	Components
ZYN	Zeyen	1988-12-01	1994-06-01	53,053	6,544	HHZ
WSB	Westerbork	1988-12-01	1994-07-01	52,917	6,611	HHZ
RLD	Rolde	1989-02-01	1994-06-01	53,000	6,659	HHZ
LGV	Laaghalerveen	1989-09-01	1994-06-01	52,929	6,504	HHZ
BVS	Bovensmilde	1989-09-01	1995-01-01	52,997	6,460	HHZ
MWD	Marwijksoord	1989-09-01	1994-04-01	52,960	6,634	HHZ
WIT	Witteveen	1993-11-16	2013-12-01	52,814	6,670	HHZ

Table 1. Surface stations in operation before 1995. The first six stations belong to the Assen array. Station WIT was an existing 3C broad-band station.

2.2 1995-2014

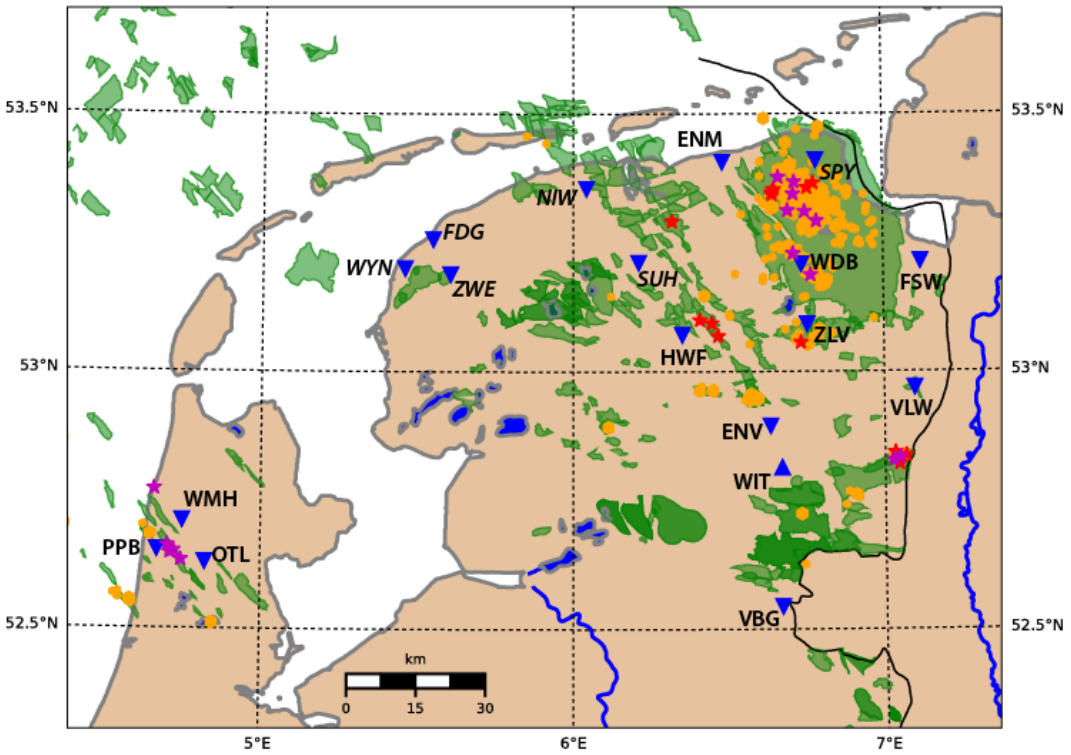

Figure 2. Overview of seismic networks operational in 1995-2014. Surface sensors are indicated by triangles, inverted triangles indicate borehole systems and accelerometers are denoted by stars. Red stars indicate accelerometers in operation before 2000, magenta indicates in operation after 2000. Green polygons denote gas fields, orange dots are induced earthquakes 1995-2014. Names of borehole stations are indicated. Names of borehole stations not contributing to the database are in italics.

In this period, the surface network around Assen was replaced by a borehole network, combined with the installation of accelerometers at the locations of previously felt events (Figure 2). Until 2003, the region around Roswinkel (Drenthe, south of Groningen) was most active together with the region north of Amsterdam around Alkmaar.

Borehole network

In 1995, the borehole network was extended with seven 200 m deep boreholes in the northeast of the Netherlands and three 200 m deep boreholes around Alkmaar in the northwestern part of the Netherlands, see Table 2. The additional borehole stations have 3-component geophones at 50, 100, 150 and 200 m depth.

Station	Name	Latitude	Longitude	Operational since	Triggered until
FSW	Finsterwolde	53.2135	7.1195	22-07-1992	29-04-2010
ENM	Eenrum	53.4064	6.4817	12-04-1995	22-01-2010
WDB	Woudbloem	53.2083	6.7355	12-04-1995	29-04-2010
ZLV/ZL2	Zuidlaarderveen	53.0921	6.7533	12-04-1995	18-05-2010
ENV	Elp (Enerveen)	52.8944	6.6337	20-06-1995	04-12-2009
VLW	Vlagtwedde	52.9682	7.0972	23-05-1995	29-10-2010
VBG	Venebrugge	52.5440	6.6693	28-04-1995	01-09-2010
HWF	Haulerwijk	53.0710	6.3512	02-06-1995	24-11-2010
OTL	Oterleek	52.6289	4.8227	21-04-1995	11-10-2010
PPB	Philistijnse Polder	52.6526	4.6700	10-02-1995	16-10-2010
WMH	Warmenhuizen	52.7096	4.7498	21-04-1995	11-10-2010

Table 2. Borehole stations in operation since 1995

Additional stations were installed to cover a larger region to the west of the Groningen field (Table 3, NIW, SUH) and to cover the north-eastern part of the Groningen field (SPY). Station SPY was co-located with a LOFAR-node (Low Frequency Array for the Radio-astronomy). Stations have a 30 m vertical spacing between the sensor elements. This was due to the fact that at that time drilling costs could be reduced considerably if depth was limited to 120 m. The last three stations (FDG, ZWE and WYN) were installed in the western part of the province of Friesland with the aim to monitor seismicity due to salt mining. These stations also have 3-component sensors at 30, 60, 90 and 120 m depth. These stations delivered continuous data from the start and therefore do not contribute to the triggered dataset. Data is available from the KNMI website.

At station ZLV, two strings were installed within the same borehole with a vertical offset of 25 m. ZLV has sensors at 0, 50, 150 and 200 m depth, ZLV2 at 25, 75, 125 and 175 m depth. ZLV2 was used for experiments. From 2002-09-18 onward, ZLV2 was recording at 244 Hz sampling rate, employing a 70 Hz anti-alias filter. These experimental set-ups are not included in the current dataset.

Station	Name	Latitude	Longitude	Operational since
NIW	Niawier	53.3548	6.0430	2009-05-20
SUH	Surhuizum	53.2113	6.2110	2009-08-26
SPY	Spijk	53.4098	6.7838	2010-07-08
FDG	Firdgum	53.2562	5.5481	2009-10-13
ZWE	Zweins	53.1885	5.6045	2010-03-24
WYN	Wijnaldum	53.1995	5.4578	2010-03-03

Table 3. Borehole stations added in 2009-2010.

Stations listed in Table 4 have additional surface sensors. These are installed separately from the string and added to the A/D board. In Table 4, we specify the installation date or, if not known exactly, the date of the first event in the database recorded by the sensor in question.

Station	Surface sensors operational since	Station	Surface sensors operational since
FSW	1992-07-22*	**PPB**	1998-05-15
ZLV	1996-02-15	**VLW**	1998-07-24
HWF	1998-03-29*	**WDB**	1998-07-24

*Table 4. List of borehole stations equipped with surface sensors. The * denotes stations whose installation date is unknown and was replaced by the date on which the first records were inserted in the database.*

Accelerometer network

The first accelerometers were installed in the period 1996-1997, followed by episodic updates and a relocation of sensors depending on the actual seismicity as well as possible repairs of sensors that were malfunctioning. Two main regions of seismic activity can be identified: the eastern part of the province of Drenthe (south of Groningen) near the village of Roswinkel and (later) the province of Groningen. Additional sensors have been installed at other fields in production and at gas storage facilities. Table 5 provides a complete list of stations.

Station	Name	Latitude	Longitude	Serial number	Operational since	Closed at
WSE	Westeremden	53,3444	6,7099	834	2006-10-11	2013-04-24
MID1	Middelstum-1	53,3473	6,6423	401	1996-12-20	2013-09-11
MID2	Middelstum 2	53,3434	6,6418	403	1996-12-20	1998-02-10
MID3	Middelstum-3	53,3533	6,6472	477	1998-02-10	2003-03-17
MID3	Middelstum-3	53,3533	6,6472	833	2003-03-17	2013-09-10
GARST	Garsthuizen	53,3677	6,7135	115282	2009-09-15	2014-09-17
KANT	Kantens	53,3772	6,6621	115275	2007-04-03	2014-07-01
WIN	Winneweer	53,3104	6,7471	115277	2007-04-03	2014-09-17
HKS	Hoeksmeer	53,2920	6,7850	110426	2005-04-26	2014-09-17
STDM	Stedum	53,3123	6,6921	117093	2009-09-15	2014-09-17
FRB2	Froombosch-2	53,1875	6,7655	110424	2006-03-22	2014-09-17
HARK	Harkstede	53,2292	6,7090	108752	2006-08-16	2014-09-17
ZAN1	t Zandt-1	53,3657	6,7751	403	1999-06-29	2013-10-24
ZAN2	t Zandt-2	53,3568	6,7547	622	1999-06-29	2000-07-03
ZAN2				834	2000-07-03	2002-07-02
ZAN2				477	2003-09-30	2013-09-23
ROS1	Bijl	52,8425	7,0327	368	1996-06-13	1997-01-10
ROS1	Bijl	52,8425	7,0327	402	1997-01-10	2020-01-01
ROS2	Hijmans	52,8206	7,0465	415	1997-02-20	2014-08-27
ROS3	NAM building	52,8365	7,0679	368	1997-02-20	2000-11-03
ROS4	NAM building, free field	52,8365	7,0679	681	1998-12-17	2010-01-01
ROS5	Bourquin	52,8336	7,0479	833	2000-01-04	2003-02-18
ROS5		52,8336	7,0479	834	2003-02-18	2006-03-22

ROS6	Duin	52,8275	7,0283	368	2000-11-03	2014-01-01
ANN	Annen	53,0566	6,7328	404	1996-12-20	*
KOM	Kommerzijl	53,2913	6,3188	405	1997-01-10	2015-12-08
NRG	Norg	53,0692	6,4665	478	1997-07-17	2018-02-15
LAN	Langelo	53,0936	6,4458	475	1997-07-17	2018-02-15
SBG	Steenbergen	53,1000	6,4081	476	1997-07-17	2018-02-15
ALK3	Alkmaar/Bergen	52,6471	4,7122	3685[1]	2002-08-09	2013-01-01
ALK3	Alkmaar/Bergen			3025/11506	2013-01-01	2019-07-25
ALK4	Alkmaar/Bergen	52,6509	4,7233	3122/64048[1]	2002-08-09	2019-07-24
ALK5	Alkmaar/Bergen	52,6612	4,7032	3121/64046[1]	2003-01-29	2019-11-18
ALK1	Alkmaar Stadhuis	52,6328	4,7467	3026/13526	2008-12-02	2019-11-19
PET	Petten	52,7706	4,6595	3024/13528	2009-04-21	2019-07-24
SMO1	Schiermonikoog-1	53,4796	6,2089	4255/51265	2010-07-01	2019-08-01
SMO2	Schiermonikoog-2	53,4800	6,1526	4256/51266	2011-05-13	2019-08-01

Table 5. Accelerometers installed in the north of the Netherlands. The serial number is equal to the identification number in the data streams. For systems that did not contribute data (ALKx, PET, SMOx) the serial number of sensor and data logger are given. Note [1]: stations ALK3, ALK4 and ALK5 did operate with different sensors/data loggers (Kinemetrics-ETNA). All other stations were equipped with GeoSig instruments (see chapter 3).

3. Data

Prior to the real-time digital waveform collection, which started in 2010 (Dost et al., 2017), data was recorded in a triggered mode. This means that small events may have been missed, but also larger events at some (distant) stations were not triggered. Different measurement systems were in operation:

Accelerometer data

For these systems, no ring buffer was available and therefore there was no possibility to retrieve data in case the system did not trigger. Data was stored in proprietary format from the manufacturer. For the first (AC-23/SMACH-SM2) systems the format was a so-called “smr” format, for the AC-63/GSR-18 systems the format was the “gsr” format.

For all formats, conversion software was written at KNMI to convert the data into SAC format (smr2sac and gsr2sac). Since SAC is an analysis format and is not designed to keep all necessary information on the measurement system (e.g. Dost et al., 2002), data are converted to the standard exchange format SEED (Standard for the Exchange of Earthquake Data). The SEED format consists of datafiles with a small and efficient header that identifies the station and channel recording the data and a separate header file containing details of the instrumentation used. The latter is called a dataless SEED file and is defined in the SEED manual (for a tutorial on SEED, see Ringler and Evans, 2015). A more modern and flexible form has been developed by the Federation of Digital Seismic Networks (FDSN) and is known as the FDSN Station XML file.

Borehole data

A ring-buffer was kept at the stations that could hold a limited amount of continuous waveform data, segmented in blocks of 128 s (15360 samples). Relevant files could be retrieved afterwards. Initially, the buffer contained only one or two days of data, later this was extended to a week. The sampling

rate amounts to 120 Hz for all borehole stations, except for station FSW that operated at 121.12 Hz until 5-5-1996. The difference in sampling rate is due to the initial use of a 12 bit AD board at FSW, which was replaced with a 16 bit version (Dost & Haak, 2002). Data blocks are 126.82 s long for the alternative sampling rate, since the blocks contain a fixed number of samples.

Apart from the data collected per local event, data from large teleseismic events were collected. First, data were collected mainly from deep events showing P-onsets at frequencies around 1 Hz, later also other events were selected that could be used in a receiver function study.

Data were recorded in the IASPEI format (Lee, 1989).

In the next chapters, we will assemble all necessary information on the measurement system, referred to as meta-data.

3.1 Instrument response

In this section we describe characteristics of the measurement system in detail, including information on the quality of the timing, the full response information and known problems in data quality.

3.1.1 Frequency response of the GeoSig accelerometer system

The accelerometers deployed by KNMI in the Netherlands in the period 1996-2013 were GeoSig instruments. Two sensor-data logger combinations were deployed: the AC-23 sensor combined with a SMACH-SM2 data logger and the AC-63 sensor combined with a GSR-18 data logger. The frequency response information we received from the manufacturer is described in the following chapter.

AC-23:

According to the manufacturer, the transfer function for the AC-23 (for acceleration) is:

$$T(s) = \frac{sS}{(s - s_1)} \frac{k_0}{(s - s_2)} \qquad [1]$$

with s_1 = (-0.9425, 0.00); s_2 = (-905.2, 0.8831), where s is given in rad/s and the numbers in between brackets are coordinates in the complex plane: (Re{s_1},Im{s_1}). The parameter s is short for iω, which is the imaginary unit times the angular frequency. S stands for the sensitivity of the sensor. Equation 1 is different from the information that was provided by the same manufacturer earlier (Dost & Haak, 2002). The normalization constant k_0= 905.2.

Since the output data is stored in the ".smr" files in cm/s^2, S=100, converting input in m/s^2 to cm/s^2.

So, the low frequency part is determined by the pole defined by a corner frequency of 0.15 Hz, the high frequency part by one pole at 143.4 Hz.

SMACH-SM2

The data logger consists of a 16-bit analogue-to-digital converter (ADC) based on the sigma delta technique and only adds a digital filter from the decimation process (64 kHz down to 200 Hz sampling). The filter is an Hogenauer filter or CIC filter (Hogenauer, 1981) and its frequency characteristic is given by:

$$T(s) = [\sum_{k=0}^{RM-1} z^{-k}\ ]^N \ ; \ \ z = e^{\frac{s}{R}} \qquad [2]$$

with R= sampling rate reduction, M=differential delay (design parameter) and N= number of cascaded comb stages. In our case, there are three stages (N = 3) with a total sampling rate reduction of 320 (R = 8, 8 and 5) and M is taken to be 1. The frequency response is not available in a simple form, comparable to the transfer function of the accelerometer. Therefore, we looked for a best fitting simple description (two stages of a two pole low pass filter) that approximates the transfer function of the Hogenauer filter:

$$T(s) = \frac{\omega_2^2}{(s-s_3)(s-s_4)} \frac{\omega_2^2}{(s-s_3)(s-s_4)} \qquad [3]$$

Although multiple acceptable solutions for the amplitude response could be found, a joint match of amplitude and phase is more difficult. The best approximation consists of the following parameters: ω_2= 2π*107.= 672.30 rad/s, s_3= (-584.90, 331.48) and s_4=(-584.90, -331.48).

Figure 3 shows the amplitude and phase response of the Hogenauer filter, calculated using equation 2 and the approximation in equation 3.

Since all anti-aliasing filtering is dealt with in the ADC, no additional anti-aliasing filters were applied.

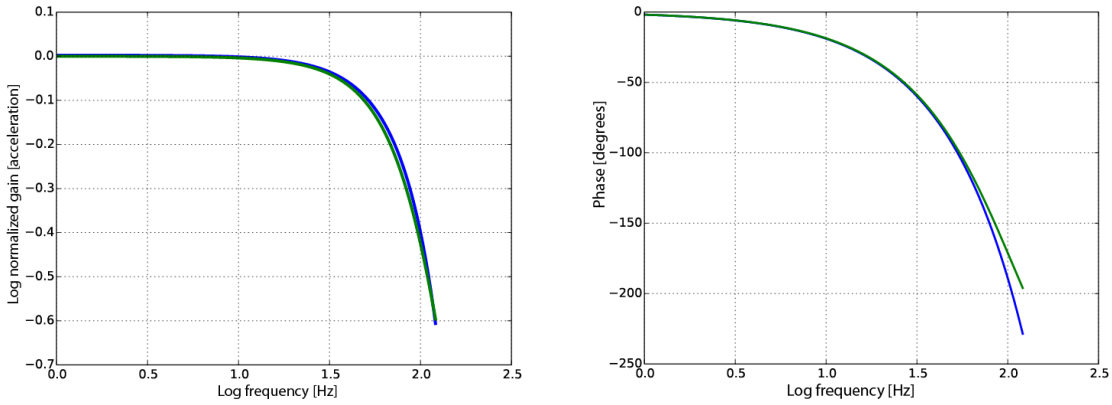

Figure 3. Comparison between frequency response of the Hogenauer filter (blue) and the proposed approximation (green).

The **overall response** for the AC-23/SMACH-SM2 systems is given by:

$$T(s) = \frac{sS}{s-s_1} \frac{k_0}{(s-s_2)} \frac{\omega_2^2}{(s-s_3)(s-s_4)} \frac{\omega_2^2}{(s-s_3)(s-s_4)} \qquad [4]$$

consisting of one zero and four poles, given by:

s_1 = (-0.9425, 0.00); s_2 = (-905.2, 0.8831); s_3= (-584.90, 331.48) and s_4=(-584.90, -331.48), all expressed in rad/s. The overall normalization factor is $k_0*\omega_2^4$= 1.85E14. The complete amplitude and phase response is shown in Figures 4 and 5.

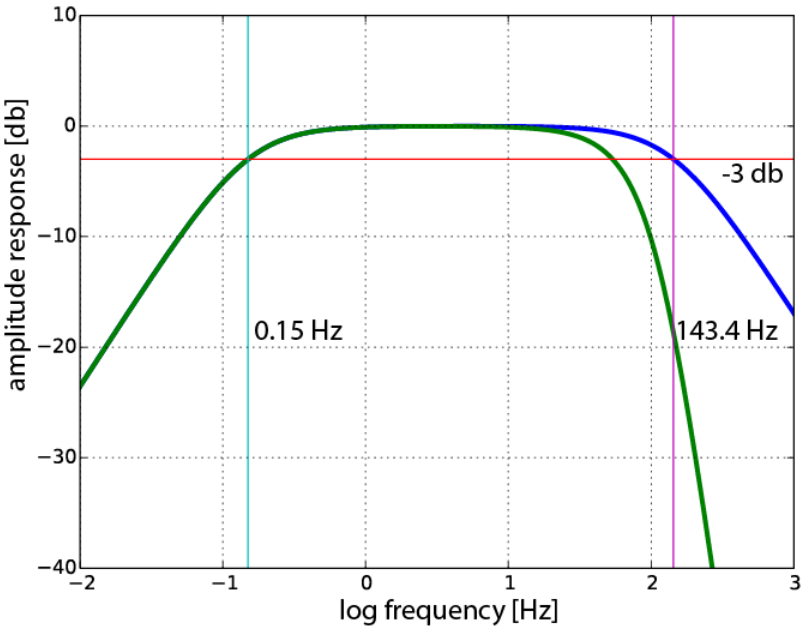

Figure 4. Amplitude response of the AC-23 sensor (blue) and the AC-23/SMACH-SM2 combined system (green). The turquoise and pink vertical lines indicate the corner frequencies. The red horizontal line shows the -3db level of the AC-23 sensor.

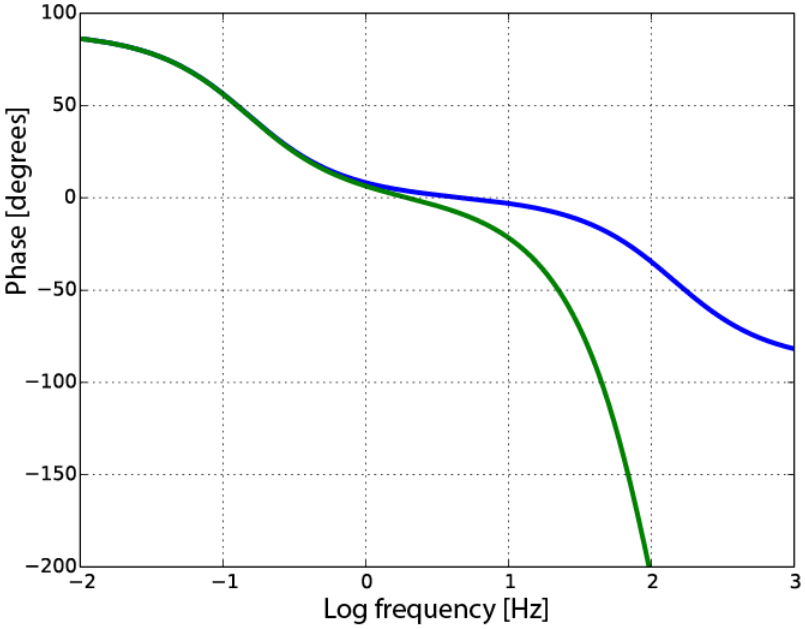

Figure 5. Phase response of the AC-23 sensor (blue) and the AC-23/SMACH-SM2 combined system (green)

AC-63:

According to the specifications of the manufacturer, the sensor is characterized by a two pole, low pass Butterworth filter. Its transfer function for acceleration is:

$$T(s) = \frac{S\,k}{s^2 - 2\omega_0 h_0 + \omega_0^2} = \frac{S\,k}{(s - s_1)(s - s_2)} \qquad [5]$$

With $s_{1,2}$= (-439.82, ±448.71) in rad/s. These poles are valid for f_0= 100 Hz and h_0= 0.7 (ω_0= 2π f_0). The factor k is equal to 3.9478E5 (normalization constant). Since the output of the sensor is given in g, assuming an input in m/s^2, the gain factor S= 1/9.81= 0.10194.

GSR-18 data logger

The data logger is, comparable to the SMACH-SM2, based on a sigma delta ADC. The manufacturer did not release detailed information on the response, but in the manual a remark was made that the filter cut-off frequency for the 200 sample-per-second sampling rate was at 50 Hz, comparable to the filter of the SMACH-SM2 data logger. However, since another ADC was used at higher sampling rates, the description for the SMACH-SM2 cannot be copied. All anti-aliasing is taken care of in the ADC, so no analogue anti-aliasing filter is applied. In the overall description, the effects of the data logger has not been taken into account.

The **overall response** is therefore given by equation 5 with the parameters:

$s_{1,2}$= (-439.82, ±448.71) in rad/s and k= 3.9478E5.

The corresponding amplitude and phase response is shown in Figure 6.

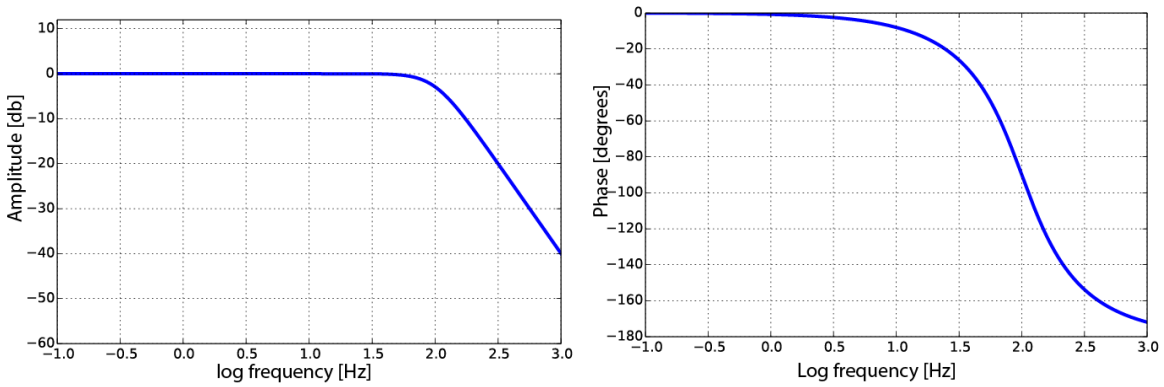

Figure 6. Amplitude (left) and phase (right) response for the AC-63 sensor

The amplitude is flat for acceleration up to 50-60 Hz.

3.1.2 Frequency response of the borehole geophone system

The development of the borehole geophone systems and their responses until 2002 have been described in detail in Dost and Haak (2002). For details, we refer to this report. In the period 1995-2010 all boreholes did operate employing the same electronics and A/D converter. This includes the sensor, a 4.5 Hz SM6 geophone, followed by a shaping filter to move the corner frequency to 1 Hz, a high pass filter at 0.15 Hz to minimize low frequency noise and an anti-alias filter (8-order Butterworth) at 28 Hz. Only station FSW operated using different settings from 1992 until 1996-05-05.

The response for velocity is:

$$T(s) = \frac{s^2 S}{(s^2 + 2h_s\omega_s s + {\omega_s}^2)} \frac{(s+\omega_s)^2}{(s+\omega_n)^2} \frac{s^2}{s^2 + 2h_f\omega_f + {\omega_f}^2} \prod_{k=3}^{6} \frac{\omega_3^2}{s^2 + 2h_k\omega_3 s + \omega_3^2} \quad [6]$$

which can also be written in a form of poles and zeroes:

$$T(s) = \frac{s^2 S}{(s-s_1)(s-s_1^*)} \frac{(s-s_2)^2}{(s-s_3)^2} \frac{s^2}{(s-s_4)(s-s_4^*)} \prod_{k=3}^{6} \frac{\omega_3^2}{(s-s_{k+2})(s-s_{k+2}^*)} \quad [7]$$

Where * indicates the complex conjugate. Poles are s1=(19.990, -19.996), s3=(-6.28931, 0.0), s4=(-0.666667, -0.700877), zeroes are s2=(-28.4377,0.) and 4 zeroes of value (0.,0.)

The 8-order Butterworth poles are given by:

s5=(-34.3278, -173.108), s6=(-98.348, -145.623), s7=(-147.079, -96.3482), s8=(-174.203, -29.8213)

The poles are marginally different from Dost and Haak (2002), due to a calculation based on the actual components used in the realization of the Butterworth filter. The factor ω_3^8 in equation 7 is the normalization factor for the 8th order Butterworth filter and has a value of 9.1770E17. However, the choice of resistances and capacitors brings small changes to the poles and zeroes and the ω_3 values for all four stages. We calculated the poles and corner frequencies for the different stages and found the coefficients listed in Table 6.

Stage	Corner frequency	Damping	Planned corner frequency	Planned damping
1	176.479	0.389	175.929	0.390
2	175.723	1.119	175.929	1,111
3	175.829	1.673	175.929	1.663
4	176.737	1.971	175.929	1.962

Table 6. Realized and planned corner frequency and damping of the 8th order Butterworth filter.

With these newly found corner frequencies the overall normalization factor becomes **9.2871E17**.

This change in the value of the poles and zeroes gives no measurable change in the frequency response. The sensitivity of the system is given in Dost and Haak (2002), p28 (New System) as S= 28.8*1000*0.956*4= 110131.2 V/m/s. In the document, a factor of 4 is missing in the line, but the total sensitivity in Counts/m/s is correct.

The factor 1000 in the calculation of S is based on general information on the amplification of the operational amplifier used. We can calculate the exact value by taking into account the components that were used in practice.

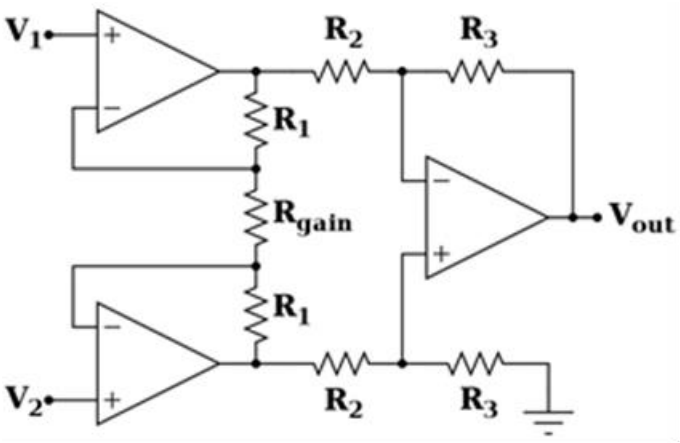

Figure 7. Electronics scheme used in the amplification stage.

The scheme in Figure 7 was applied with R_1= 3320 Ohm, R_2=110 Ohm, R_3=2210 Ohm and R_{gain}= 133 Ohm. The total amplification of this system is: $\frac{V_{out}}{(V_2-V_1)} = (1+\frac{2R_1}{R_{gain}})\frac{R_3}{R_2}$, which amounts to 1023 instead of 1000. We upgraded the original value with this new value. Therefore the total sensitivity increases to 28.8*1023*0.956*4= 112664.2 V/m/s.

Due to the influence of the other electronic components, the normalization factor of the whole system may be different at a chosen normalization frequency, although the overall sensitivity should remain the same. For a normalization frequency of 10 Hz, the normalization factor of the total system is 7.9814E17, a factor 1.164 smaller than the normalization frequency of the Butterworth filter. The gain of the system should therefore be 112664.2* 1.164= 131141.13 V/m/s.

In the XML description, the first stage is the description of the system without the data logger. The normalization factor, frequency and stage gain are filled in according to the previous description. The second stage describes the data logger response, which has only a stage gain of $\frac{65536}{20}$ Counts/V. An example of a header file stored in XML is given in Appendix A.

The **overall gain** is 131141.13*3276.8= **4.29723E08** Counts/m/s.

The amplitude and phase response of the whole system is shown in Figure 8.

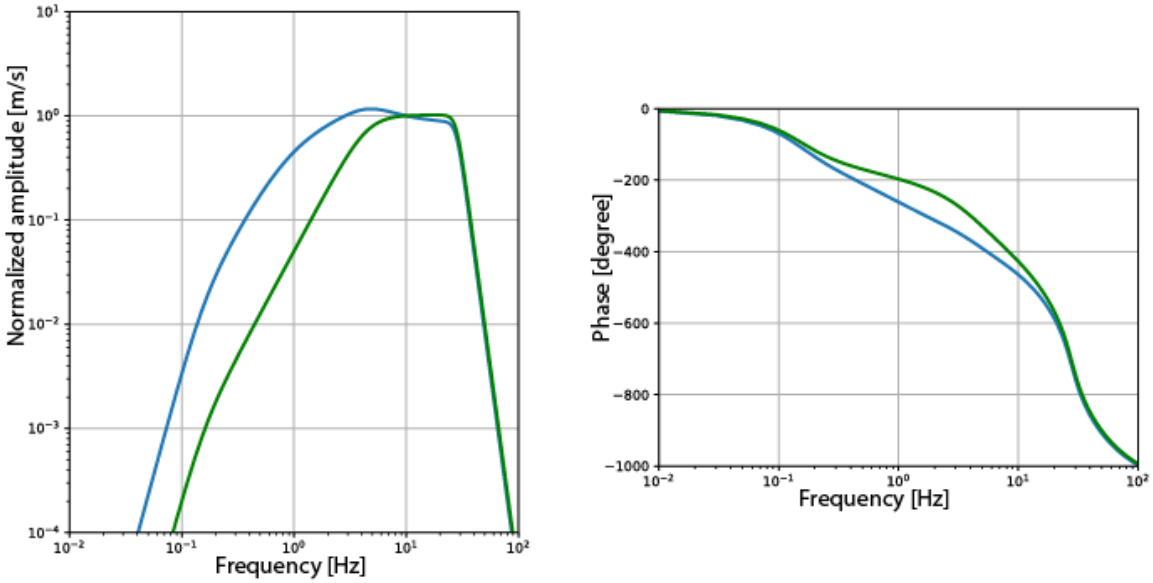

Figure 8. Normalized amplitude response (left) and phase response (right) of the borehole systems in operation 1995-2010. FSW response until 1996-05-05 in green, other boreholes' responses in blue.

In the period from 1992 until 1996-05-05, station FSW was operated without the shaping filter. In addition, the data logger was only 12 bits and its gain setting was different (Dost & Haak, 2002). In equation 7, pole s_3 and zero s_2 are omitted. This has consequences for the normalization constant at 10 Hz, which changes to 9.5209E17. This value is higher than the value of the normalization constant of the Butterworth filter, so the correction factor becomes 0.9754.

The sensitivity of the first stage of the response S, describing the sensor and electronics, becomes: S=28.8*1023*0.956*100 = 2.816606E6 V/m/s. Multiplied by the correction factor this value becomes S= 2.747317E6 V/m/s. In stage 2 of the response the data logger is described, which provides a factor 4096/20 = 204.8 Counts/V.

The **overall gain** of this response becomes 2.747317E6 * 204.8= **5.6265E8** Counts/m/s.

Consequences:

The metadata of all boreholes installed in 1995 are described in three epochs, covering the period 1995-2009/10, 2009/10-2016 and from 2016 up to present. In 2009/10 the operation of these boreholes changed from a triggered system to a continuous data streaming system. The hardware set-up did not change, although A/D boards and PC's were updated. This update resulted in the reduction of the overall gain by a factor of 4. Calculated, but unfortunately not documented, values for the overall gain factor are 1.07434E8 for the second epoch. The overall gain factor for the first epoch was re-evaluated at the start of the second epoch and calculated as 4.29735E8.

The latter value is 0.003% higher than the overall gain calculated and documented in the current report (4.29723E8). M_L is calculated as: $M_L = \log_{10} A - \log_{10} A_0$, where A is the arithmetic average of the maximum value of the horizontal components and A_0 a correction for the attenuation at distance (e.g. Dost et al., 2018). The use of an overall gain factor, which is 1.00003 higher than the value calculated in this report, adds a constant factor of 0.000013 magnitude units to the reported magnitudes. This difference is well below the precision that magnitudes are communicated. Therefore, we did not modify the overall gain in the data archive, but used 4.29735E8 for the first

epoch. For the third epoch, dataloggers were replaced with Kinemetrics dataloggers and electronics were simplified by removal of the analog shaping- and anti-alias filter.

For the first epoch, magnitudes have been calculated using the gain settings listed in Dost and Haak (2002), based on the knowledge at that time. The re-evaluation of the gain factor S in equation 6, resulting in a 2.3% higher value for the amplification of the system (1023 vs 1000, see p12), has also little effect on the calculated magnitudes. Similar to the previous discussion on the overall gain, a higher value of S implies a smaller value of A in the equation for M_L. In this case a factor 1.023 gives a constant factor of -0.0099 magnitude units that needs to be added to M_L. Since event magnitudes are averages over multiple stations and the uncertainty in magnitude is always > 0.1 magnitude unit, this change in gain setting will also not influence the magnitude estimates in the first epoch, within the precision that magnitudes are communicated.

The dataset presented is used in Seismic Hazard and Risk Analysis (SHRA) calculations for the Groningen gas field. Although magnitudes are available in two decimal places, only one is used in the calculations. The second decimal place is only used to stabilize the inversion procedure, so a change of 0.01 magnitude unit will not influence the results (pers. comm., J. van Elk). The same holds for the calculation of the b-value from the frequency-magnitude relations. Data are binned in 0.1 magnitude intervals, so only in very special circumstances a change of 0.01 magnitude units may modify a specific binning result.

3.2 Polarity and orientation

In this section of the report, we will look in detail on the polarity and orientation of the accelerometer and borehole network. A short paragraph concerning the vertical polarization is followed by a more elaborate examination of the orientation of the horizontal components. For the accelerometers, this was the most elaborate part, since the dataset is small and only consists of triggered local events. For the boreholes orientations were already determined, using check shots at short distances (Diephuis & Asmussen, 1995), explosions and local events (Ruigrok et al., 2019).

3.2.1 Vertical component

In the description of the FDSNStationXML format, the polarity of the vertical component is defined as positive down from the horizontal. Therefore, if a sensor has a positive movement downwards (pointing inside the earth) the dip= 90 degrees, while for a sensor that has a positive movement upwards, the dip= -90 degrees.

3.2.1.1 Accelerometers

For the AC-23 sensor, the manual states that the vertical component is positive downwards for the time period in which the sensors were ordered and delivered.

For the AC-63 sensor, the vertical component is positive upwards, so this sensor has a dip -90 degrees. The manual does not specify any changes over time for this sensor.

3.2.1.2 Boreholes

Using teleseismic events, we compared the polarity from the vertical channel of borehole stations with broad-band stations in- and outside the region. In order to make a reliable virtual comparison, we corrected the borehole recordings for the instrument response. This is not needed for the broad-band systems, since they have a flat response to velocity in the frequency range we are interested in (roughly 0.5-3 Hz). Figure 9 shows results for station FSW at 225 m depth compared to broad-band stations HGN and WIT. All have clearly the same polarity and the convention is to have the positive motion upwards for the vertical component. One more check on the polarity of the broad-band stations in Figure 10 shows consistency of polarity over all broad-band stations, including one in Belgium. Recordings are from the 2007-11-29 M7 Martinique event with a deep source depth (156 km).

So, although the boreholes in their original set-up have a polarity different from the broad-band stations, positive down, this was corrected for in the electronics. Apart from 2007, we found other teleseismic recordings which show the same results. At an earlier 2003, May 26 M7 Honshu event we found that station WIT did have a different polarity. It appeared that the polarity in this station was changed at September 29, 2003 (Reinoud Sleeman, pers. comm.). This information will be added to the XML information of station WIT.

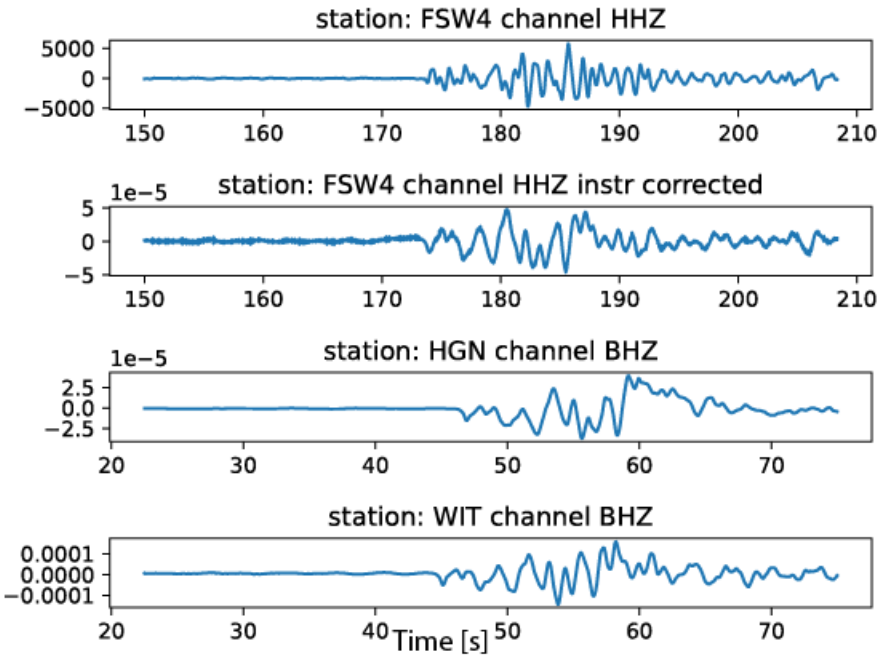

Figure 9. Borehole channel FSW4-HHZ recordings of the 2007-11-29 M7 Martinique event compared to BHZ component recordings from broad-band stations HGN and WIT.

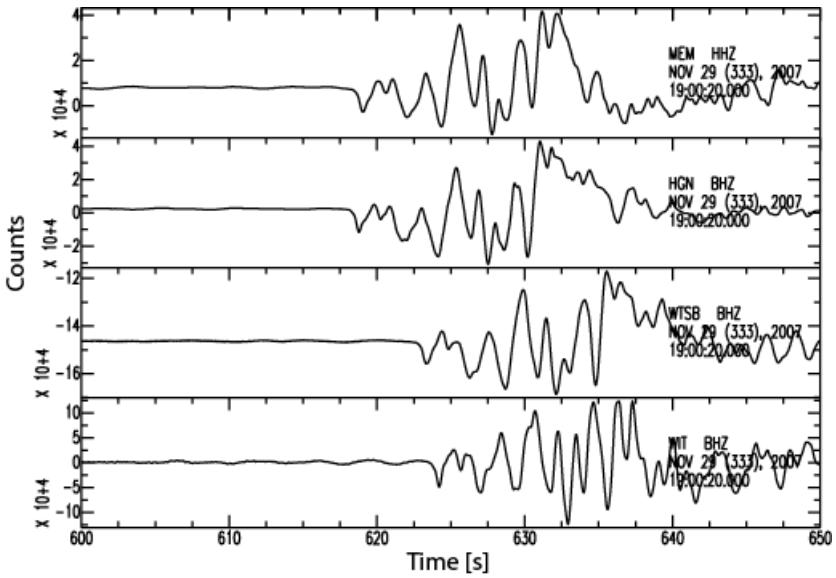

Figure 10. Comparison of broad-band Z-component polarity for P-wave recordings of the 2007-11-29 M7 Martinique event in stations MEM (Belgium), HGN, WTSB and WIT.

Now we have shown that one of the boreholes (FSW) at its 4th, 225 m deep, borehole level has the same polarity as broad-band stations elsewhere, we can compare all boreholes at the same level. In Figure 11, the Z-components of all boreholes at the 4th level are plotted, again based on the 2003-05-26 M7 event. It is clear that all show the same polarity including the borehole stations near Alkmaar (OTL, PPB and WMH).

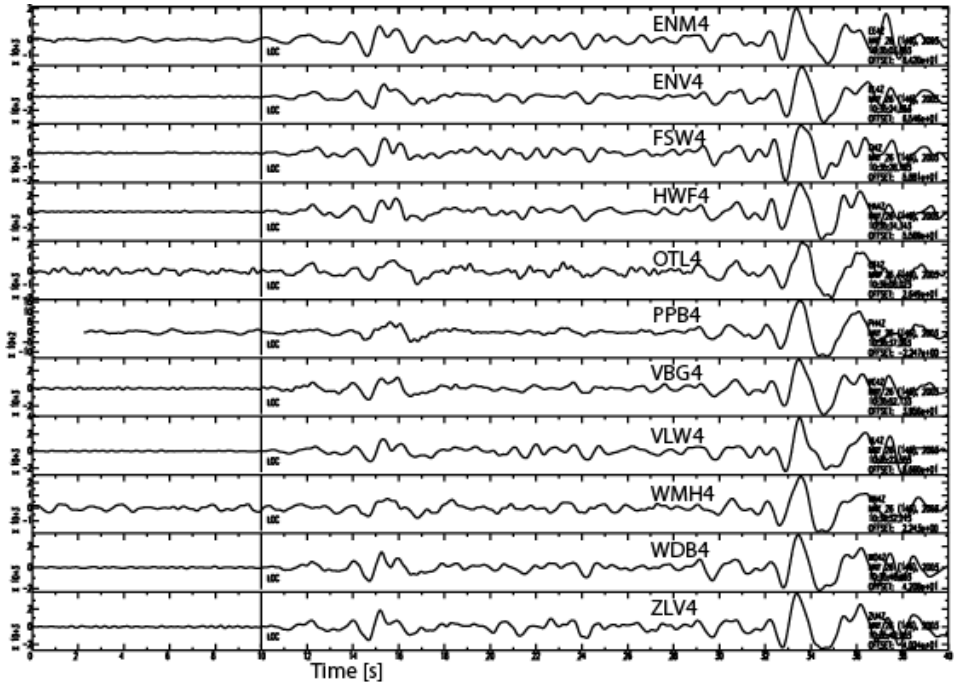

Figure 11. Vertical components of the 4th level of borehole recordings of the M 7 May 26, 2003 event.

Finally, a check on all Z-components has been carried out by plotting all levels at all boreholes in Figure 12. There are no visible changes in polarity of the Z-component over all levels.

Other observations are:

- Malfunctioning of the Z-component of the surface sensor at ZLV (lowest trace in panel) and missing records for station ZL2. We therefore added results for ZLV and ZL2 for the 1999-03-28 M 6.6 event in India in Figure 13. All levels show the same polarity.
- All levels, including the surface levels, show similar amplitudes. This is expected at these low dominant frequencies (< 1 Hz), since the wavelengths are larger than the depth of the sensors.

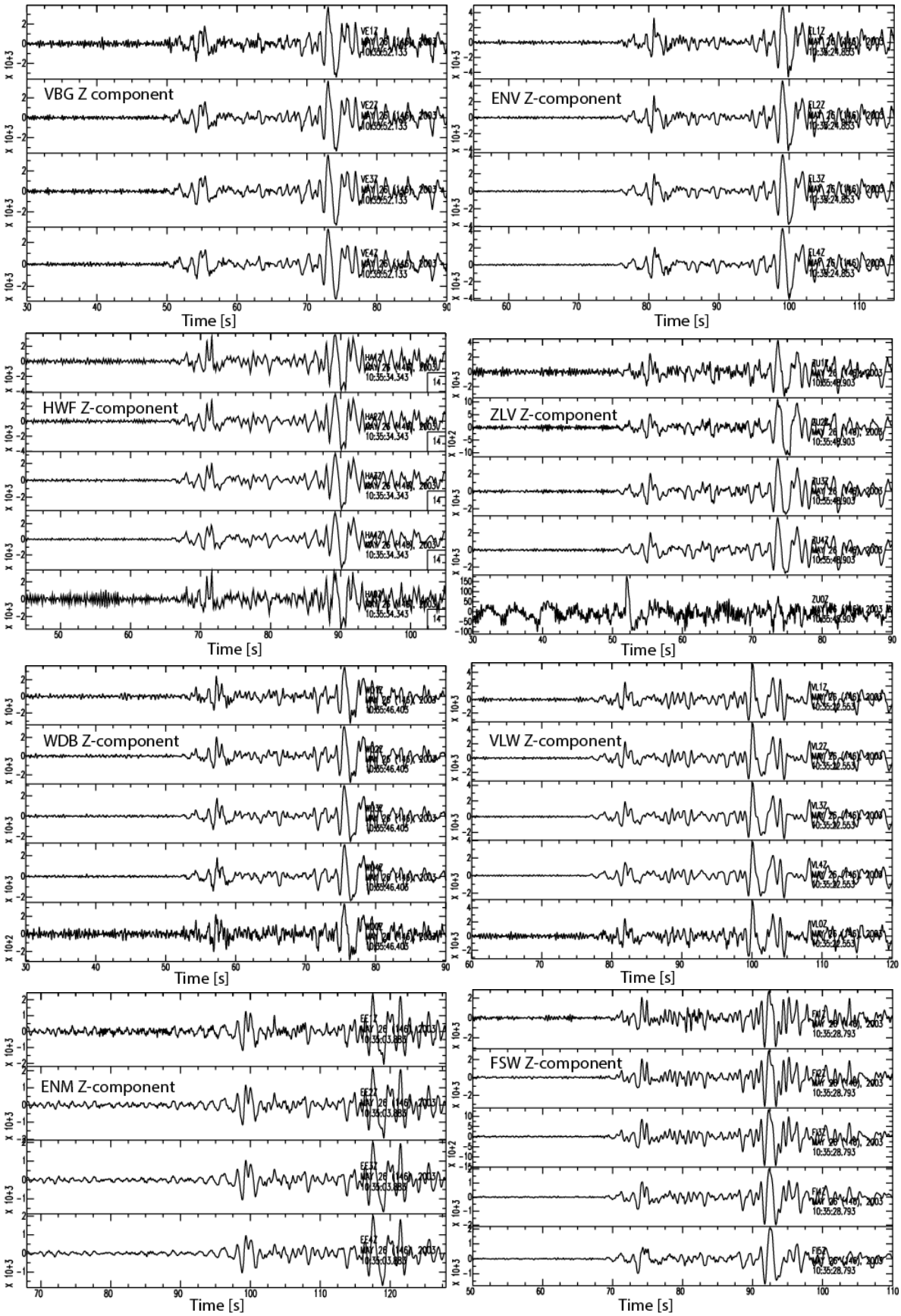
VBG Z component
ENV Z-component
HWF Z-component
ZLV Z-component
WDB Z-component
VLW Z-component
ENM Z-component
FSW Z-component
Time [s]

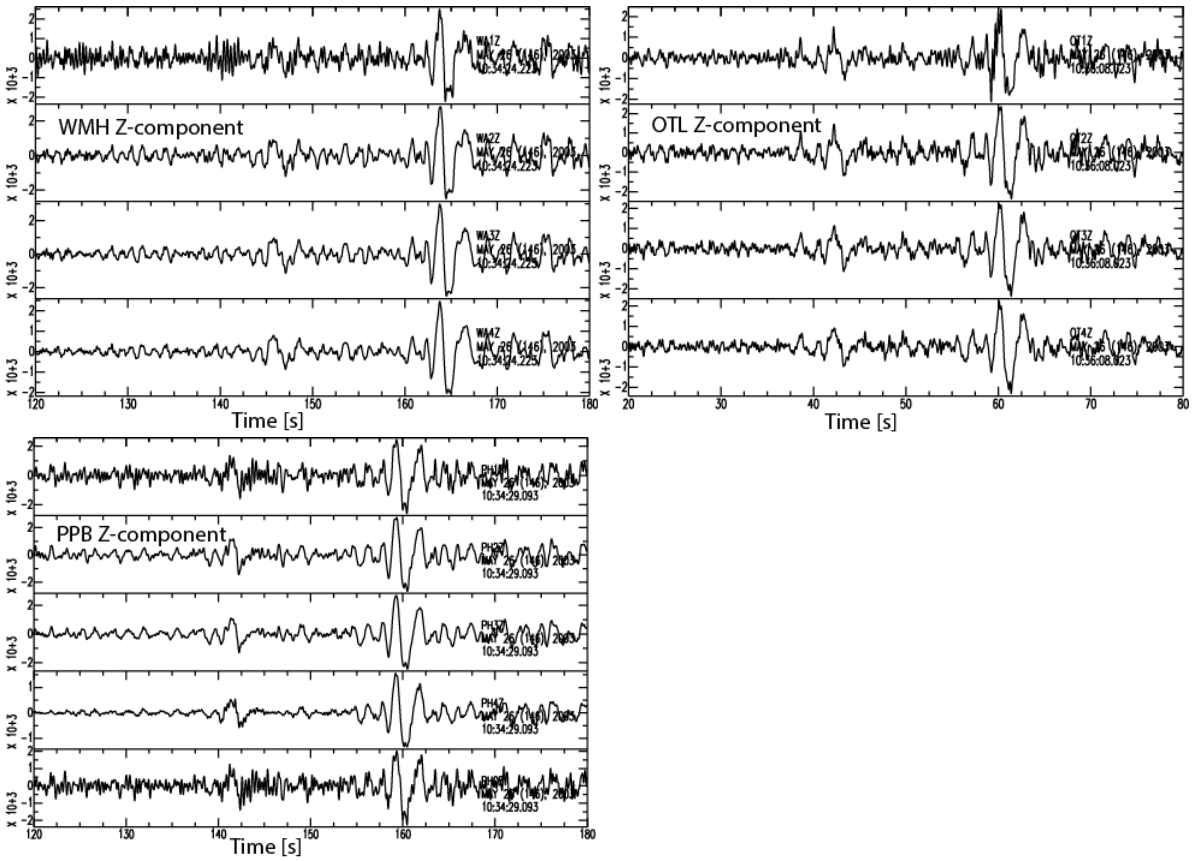

Figure 12. Z-components of all borehole levels for all borehole stations plotted for the 2003-05-26 M 7 Honshu event. For stations with 5 traces displayed, the lowest trace is the surface sensor, except for FSW where the surface sensor is shown as the first trace.

Looking at the development in time of the borehole records, we show in Appendix B the recordings in 6 stations from the 156 km deep, 2007-11-29 M 7.4 Martinique event (Figure B1).

Now going back to the early period, we found the 625 km deep, M 6.8 1997-09-04 Fiji event, recorded in all operational boreholes. Figure B2 shows similar panels as in Figures 12 and 13. Apart from malfunctioning of a few components, partly caused by damaged pre-amplifiers, we find at station PPB the second level showing a reversed polarity. For an overview of known malfunctioning, we refer to Appendix G.

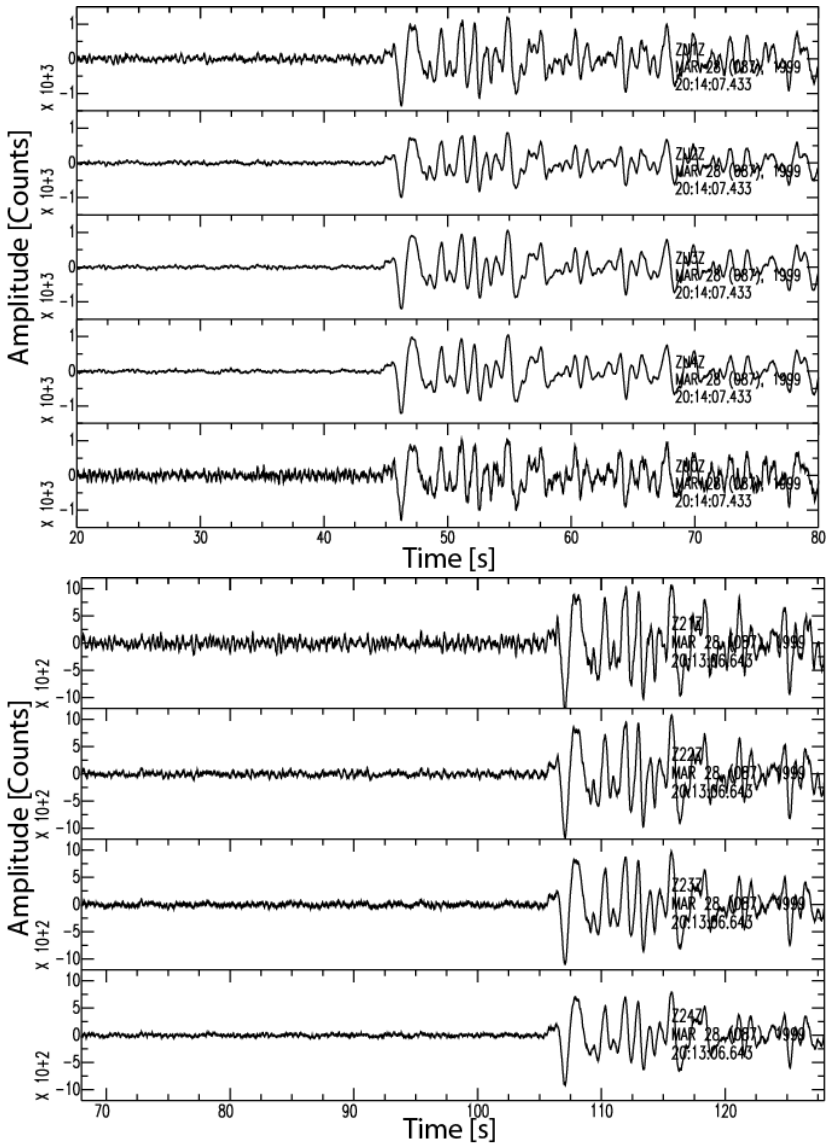

Figure 13. See Figure 12, now for the 1999-03-28 M 6.6 Indian event and stations ZLV and ZL2.

In the calibration reports (Diephuis & Asmussen, 1995), a possible change for stations ENM and FSW is indicated. However, looking at teleseismic events, we do not see this change in vertical polarity. There may have been a problem during the testing, so we should be careful looking at the polarity of the horizontal components of these stations.

3.2.2 Horizontal components

In the description of the FDSNStationXML format, the polarity of the horizontal components is defined by the "azimuth of the sensor in degrees clockwise from the geographic (true) north". The uncertainty in the azimuth can also be specified.

3.2.2.1 Accelerometers

The accelerometers that were installed over the years since 1996, were located in buildings and supposed to be aligned according to the manual, which means that the X component (HG1 in the data files) should point to the North. No further check was carried out, mainly because these sensors were primarily used to measure peak amplitudes in the field at locations where in the past felt earthquakes occurred. In this report we will investigate if we can confirm the settings. For this, we will analyze the waveforms with respect to known locations of local events. These data are triggered, so only events are available. An overview of recorded events is shown in Table 7:

		#records in stations																
start		1996	1997	1997	1998	2000	2000	1996	1998	1999	1999	2006	2006	2005	2007	2007	2009	2009
year	#events	ROS1	ROS2	ROS3	ROS4	ROS5	ROS6	MID1	MID3	ZAN1	ZAN2	WSE	FRB2	HKS	KANT	WIN	GARST	STDM
1996	2	2																
1997	7	6	2	5														
1998	3	3	3	2														
1999	6	6	5	4	1													
2000	3	1	3	1	1	1												
2001	1	1	1		1	1	1											
2002	3	1	3			1	2											
2003	5	1	1					1	4		2							
2004	1	1	1				1											
2005	0																	
2006	10	2	2		1		2		2	1	3	1		5				
2007	3										2	2						
2008	4							2	1	1	3	1				1		
2009	8							2	1	3	3	6		1		3		
2010	5							1		1	1	2	1	1	1		1	
2011	10							4	2	1	2	9	1	1	1	2	3	1
2012	3							2				2	1	1	1	2	3	1
2013	7									2		4		2	2	4	4	
2014	1													1	1	1	1	
Total	82	24	21	12	4	3	6	12	10	9	16	27	3	12	6	13	12	2

Table 7. Overview of the number of station recordings for specific events in the period 1996-2014. The row 'start' lists the years the stations became operational.

From the operation manual, we noted that there are two different orientations: 1] for the AC-23 system the movement of data recorded on the X (HG1, North), Y (HG2, East) and Z (HGZ, up) components are negative in the indicated direction; 2] for the AC-63 system the movement of data recorded on the components is positive in the North (X, HG1), West (Y, HG2) and Up (Z, HGZ) direction. In the analysis of the orientation of the sensors, we multiplied all components of the AC-23 system with a factor -1 and for the AC-63 system we multiplied the Y (HG2) component with a factor -1 to be compatible with seismology standards (positive in the N, E and up direction).

From the 31 accelerometers in Table 5, only 17 recorded events (Table 7) and these are all inspected and analyzed to see if the records met the specifications, which are a record length of 15-30 seconds, including 5 seconds before triggering. For the analysis the 'Obspy' toolbox was used (Beyreuther et al., 2010). The remaining 14 stations do not contribute to the dataset. In our analysis we assume the instruments were not moved over time and there have not been indications these assumptions were violated.

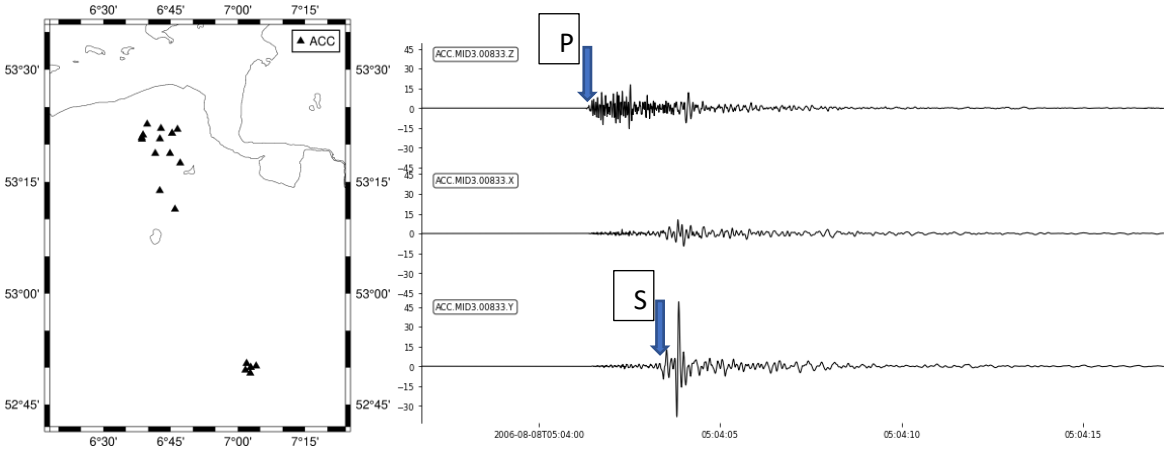

Figure 14. Left: Accelerometers in the North of the Netherlands for which analysis could be performed. The cluster of 6 accelerometers at the bottom of the figure is for monitoring the induced seismicity at the Roswinkel gas field. The upper cluster is the accelerometer network in Groningen field. Right: raw data recorded at station MID3 for the 2006, M 3.5 Westeremden event

Procedure

First of all a procedure was developed to automatically process the entire dataset and determine the orientation of each station by rotating the horizontal components in the direction of the associated event. Corrections to the theoretical azimuth that are required to obtain a minimum energy at the transverse component and a maximum energy at the radial component indicate that the orientation of the sensor needs an adjustment. As shown in Figure 14, the P and S waves are mostly separated in the 3-component recordings, with P wave mostly on vertical components and S wave on the horizontal components

For each station, the P-wave onset of each earthquake is picked using a STA/LTA procedure (based on vertical components which are band passed at 2 - 35 Hz, short time window 0.01 s (STA) and long time window 0.5 s (LTA), the trigger threshold is set at 10). Additional constraints were applied to subtract false triggers:

(1) A direct constraint on the amplitude of the vertical component, i.e. the minimum absolute value of the signal amplitude in the record should be larger than 0.2 cm/s^2.

(2) The time length between trigger-on (STA/LTA increase to 10) and trigger-off (STA/LTA decrease to 10), as real signal onsets tend to have longer and robust STA/LTA values. The largest STA/LTA on the time window between 0.2 cm/s^2 and the maximum amplitude is found. The trigger, that has the status "on" before the maximum STA/LTA and "off" after it was selected, is chosen.

As shown in Figure 15, the P wave onset is successfully picked through this procedure.

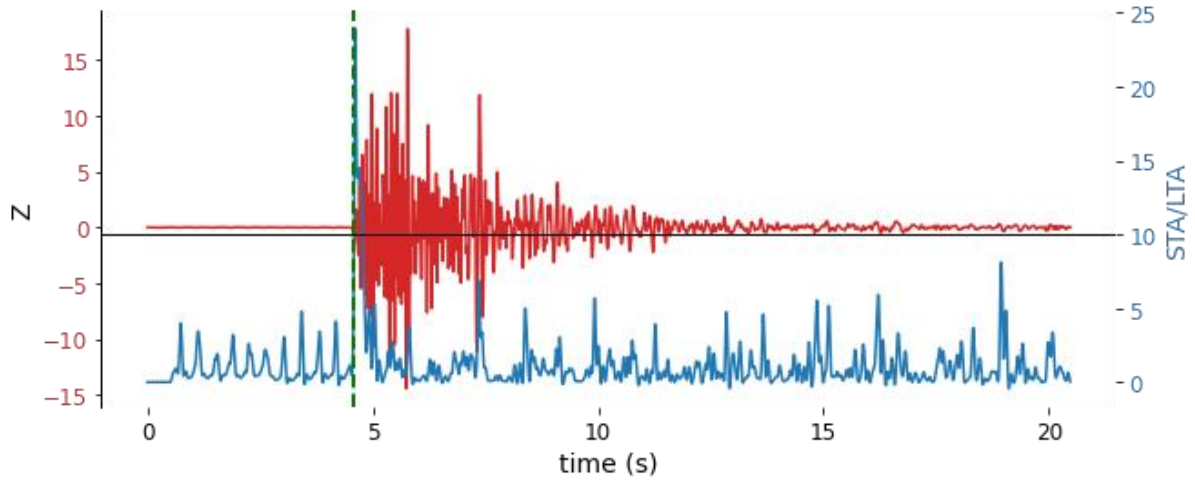

Figure 15. P wave onset (green dashed line) picked by STA/LTA (blue curve) at threshold 10.

After the P onset is picked, the 3-component data are bandpass filtered between 2 to 30 Hz (Butterworth 2nd order). A time window from -0.1 to 0.15 s (AC-63) or from -0.1 to 0.25 s (AC-23 instruments) around the onset is selected for the component analysis. Ideally, we would like to take a window as short as possible around the P-wave onset. But with the AC-23 instrument, which has only a 16-bit digitizer, the resolution is low around the onset, thus a window of -0.1 - 0.25 s is chosen, after testing multiple values.

The next step in the procedure is to carry out the rotation, defined as

$$\begin{bmatrix} R \\ T \end{bmatrix} = \begin{bmatrix} cos\theta & sin\theta \\ -sin\theta & cos\theta \end{bmatrix} \begin{bmatrix} X \\ Y \end{bmatrix} \quad [8]$$

with R and T the radial and transverse component and θ the source-receiver azimuth. The rotation is executed as a grid search taking 1 degree steps from 0 to 360 degrees. The optimal value for the angle of rotation is found when the energy at the transverse component is minimized. In Figure 16 an example of this procedure is shown and this also shows that there are two minima, 180 degrees apart. To solve this problem, we also compute the multiplication of the vertical and radial component, which should be positive for a P-wave and a North, East, Up positive axis definition (e.g. Jepsen & Kennett, 1990). A joint interpretation of both measures is expected to provide a unique solution. Figure 16 shows the combined interpretation of both measures.

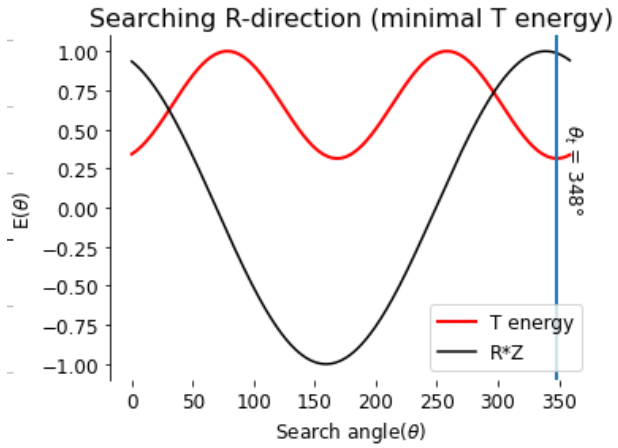

Figure 16. Results of a rotation after a grid search over a step length of 1 degree. In red the energy on the transverse component is shown, in black the energy of the multiplication of the radial and vertical component. A unique solution is found for an azimuth θ=348^o .

Event coordinates are taken from the KNMI catalogue and, together with the station location, the azimuth from the event to the station can be calculated. Equation 8 is used to calculate the radial and transverse components, assuming X=N (HG1) and Y=E (HG2). In case the experimentally determined rotation differs from the theoretical value, a correction needs to be applied to the orientation of the components HG1 and HG2 before rotation. In the following we will determine this correction.

Testing the procedure with G-network stations

The procedure was first tested on the G-network borehole stations, as the data quality is high and the orientations of horizontal components are well constraint (Hofman et al., 2017). Results are presented in Figure 17. An important observation from these results is that very stable results are obtained for borehole sensors at depth (Figure 17b,c,e,f), while the results on the surface accelerometer show a high variability (Figure 17a).

After selecting events with magnitude larger than 2.5, to ensure a good signal to noise ratio and a distance larger than 2 km to minimize the effects of location uncertainty, the variation in azimuth becomes less, but is still clearly visible (Figure 17d). Although the effect is not very convincing in this example, we decided to use the limits in magnitude and distance to be sure that the effects of small distances and low magnitudes are minimized.

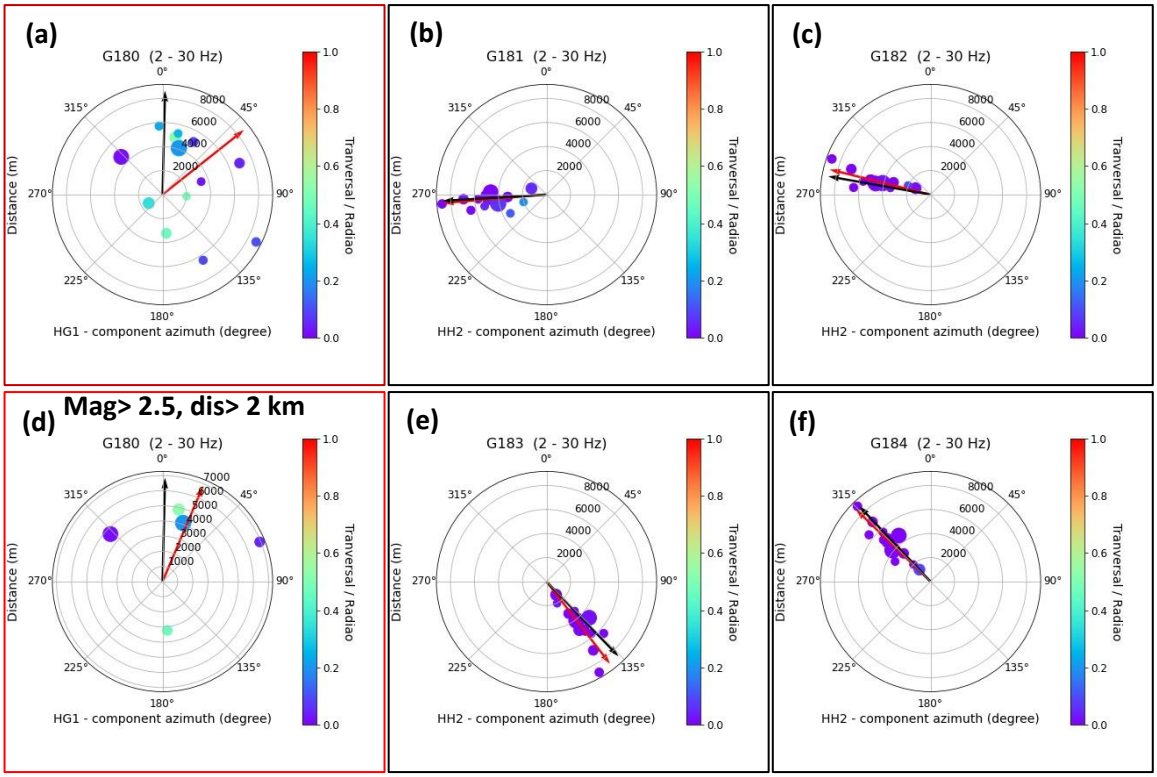

Figure 17. Results of the procedure to G-network surface accelerometer (G180) and borehole geophones (G181, G182, G183, G184) at station G18. Black color arrows indicate azimuth of HH2 component (for geophones in borehole) and HG1 components (for the accelerometer at surface). While Red color arrows are calculated results from our procedure.

There are several possible reasons for the large uncertainty in azimuth determination from the surface accelerometers. First of all the P-wave does have a near-vertical incidence angle, which results from a large velocity contrast at the bottom of the Northsea group (Vp ~2.7 -> 2.0 km/s) at a depth of app. 0.8 km (Romijn, 2017) and a further velocity reduction close to the surface. The Northsea group consists mainly of unconsolidated sediments. As the direct P-wave particle motion is mostly in vertical direction, the amplitudes on horizontal components are small. Near surface heterogeneity and local high velocity contrasts at shallow depths may result in multiple reflections and scattering and P to S converted waves. These interfering waves may have amplitudes as high as the direct P-SV waves at the horizontal components. The direction inferred from the minimal energy determination of these complex wave groups may result in erroneous orientation.

A similar observation was made in a number of papers on the Mississippi embayment (e.g. Langston 2003, Chiu et al., 2011 and Li et al., 2014).

In some cases, although the very beginning P-wave onset of the R and Z may be in phase, the rest of the waveform appears out of phase, as shown in Figures 18 and 20. However, the example in Figure 18 also shows that if we apply a small time correction to the radial component of app. -0.015s, the Z and R components are in phase and show a high correlation. This observation suggests that the P-S conversion plays a dominant role, similar to the findings by Li et al. (2014), who found a 0.3 s difference between P on the Z and P-S on the R-component. So, it is essential to keep the window length as small as possible and at the same time to guarantee sufficient signal-to-noise ratio. If it is possible to estimate a station delay between the radial and vertical component, this delay should be corrected for before calculating R*Z in the automated procedure. Due to limited time, this was not yet

implemented in the automated procedure, but is worthwhile to further explore. However, the correction was applied manually in several cases. We will come back to this in the results section.

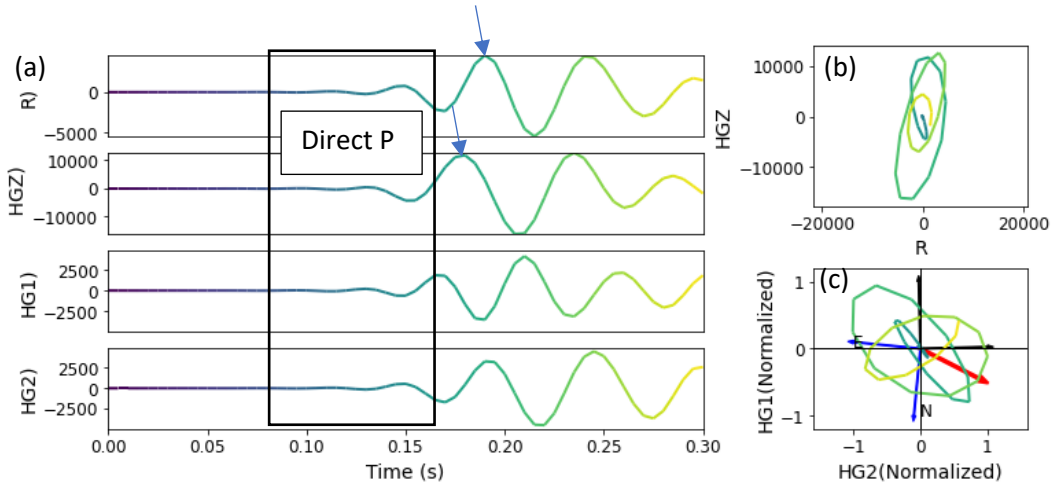

Figure 18. (a) P-wave window used for the analysis from the M2.5 event at G180. The blue arrows indicate the maximum of the waveforms at the Z and R component (b) Particle motion in the R-Z plane and (c) Horizontal particle motion, the inferred radial direction (red arrow) and the inferred N and E direction (blue arrow). Assumed "true" N and E directions, obtained from station meta-data, are shown as black arrows.

Results

Events with magnitudes larger than 2.5 and epicentral distances larger than 2 km are used to ensure good signal level and decrease the influence of uncertainties on earthquake locations. For the AC-23 instruments, it is also required to have the horizontal signal amplitude larger than 0.2 cm/s^2 (4 times larger than the minimum resolvable acceleration level of 0.05 cm/s^2).

Since the automated method, referred to as Method 1 in the rest of this report and explained in the previous section, sometimes created large variations in orientation, we decided to do an additional manual check for each station (Method 2). This enabled us to clarify the cause of this difference and take decisions on the correct values. Results from method 1 have been corrected in case of clear errors in the automated procedure. A difference of 180° between results from both methods was in most cases the reason and could be attributed to the time difference between R and Z. Stations WSE, ZAN1 and ROS3 were affected. For both methods we average the orientations for each station.

An example of the resulted X component orientation is shown in Figure 19, for the station MID3. Relatively stable results are obtained at this station with an average orientation of -55° (305°). The averaging of angles is calculated from:

$$\bar{\theta} = tan^{-1}\left(\frac{\frac{1}{N}\sum \sin(\theta)}{\frac{1}{N}\sum \cos(\theta)}\right)$$

Over N events. The standard deviation is calculated by:

$$\sigma = \sqrt{\frac{\sum(|\theta - \bar{\theta}|)^2}{N}}\ ; if\ |\theta - \bar{\theta}| > 180;\ |\theta - \bar{\theta}| = 360 - |\theta - \bar{\theta}|$$

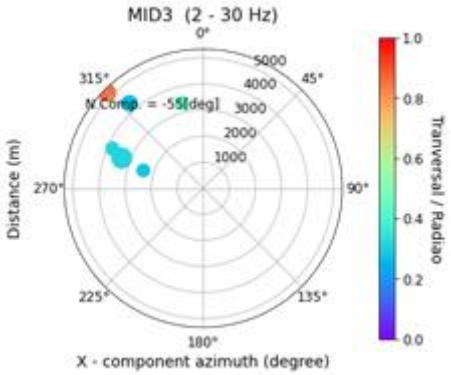

Figure 19. Orientation of the HG1 (N) component from 6 events.

A list of average orientations and their uncertainties, estimated at all accelerometers that recorded at least one event, is presented in Table 8. In general the two methods give comparable results. Stations with only 1 or 2 event recordings , such as KANT and FRB2, show larger differences. For the final result in the last two columns, the results from the two methods are averaged. For the averaging we used a weighted arithmetic mean:

$\bar{x} = \frac{N_1\bar{x}_1+N_2\bar{x}_2}{N_1+N_2}$ and accompanying weighted standard deviation $\bar{\sigma}^2 = \frac{N_1^2\sigma_1^2+N_2^2\sigma_2^2}{(N_1+N_2)^2}$

Please note that a standard deviation of 30 degrees was assigned to orientations based on measurements in only one station. After averaging, we kept the uncertainty at 30 degrees for these stations. For ROS5 and ROS6 no event was recorded that could meet our specifications in magnitude and distance range. Therefore we released the specifications for ROS5 to include a distance of 916 m and M = 2.1. For ROS6 we selected a M 2.4 at 1774 m epicentral distance. For event information we used the KNMI online catalog, except for the M 3.6 Huizinge event. For this event we used the relocation results (Dost & Kraaijpoel, 2013).

	Method 1			Method2			Averaging X azimuth	
Station	Mean	Std	N	Mean	Std	N	**MEAN**	**STD**
MID1	9	26	2	28	28	2	**19**	**19**
MID3	309	21	6	315	23	6	**312**	**16**
ZAN1	268	22	3	267	25	3	**268**	**17**
ZAN2	30	18	5	30	24	4	**30**	**15**
WSE	20	34	6	18	27	6	**19**	**22**
ROS1	353	20	3	352	4	5	**352**	**8**
ROS2	9	42	4	13	24	4	**11**	**24**
ROS3	346	5	4	339	5	4	**343**	**4**
ROS4	65	38	2	73	8	2	**69**	**19**
ROS5*	331	30	1	310	30	1	**321**	**30**
ROS6*	322	30	1	330	30	1	**326**	**30**
GARST	351	24	7	361	14	4	**355**	**16**
KANT	80	30	1	20	37	3	**35**	**29**
WIN	358	52	7	322	58	5	**343**	**39**
HKS	354	26	4	363	29	3	**358**	**19**
STDM	54	30	1	60	30	1	**57**	**30**
FRB2	39	30	1	20	30	1	**30**	**30**

Table 8. Orientation of the North component at acceleration stations. Method 1 is an automated procedure, Method 2 a manual procedure. Mean and standard deviations (std) are shown for each station and a final mean and standard deviation based on the other two results. N denotes the number of events used in the analysis.

As explained earlier, we find at stations a small delay between the vertical and radial component, which influences the RZ calculations. As an example of this effect on the processed accelerometer data, Figure 20 shows data from station WSE, where RZ is mainly negative in the raw data. The RZ component is shown in detail in Figure 21. Only the first samples are positive, while the average RZ value is negative over the selected time window. Figure 20 and 21 show results without a time shift applied. In Figure 22 the effect of the time shift is demonstrated.

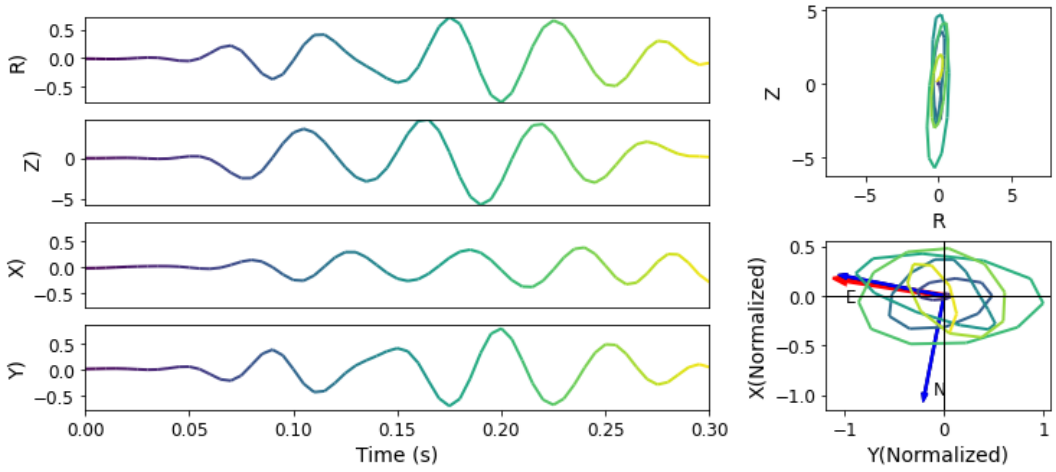

Figure 20. (a) P-wave data used for polarization analysis, for station WSE event 2009-04-14 M2.6. Estimated radial component is shown on the top panel. (b) particle motion on the estimated R and Z plane. (c) particle motion on horizontal components. With the radial direction indicted by red arrow, N and E direction indicated by blue arrow, related to X-Y.

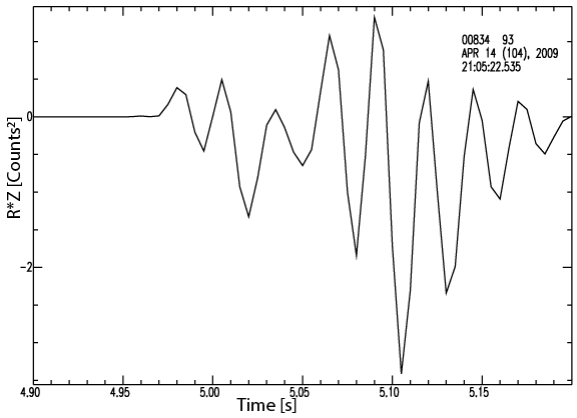

Figure 21. RZ for station WSE, event 2009-04-14

We looked in more detail at station ZAN1 to see if a constant time shift can be applied as a station effect. Figure 22 shows a good correlation between vertical and radial components after a time correction of -0.054s is applied to the radial component of multiple events. The station-event distance of these examples are 4.9 and 7 km for the 2008-10-30 and 2011-06-27 events. For an event at 2009-05-08 at an epicentral distance of 1.6 km, this delay has not been found for station ZAN1. It may be due to a steeper incidence angle for these short distances.

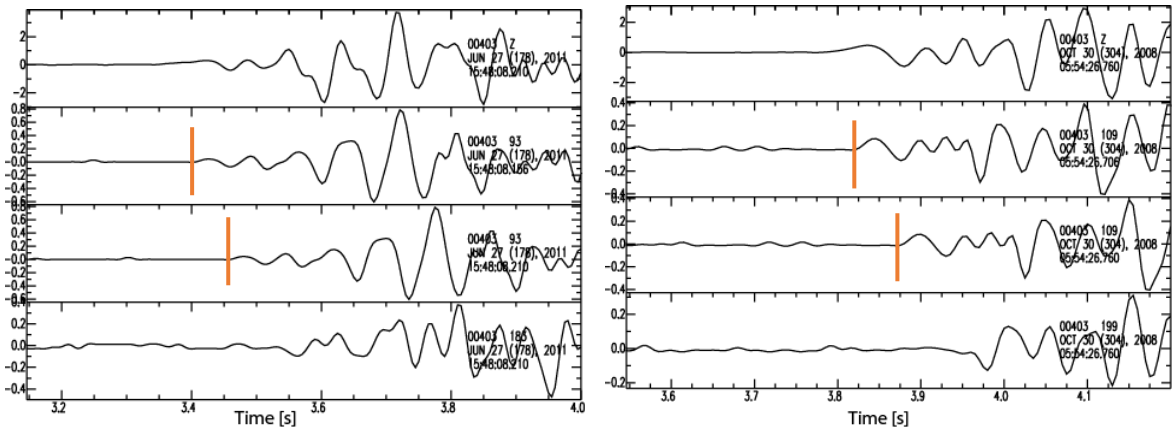

Figure 22. P-onset for station ZAN1 for event 2011-06-27 (left) and 2008-10-30 (right). From top to bottom: vertical component, radial component, shifted in time over -0.054s, original radial component and the transverse component. The onset of the shifted component is indicated by an orange line.

Please note that the orientation of the accelerometers in table 8 and in the Station XML files may have high uncertainties, especially in case only a few seismic events could be used in the analysis. Estimated uncertainties are listed in the Station XML files.

3.2.2.2 Boreholes

For the borehole systems that were installed in 1995, NAM (Diephuis & Asmussen, 1995) organized checkshots at all station locations to determine the orientation of the horizontal components. This documentation is added to this report as Appendix.

		level 1	level 2	level3	level4	level 0
FSW	NS	204	11	214	278	158
ZL2	NS	25	350	160	44	
ZLV	NS	64	133	222	130	0
WDB	NS	94	232	131	250	
ENV	NS	322	337	207	311	
ENM	NS	122	177	164	91	
VBG	NS	340	294	104	90	
VLW	NS	202	252	123	89	0
HWF	NS	166	257	342	199	0
OTL	NS	89	191	325	115	
PPB	NS	355	135	276	116	0
WMH	NS	260	9	280	210	

Table 9. Orientation of the horizontal (NS) component in degrees of the borehole stations operated in the period 1995-2011. Level 0 for FSW has station name FSW1, since the surface sensor was added from the start. For all other stations level 0 corresponds to station name XXX0.

Figure 23 shows 3C recordings over boreholes WDB after resolving the 180 degree ambiguity. In Appendix C results for all other boreholes are given. For most boreholes and depth levels it can be seen quite clearly that, for the upgoing wave, the vertical component (red line) and radial component (blue line) are in phase. For traces at or near the Earth's surface, it is harder to estimate the orientation and to resolve the 180 degree ambiguity.

Now the polarity of the Z-component is known for all borehole stations, the possible 180 degree ambiguity is resolved. This is done by checking whether the (first) upgoing P-wave has a consistent polarity on the vertical and radial components.

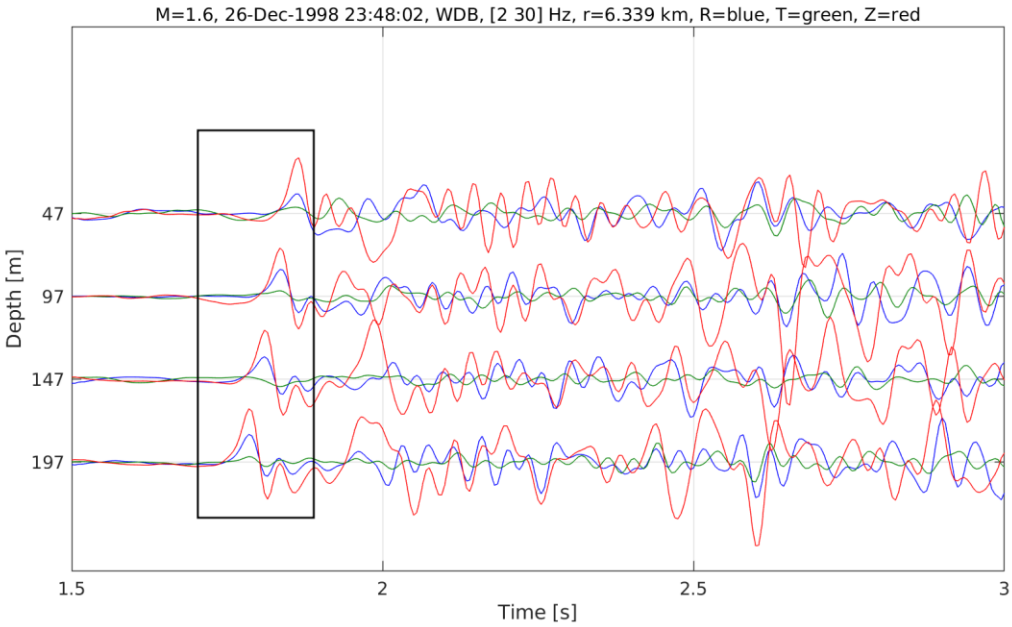

Figure 23. Overview of the vertical (red), radial (blue) and transverse (green) components for borehole station WDB, levels 1-4. The P-onset is indicated with a box.

The orientation of the horizontal components for FSW, ENM, PPB and VBG are similar to the ones listed in the NAM report (Diephuis & Asmussen, 1995). All others are 180 degrees different. This is due to the fact that the authors suspected a difference in the vertical component. Instead this appeared to be the case for the horizontal components of these stations. In Table 9 the orientations θ of the N-component (HH1) are listed. The E-component (HH2) has an orientation of θ +90 deg. This information is part of the stationXML files.

FSW1 is a surface geophone. Data quality on check shots was insufficient to estimate orientation. However, we could apply other techniques (see below) to find an accurate orientation. The other surface sensors could not be oriented well, so these are given an orientation 0, which means unknown in SEED convention.

FSW1 is located on the Earth's surface. To derive the orientation of the horizontal components from the recordings is challenging, as was the case for the surface accelerometers (Section 3.2.2.1). On the one hand, the P-wave incidence is nearly vertical due to low P-wave velocities in the near surface. That results in low signal levels on the radial component. On the other hand, there are high noise levels due to near-surface scattering. A solution is to use S-waves instead. They do have high signal-to-noise levels on the horizontal components. The polarization of S-waves in the horizontal plane, however, is a-priori unknown. What is known, is that the incoming S-waves must have (nearly) consistent polarization over the different borehole elements. Moreover, for all non-surface borehole elements, the orientation is well known from check shots. Hence, we estimate the orientation by

- Selection a time window around S-wave arrivals
- Applying a propagation correction to map a recording at depth to the free surface
- Correlating the surface recording and the propagated depth recording for various orientation corrections
- Determining the orientation angle that yields the largest cross-correlation coefficient.

The above mentioned procedure is repeated for all the available events in the database. Only estimates are retained that have a normalized cross-correlation coefficient of at least 0.6. Using FSW2 as a reference, for instance, there are 9 events that yield an estimate with an acceptable coherence (Figure 24). From these 9 events, the mean orientation angle, and its standard deviation, are taken. The same is done for the other three depth levels as a reference (FSW3, FSW4 and FSW5). From the resulting four estimates, the weighted mean is taken, which yields 157.9+-3.8.

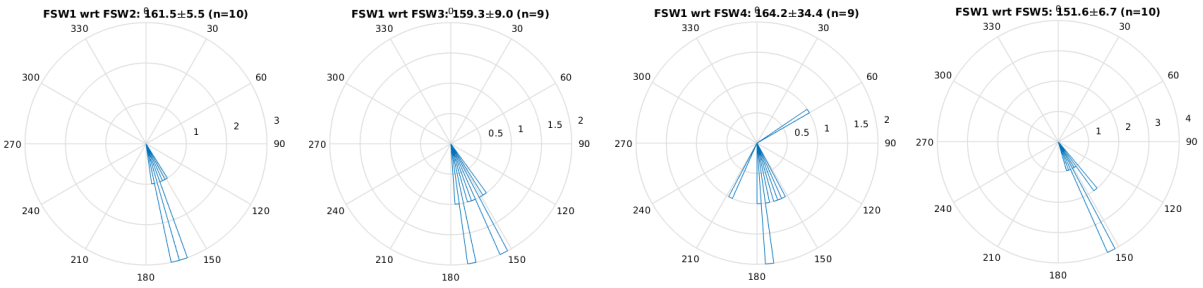

Figure 24. Rose diagram of orientation angles estimated with S-wave coherence between the surface sensor (FSW1) and four sensors at depth, from left to right FSW2, FSW3, FSW4 and FSW5. Above each rose diagram, the average orientation angle, its standard deviation and the amount of usable events, is listed.

The orientations of the borehole sensors have been obtained using local check shots and have been checked later using regional events. Results are comparable, apart from a 180 degree correction. Estimated uncertainties in the orientations are on average 5-10 degrees

3.3 Timing

Both accelerometer and borehole-geophone systems were synchronized in time by either a DCF-77 or a GPS receiver.

Accelerometers:

In the AC-23/SMACH-SM2 accelerometer set-up a flag was set in the native format indicating whether the time was synchronized or not. In addition information was kept on the time since the last synchronization. Unfortunately, this flag could not be used in the AC-63/GSR-18 setup. Information on timing quality is kept and stored in blockette 1001 in the SEED files. See chapter 4 for more details.

Boreholes:

Since the data logger part of the borehole systems was designed at KNMI, the DCF signal could be recorded as a separate channel. In this chapter we will explain how time corrections could be retrieved from the recorded time-channel.

The DCF signal consists of a series of second pulses. The minute mark can be recognized by the omission of the last second pulse before the minute mark. Figure 25 shows an example of the pattern of recorded second pulses and the determination of the minute mark. The time of the minute mark is relative to the start time of the record, so in the example the start time is 07:39:28.18 and the time of the minute mark is at 31.82s after the start time.

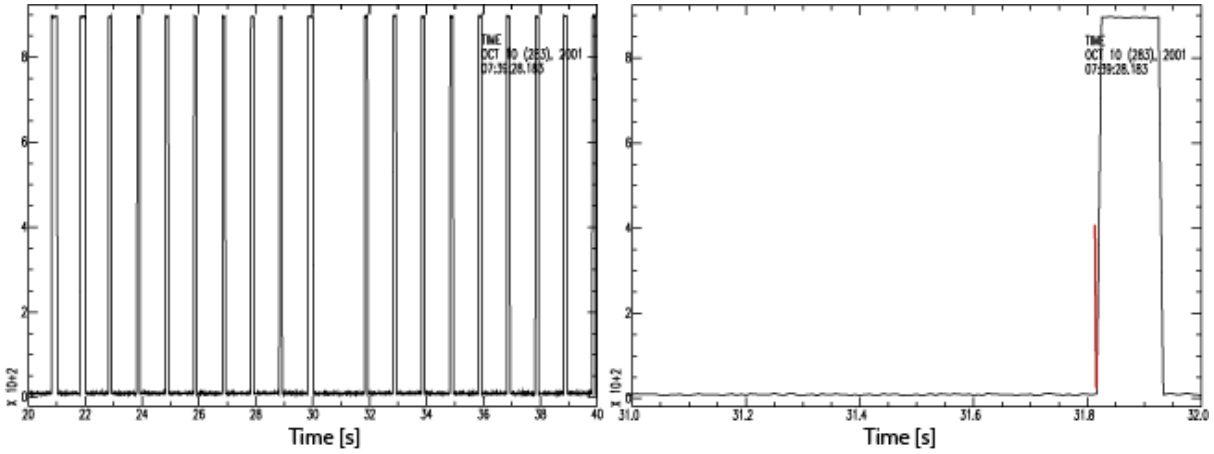

Figure 25. DCF timing signal recorded as a separate channel at each triggered file. Left: 20 second time section where the second before the minute is omitted. Right: detail of the timing of the minute mark (red)

For station FSW there is a different timing signal for the period 1992 until May 5, 1996, when this borehole station did operate in a different set-up (see response section). Only the minute mark is recorded, see Figure 26, and the correct time can be found on the onset of the pulse.

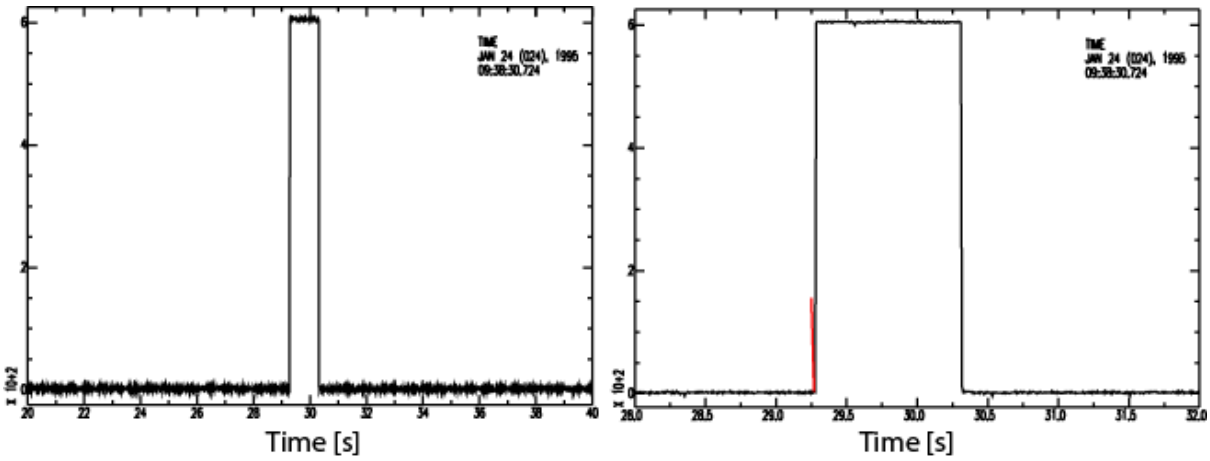

Figure 26. DCF timing signal recorded as a separate channel at FSW recordings < 1996-05-05. Left: 20 second time section where the minute mark is recorded. Right: detail of the timing of the minute mark (red).

Sometimes the timing signal shows erroneous second or minute marks due to bad reception. Care should be taken not to misinterpret the spurious pulses (Figure 27). In some instances spurious pulses may be so abundant that the minute mark cannot be identified. If this is the case, then timing cannot be trusted and the record should not be used for timing critical studies.

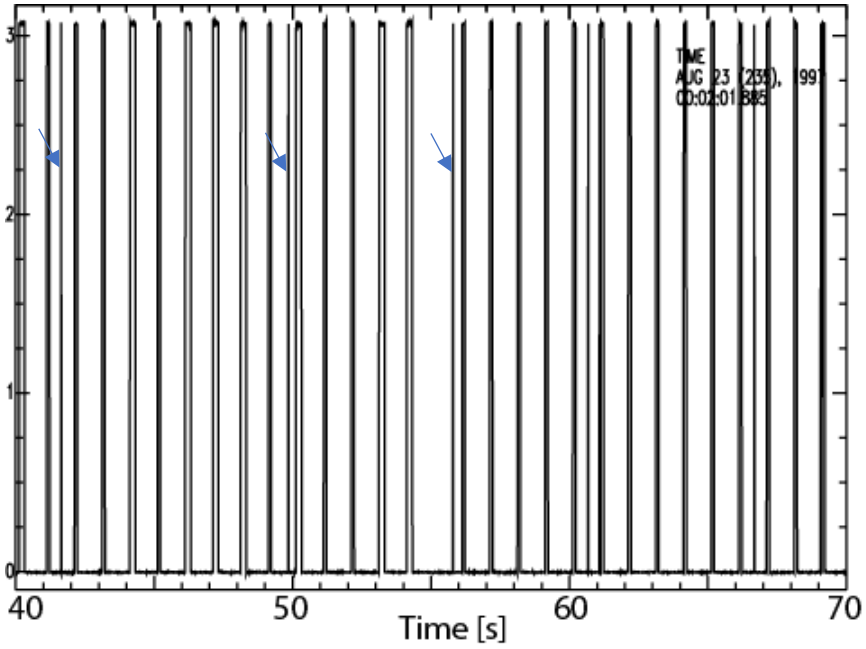

Figure 27. DCF timing signal (start at 1999-08-23 00:02:01.885) containing erroneous second marks, marked by blue arrows.

4. Data conversion:

As mentioned before in Chapter 3, the data collected in a triggered mode are stored in a local format and converted to SAC format. The conversion to SEED will be done in the form of miniSEED datafiles and accompanying meta-data in standard seismological XML format (https://docs.fdsn.org/projects/stationxml) . In the XML format the station details are documented (location and channel details), including e.g. the uncertainties in the orientations. An example of azimuth information including uncertainty for channel ROS1.HG1 is:

<Azimuth unit="DEGREES" minusError="8.0" plusError="8.0" measurementMethod="Event calibration">172.0</Azimuth>

Information on the uncertainty can be accessed by reading the xml text. We are currently not aware of software that reads in the uncertainty in azimuth.

For the data conversion we used routines from the Obspy-software to construct miniSEED volumes.

Acceleration data

An overview of the acceleration data obtained from the SEED files, using Obspy-scan is given in Figure 28 and shows a similar pattern as Table 7. The period 1995-2006 is dominated by ROS1-6, located outside Groningen and recording local events. After production from the Roswinkel gas field stopped, seismicity dropped quickly. Since 2006 only events in Groningen were recorded.

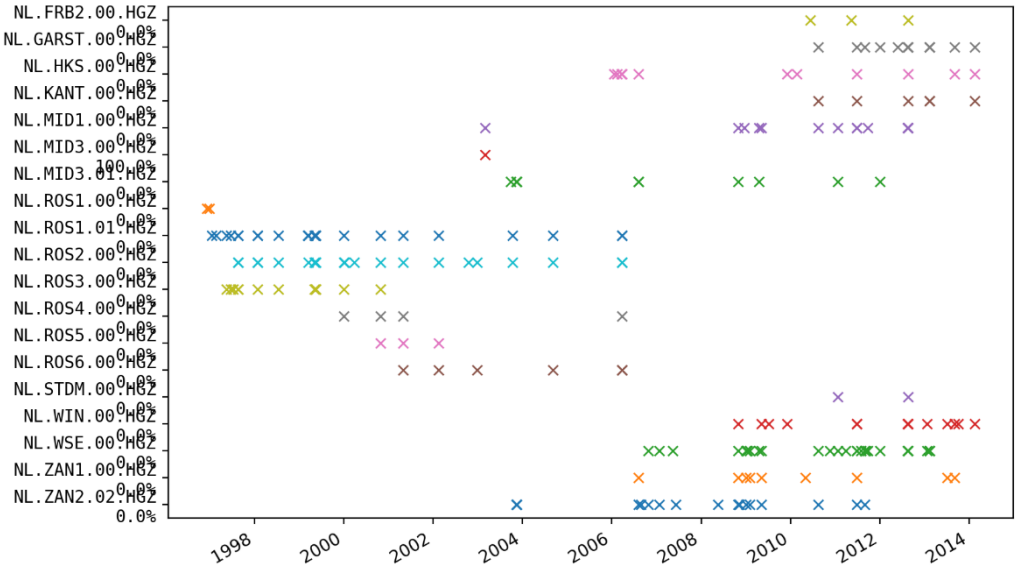

Figure 28 Overview of the total accelerometer dataset. Each record is indicated with a cross, while each station is marked with a different color

The implementation of the response information in XML is straightforward. Concerning the orientation and timing information (see Chapter 5), we think it is worthwhile to explain how the information in table 9 and Appendix A was implemented.

For the AC-23 system, all three components were multiplied with a factor -1 before analysis. The raw data are kept unchanged, so in the XML file we added 180 degrees to the orientation. For the AC-63 system the EW component was multiplied with -1, so in the XML file 180 degrees was added to the orientation of the EW component.

Information on the timing was added to the timing quality flag in the miniSEED header. For a known synchronized record we put the timing quality flag at 100%, while for the others we put the flag at 0%.

Please note that reading the flags using Obspy routine get_flag does not work correctly for SEED files containing multiple stations. Alternative is to read from blockette 1001 using tr.stats.mseed.blkt1001.timing_quality, where tr is the Trace() object corresponding to a single record. This only works if one reads the miniSEED file with option “details=True”.

Borehole data

Similar to the acceleration dataset, we display in Figure 29 an overview of the borehole dataset. In order to limit the complexity of the figure, we selected one channel only. It is clear that stations OTL, PPB and WMH, all situated in the western part of the Netherlands close to Alkmaar, recorded only a few events. This is due to the limited seismicity in the region. In addition station ZL2 was discontinued after 2001 when the string was used for experiments as explained earlier.

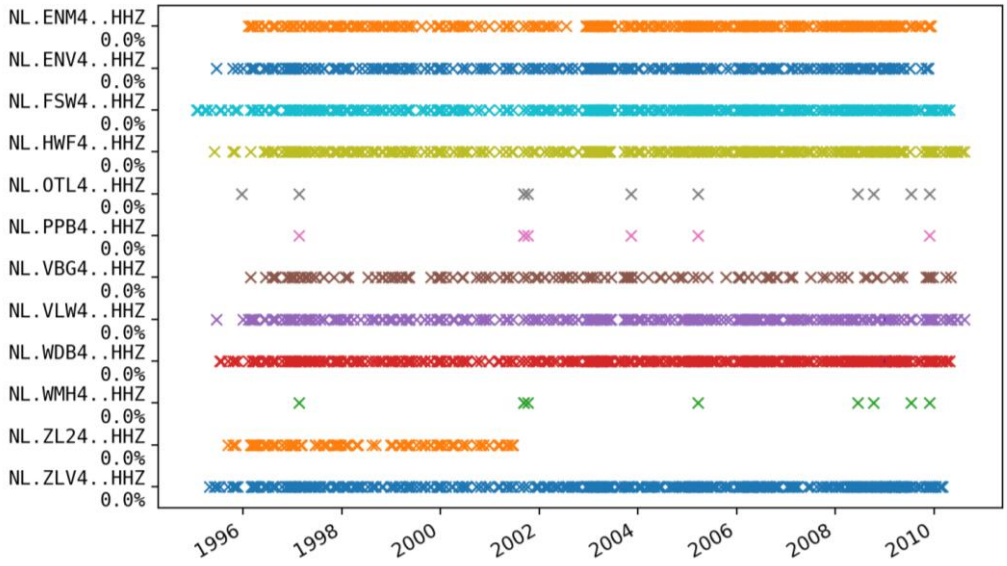

Figure 29 Overview of the total borehole dataset obtained through the Obspy-scan procedure (see Figure 28)

The borehole systems were all equipped with a DCF77 time receiver and the signal of the time receiver was recorded as a separate channel. In the SEED volumes the time mark has been included and given a channel code HY1.

In order to assure data completeness, we took the KNMI induced event catalogue and collected all existing raw data per event. In table 10 we specify the number of events and the number of miniSEED files produced. These numbers may differ and we will give an explanation why this is the case.

year	#events	#files	year	#events	#files	year	#events	#files
1995	18	18	2001	23	20	2007	32	32
1996	41	41	2002	25	25	2008	49	49
1997	42	41	2003	57	55	2009	91	80
1998	23	23	2004	31	30	2010	29	23
1999	31	31	2005	36	36		total	total
2000	26	25	2006	56	55		**610**	**584**

Table 10. A list of the number of events in the KNMI catalogue and the number of miniSEED files per year.

Out of the total number of 610 events, the borehole dataset contains recordings of 596 events. The missing 14 events can be explained by events only recorded by local accelerometers (1997-07-09 06:23, 2000-03-27 10:23 and 2004-09-06 20:31) or only in borehole ZL2 after 2002-09-18, when it was operating in an experimental set-up. During the Noordlaren swarm (from 2009-02-22 until 2009-03-22) all four events at 2009-03-12 were only recorded in ZL2. As explained earlier, these files are not available in the current dataset.

The difference between the number of files (584) and the 596 events in the database is explained by the occurrence of multiple events within a short time interval. Multiple events in one SEED volume can be found for events listed in Table 11.

Finally, for 2010 an increasing number of boreholes were transferred to continuous recording, so only a limited number of boreholes produced triggered data. After 2010-08-14 all triggered systems were converted into continuous systems.

Filename	Event origin time	ML
200104281000.mseed	2001-04-28 10:00:08.29	1.5
	2001-04-28 10:00:55.51	1.1
200110101406.mseed	2001-10-10 14:06:43.35	1.0
	2001-10-10 14:06:57.24	0.8
200112041908.mseed	2001-12-04 19:08:31.06	0.2
	2001-12-04 19:08:37.83	0.0
200603251355.mseed	2006-03-25 13:54:38.14	2.1
	2006-03-25 13:55:51.17	1.7
200903141532.mseed	2009-03-14 15:32:16.31	1.0
	2009-03-14 15:32:27.70	1.0
200903171910.mseed	2009-03-17 19:10:16.55	0.9
	2009-03-17 19:10:33.60	0.9
	2009-03-17 19:10:49.31	0.9
	2009-03-17 19:11:12.38	1.0
200903171927.mseed	2009-03-17 19:27:36.41	0.7
	2009-03-17 19:28:41.32	0.7
200903202248.mseed	2009-03-20 22:48:15.16	0.4
	2009-03-20 22:49:29.96	0.5
200903220032.mseed	2009-03-22 00:32:19.11	1.2
	2009-03-22 00:34:53.49	0.6
201005301858.mseed	2010-05-30 18:58:36.12	1.5
	2010-05-30 18:58:57.99	1.2

Table 11: Overview of files containing multiple events

5. Quality control

With respect to quality control we looked at two aspects: 1] accuracy of timing and 2] consistency of the waveform amplitudes.

5.1 Timing

All instruments are equipped with an accurate time receiver, either through a DCF-77 receiver or through a GPS receiver. The DCF is mainly used for the old boreholes, while for the instruments that were installed later, mainly GPS receivers are used.

Accelerometers:

For the AC-23/SMACH-SM2 systems, a regular synchronization of the clock was organized and marked in the recording software format ('SMR' files). Therefore, we can derive from the original data if the clock was synchronized and if not, how much time passed since the last synchronization. For the AC-63/GSR-18 system this synchronization was not kept in the software (as far as we know), so we are unable to check this from the original 'GSR' format. A list of information on time synchronization for all records is given in Appendix E. Also, in the miniSEED header data a flag is added for the timing quality. We used a factor 100 in case of a synchronization and 0 if there was clearly no synchronization or if the synchronization could not be determined. Figure 30 gives examples of event sections for synchronized and non-synchronized stations.

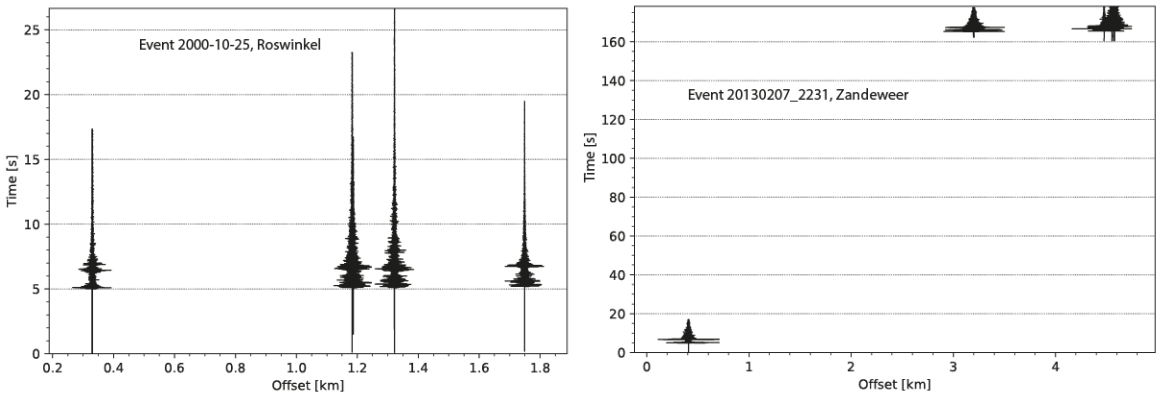

Figure 30. Examples of a full time synchronized section (left) and a section with only 1 time-synchronized station (right). In the panel on the right, the station recordings at an offset of 0.4 km are the only synchronized recordings. For each station all 3 components are plotted.

NORSAR (2021) looked in detail on timing issues for the accelerometer dataset and used QuakeML data to compare the timing of the records with theoretical times. They found in some cases differences between the calculated and observed times. Part of these differences could be explained by relocation of events for which the origin time was not yet updated. This will be done as soon as possible. Others may be caused either by a timing problem or by an inaccurate location.

Boreholes:

In an early stage the decision was made to add the timing information from the DCF receiver as a separate channel to each borehole volume (see section 3.3). NORSAR (2021) used the timing information in the HY1 channel and computed a list of timing errors (Table B14).

5.2 Amplitudes

In this section we investigate the consistency of measured amplitudes over the different networks and within individual boreholes between the elements. Due to the difference in set-up of the accelerometers and the boreholes, different techniques could be used to investigate amplitude consistency and calibration.

We collect all information we found on component malfunctioning or other known problems. For the accelerometer stations, we did look at all recordings for the determination of the orientation of the channels. For the boreholes we wrote automated procedures and over time checks were carried out.

5.2.1. Accelerometer checks

First of all a simple check was made to find out if the amplitudes are preserved in the format conversion process. In Obspy we read in the accelerometer miniSEED data, determine the maximum amplitude of the trace and compare with the raw data in SAC format. Since the output of the miniSEED data is in cm/s^2 we compared the raw SAC data in cm/s^2 with the miniSEED data before instrument correction. Please be aware that after removal of the instrument response the accelerometer data are presented in m/s^2.

The first recordings of ROS1 at the end of 1996 (December) show malfunctioning of the X (North) component. This was repaired early January 1997.

ROS6 shows significant 50 Hz electric noise at 2004-09-06 20:31 and 2006-03-25 13:55 events. The noise can be removed by application of a low pass filter. A 10 Hz low pass filter reveals useful earthquake data for the 2004 event. For the 2006-03-25 13:55 event the Y-component shows malfunctioning after filtering.

The AC-23 system was limited in resolution and it was initially not clear how large accelerations could be expected. Since the 1997 M 3.4 Roswinkel event showed large accelerations (3.04 m/s^2 at the radial component, Dost et al. 2004), the instruments were set at high saturation limits. Therefore, the noise level has been sampled poorly and this affects the recordings at small magnitude events before the P-onset. Figure 31 shows an example of poor sampling on the horizontal components.

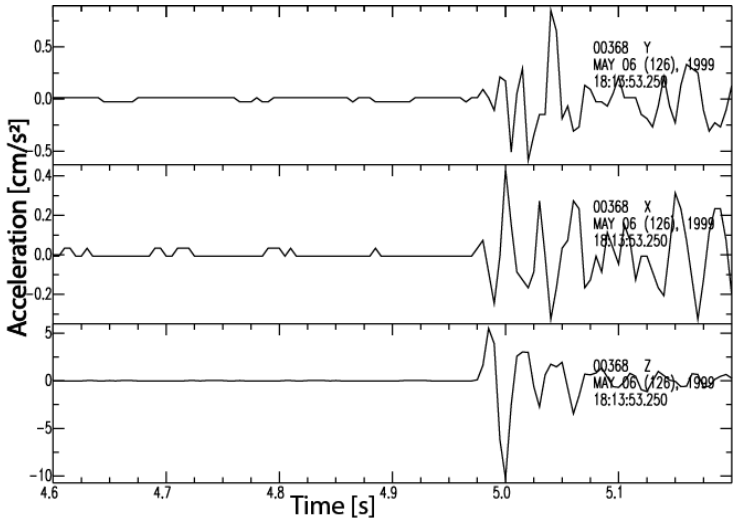

Figure 31. Accelerations recorded at station ROS3 for the 1999-05-06 M 1.4 Roswinkel event. Prior to the P-onset the noise-level on the X and Y components is sampled poorly.

Since the accelerometers discussed in this report are located at the surface and not co-located with other sensors at the same time, a comparison of amplitudes with other coexistent sensors and/or networks is not directly possible. It is possible, however, to check the consistency of amplitudes over time, through the development of the events terms. In the Groningen area, the triggered

accelerometers are coined the pre-B network. The follow-up network with continuously recording EpiSensor accelerometers is called the B network. In the following section the event-term development over these two successive networks is discussed.

5.2.2 Event terms

An earthquake leads to ground motion that can be expressed in particle displacement, velocity or acceleration. In Groningen, one is interested specifically in the largest particle velocity in the horizontal plane (PGV) as it has a correlation with damage. A ground motion prediction equation (GMPE) describes the ground-motion amplitudes at the Earth's surface as function of distance and magnitude of an event. Specifically for the Groningen gas field, an empirical GMPE has been developed that both captures the average PGV and the variability thereof (Bommer et al., 2019). This variability is subdivided in within-event and between-event variability. The within-event variability describes the variation of ground-motion amplitudes from a distance-dependent term, caused by the radiation pattern of the source, complex propagation paths and site condition. The between-event variability describes variation in average amplitude levels between different events (of the same magnitude), caused by, e.g., differences in stress drop. For each event, the average difference between measured and modeled PGV can be computed. This is called the event term.

In the development of the V6 GMM (ground-motion model) it was observed that event terms got a different character with the completion of the G-network (Fig. 19 in Bommer et al., 2019). Before 2015, event terms oscillated around 0. From 2015 and onwards, nearly all event terms were negative. This was one of the observations that prompted an in-depth investigation of the used sensors, their calibration and siting (Ntinalexis et al., 2019). Since the calibration error was found and fixed in the end of 2018 (SodM, 2021) the event terms likely oscillate again around 0 unless other issues persist. In the following we compute this distribution of event terms.

The event term is computed as described in Section 5.1 in Ruigrok and Dost (2020). We use the GMPE developed in the same reference: BMR2. This GMPE gives a good average fit to observed induced seismicity in the Netherlands. As PGV measure we use the maximum rotated value in the horizontal plane. The mean difference of the measured and modeled *ln*(PGV) are taken, where *ln* is the natural log. Thus, an event term of 0.69 would mean that the measured values are, on average, 2 times higher than the average modeled values. We use seismicity of M>=2.5 and we only compute event terms for events with more than 3 accelerometer recordings. Figure 32 shows an example of measured and modeled PGV values. In this example, the event term is 0.32, meaning that the measurements are on average 38% higher than the model.

The (pre-)B network is situated in the area where the largest events take place within the Groningen gas field. With the (pre-)B network there is mostly a good station coverage in the epicentral area until about 14 km distance. The G-network has been laid out over the entire field. For the larger earthquakes there is a good station coverage until about 30 km. In order not to obtain a biased station-distance distribution over time, we restrict the maximum offset to 14 km. For the indicated magnitude range, 20 events can be found between 2006 and 2020 with a sufficient amount of recordings within 14 km.

Figure 33 shows the event-term distribution in chronological order. The amount of events is limited to draw detailed conclusions. Yet, a few observations can be made:

- When transitioning from the pre-B network to the B-network, no difference in event-term trend can be noted. Given that the B-network stations were found to be well calibrated in earlier studies (Ntinalexis et al., 2019; SodM 2021) it is thus likely that also the pre-B network stations were well calibrated. This change from Geosig to EpiSensor instrumentation occurred mid-2013.
- When going from the (pre-)B network to the B&G-network setup, an average drop of about 0.2 can be noted. The G network became operational in addition to the B-network in 2015. Besides a vastly expanded accelerometer network, also a vastly expanded geophone network became available. Prior to 2015, magnitudes were estimated with geophones at relatively large epicentral distances. From 2015 onwards, also geophones are used that are at close range. This likely has led to (on average) a small over-estimation of the magnitude since 2015, which leads to a small over-estimation of the modeled PGVs and therewith (on average) a reduction of the event term.
- The event terms calculated for the networks have comparable values to other studies, e.g. Ktenidou et al (2018) who show average values around zero and a standard deviation of 0.32. Although hard to measure from Figure 5 in their paper, individual event terms reach up to at least twice the standard deviation.

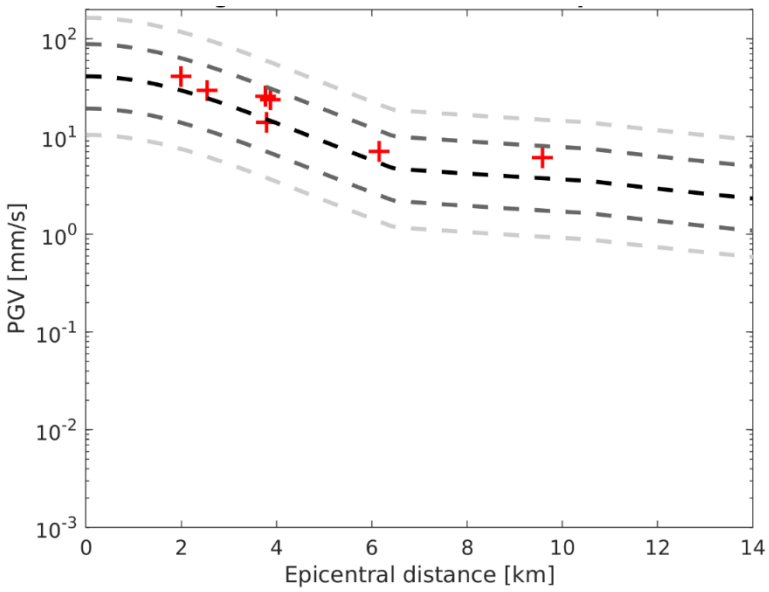

***Figure 32**: Peak ground velocity (PGV) recordings (red crosses) of the Huizinge M=3.6 event (2012-08-16, 20:30:33) in comparison with the BMR2 mean model (black dashed line), 80% confidence zone (delimited by the gray dashed lines) and the 98% confidence zone (delimited by the light-gray dashed lines).*

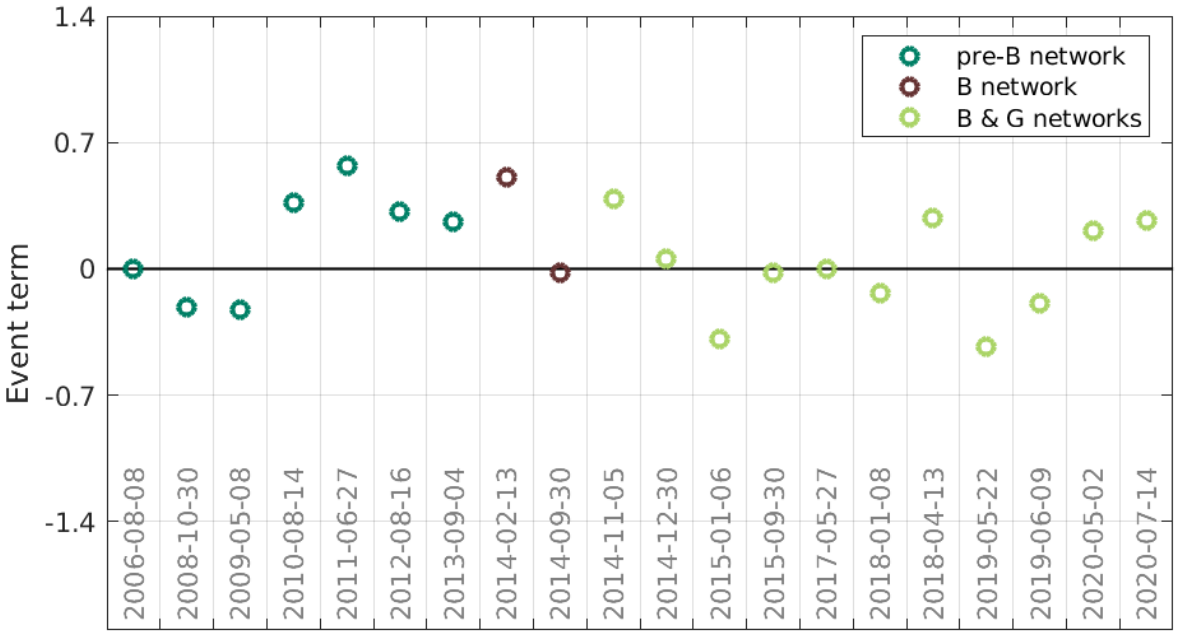

***Figure 33**: Event terms for Groningen events with magnitudes larger than 2.50 and a sufficient amount of recordings (#>3). The event terms are expressed as the mean natural log of the misfit between measurement and model. The pre-B network consists of Geosig accelerometers installed in buildings. The B-network consists of EpiSensor acccelerometeres installed in buildings. The G-network consists of EpiSensors installed in the free field.*

5.2.3 Station terms

Also for each pre-B network station, the difference in observed and modeled PGV can be computed. We call this here the station terms. These terms have a large scatter from event to event, largely due to strong fluctuations of the ground motion field in the epicentral area, caused by the radiation pattern of the source. Also, there may be some positive or negative bias due to site terms. However, on average the stations terms should be within +-0.7. If not there would be a suspicion for calibration errors. The station terms are shown in Figure 34.

There are no indications of suspicious behavior at these stations, although occasionally station terms may be larger. We looked at the largest values of the station terms for station GARST, WSE and ZAN1 and did not find disturbed records, but noted that the epicenter distance for the specific records were all between 7 and 10 km. For ZAN2 the largest value of the station term corresponds to a record at very short epicentral distance (700 m). We observe in the records a high frequency (~20 Hz) waveform package at the horizontal components, probably caused by a very local effect. The model will not explain all details.

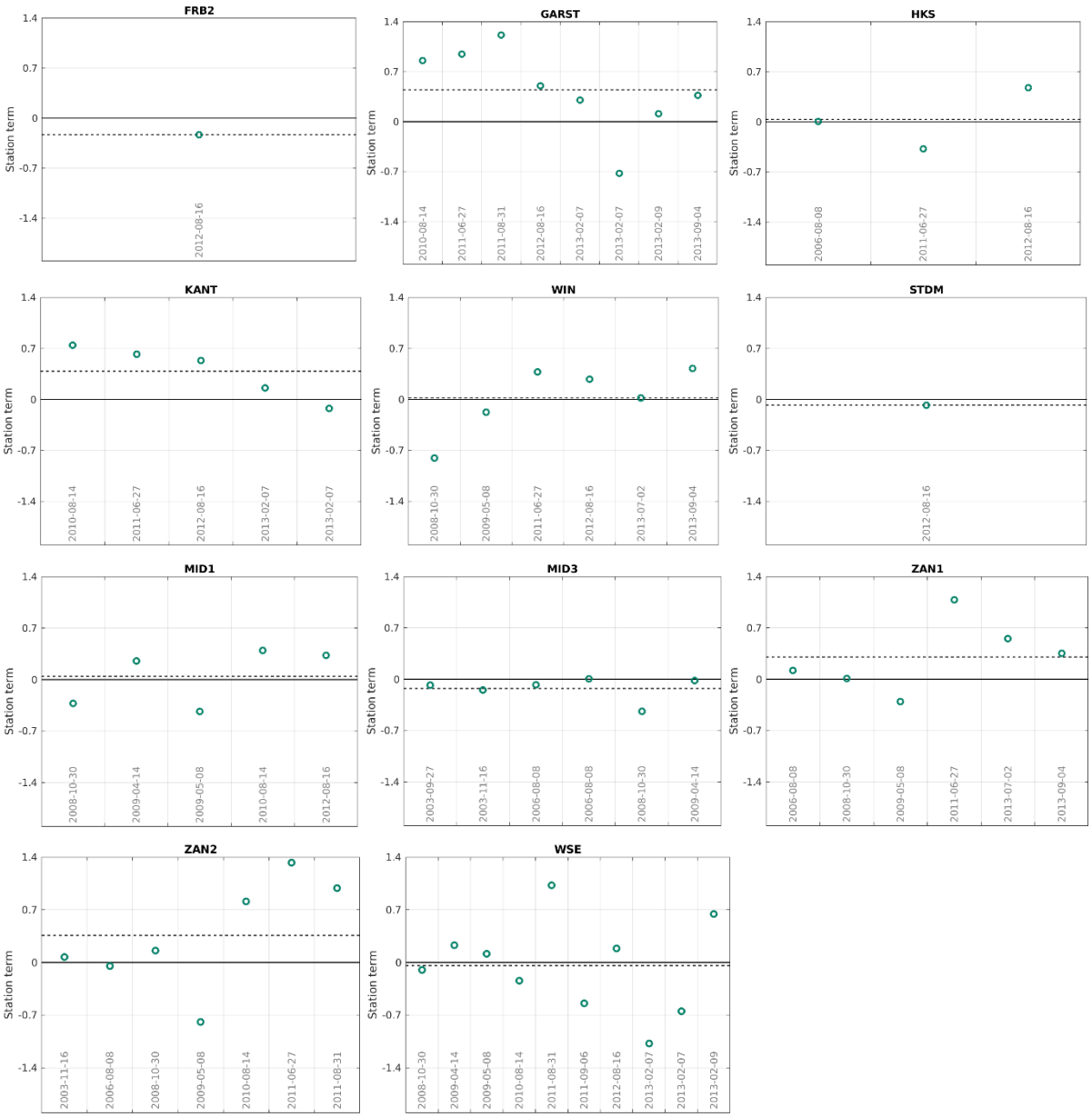

Figure 34. Station terms for Groningen events with magnitudes larger than 2.50. Averaged values are indicated by dashed lines.

5.2.4 Borehole checks

We use the amplitude in counts to quality-check the geophone channels. In Groningen, the seismic noise yields values of a few hundred counts. Hence, if the amplitude is lower than this value, this directly points to an instrumental issue. However, for larger amplitudes also significant instrumental issues may exist. To find a more complete overview of instrument malfunctioning, we normalize with the average amplitude recorded over the borehole, for a certain component. This proves to be effective, as it is very unlikely that geophones at different depth levels concurrently have the same defect. Figures 35-46 show the relative amplitudes per borehole, for all the different channels other than the surface channels. The surface channels are in practice so noisy, they disturb the results for the deeper levels. The analysis is performed on the raw data (in counts) without any frequency filtering applied.

The horizontal components HG1 and HG2 have been used without a rotation to N and E. The reason for this choice is that it allows us to identify which component was malfunctioning.

For the interpretation of the figures there are a few aspects that are important to take in mind:

- The Y-axis in the figures denotes the relative amplitude. A relative amplitude of 1 means that the maximum amplitudes recorded at a specific depth level and component, is precisely the same as the mean over the maximum amplitudes recorded over all depth levels.
- For interpretation we put a dashed line on 40% (0.4) of the mean amplitude over the borehole. When a channel reaches lower values, caution needs to be taken.
- At, or near, the Earth's surface, amplitudes are naturally higher due to amplification and the free-surface effect. Hence, values lower than about 80% can raise caution.
- For small magnitude events, high seismic noise levels at the upper geophone can push the relative amplitudes down at lower levels. Hence, if concurrently high relative amplitudes are found at the upper geophone, and low levels at the other geophones, likely there is no instrumental issue. To identify these 'noise peaks' the scale of the top geophone is from 0 to 4, whereas it is from 0 to 2 at the other geophones.
- A channel degradation can be seen as a trend over time, of either the mean or the variance. For this dataset, no algorithm has been implemented to detect such degradation automatically.
- Amplifier issues (due to lightning) were often quickly resolved and lead then only to a few cases of very low relative amplitudes.

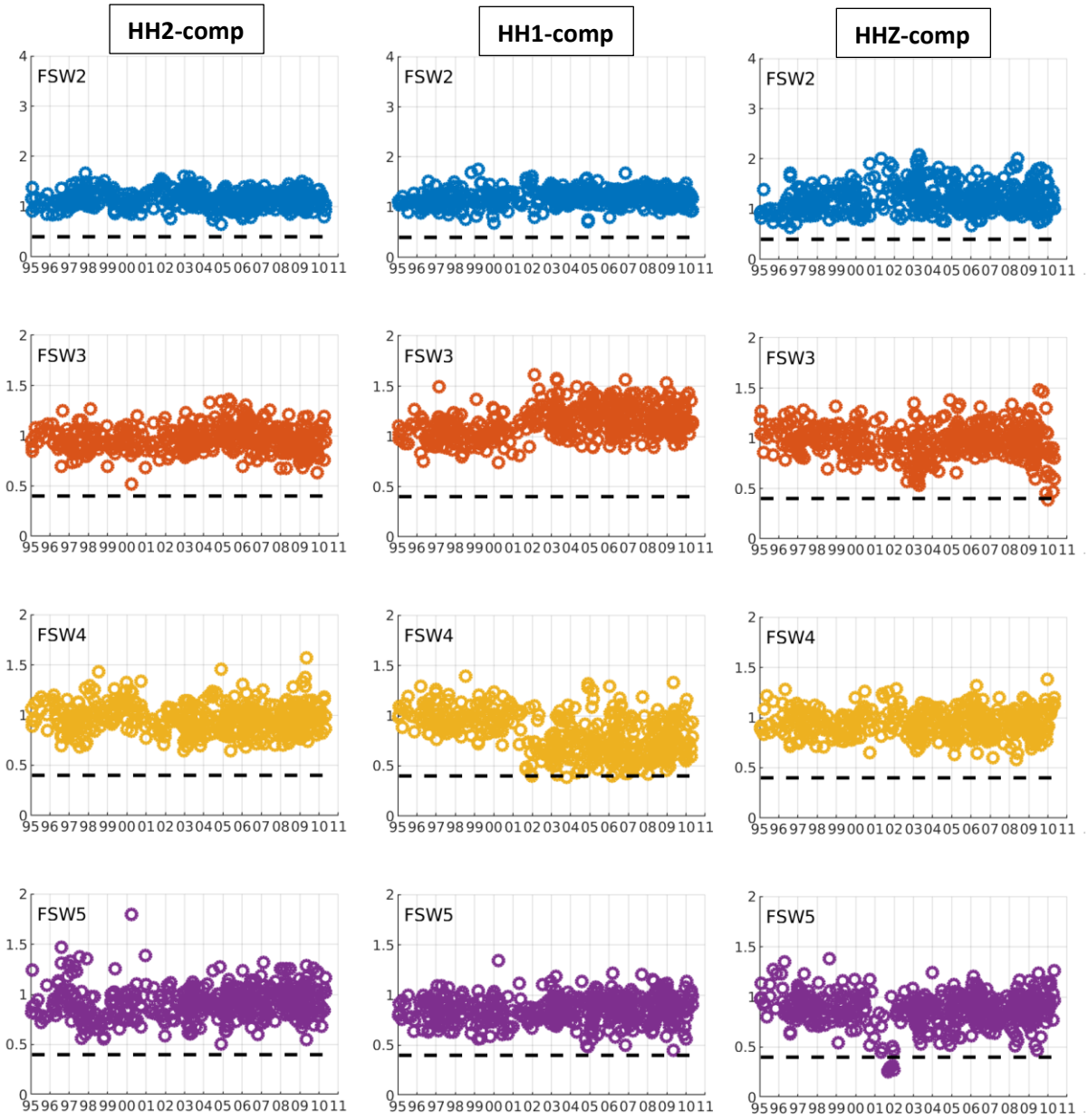

Figure 35. Maximum absolute amplitude values of individual borehole channels for station FSW, normalized with respect to the average maximum absolute amplitude of this channel recorded over all borehole levels.

For FSW a trend can be seen for the HH1 component, showing an increase in amplitude at FSW3 and a corresponding decrease at FSW4. This change occurred around mid-2001. Furthermore, an amplitude drop is observed at FSW5.HHZ for 2001. Early 2002 this was repaired.

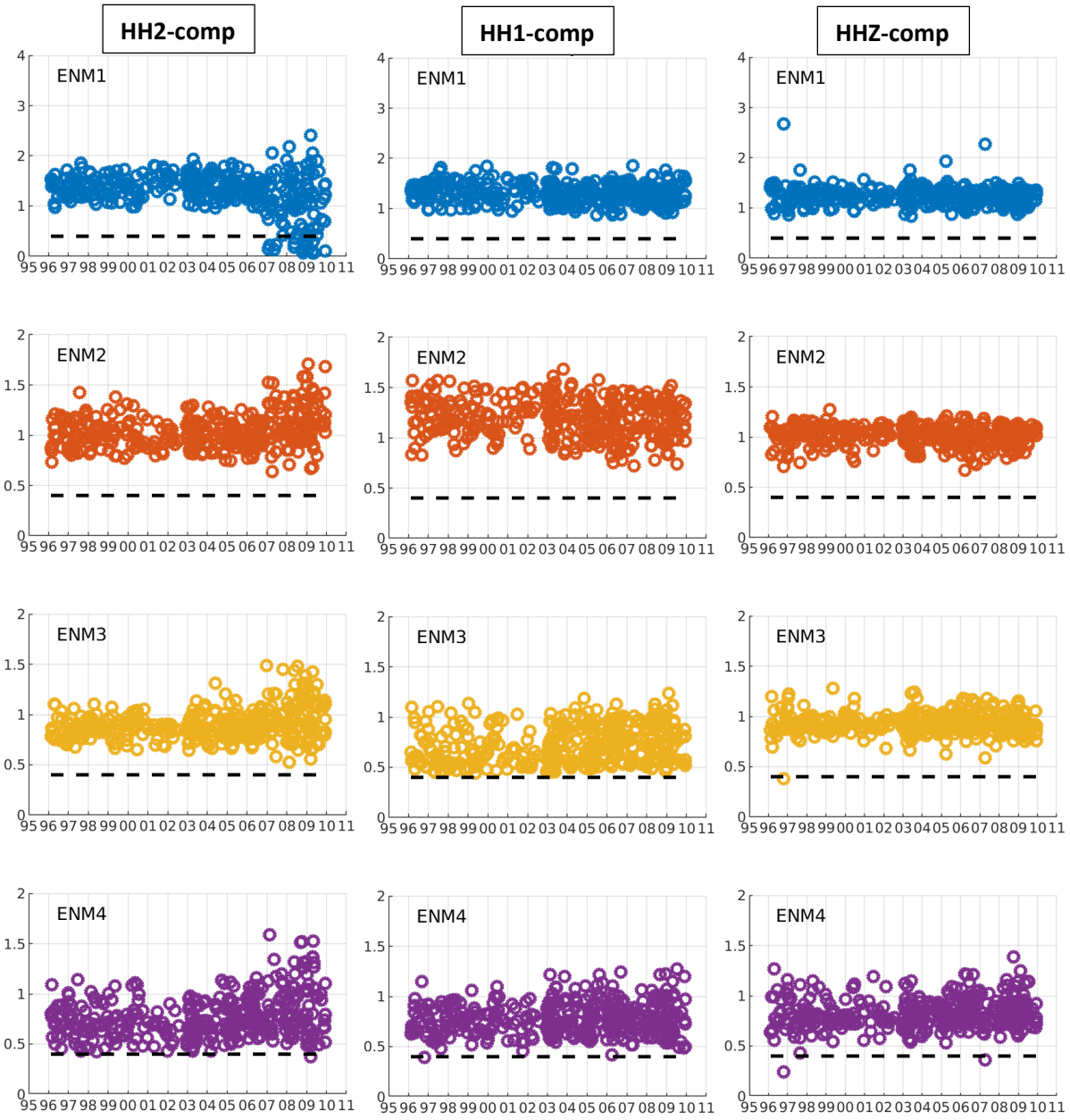

Figure 36. Maximum absolute amplitude values of individual borehole channels for station ENM, normalized with respect to the average maximum absolute amplitude of this channel recorded over all borehole levels.

ENM1.HH2 shows a larger variance from 2007. This could be due to an instrumental degradation or the addition of a (strong) noise source near the sensor. For event 1996-10-16, ENM4.HHZ drops below 0.4 due to high noise on ENM1.HHZ.

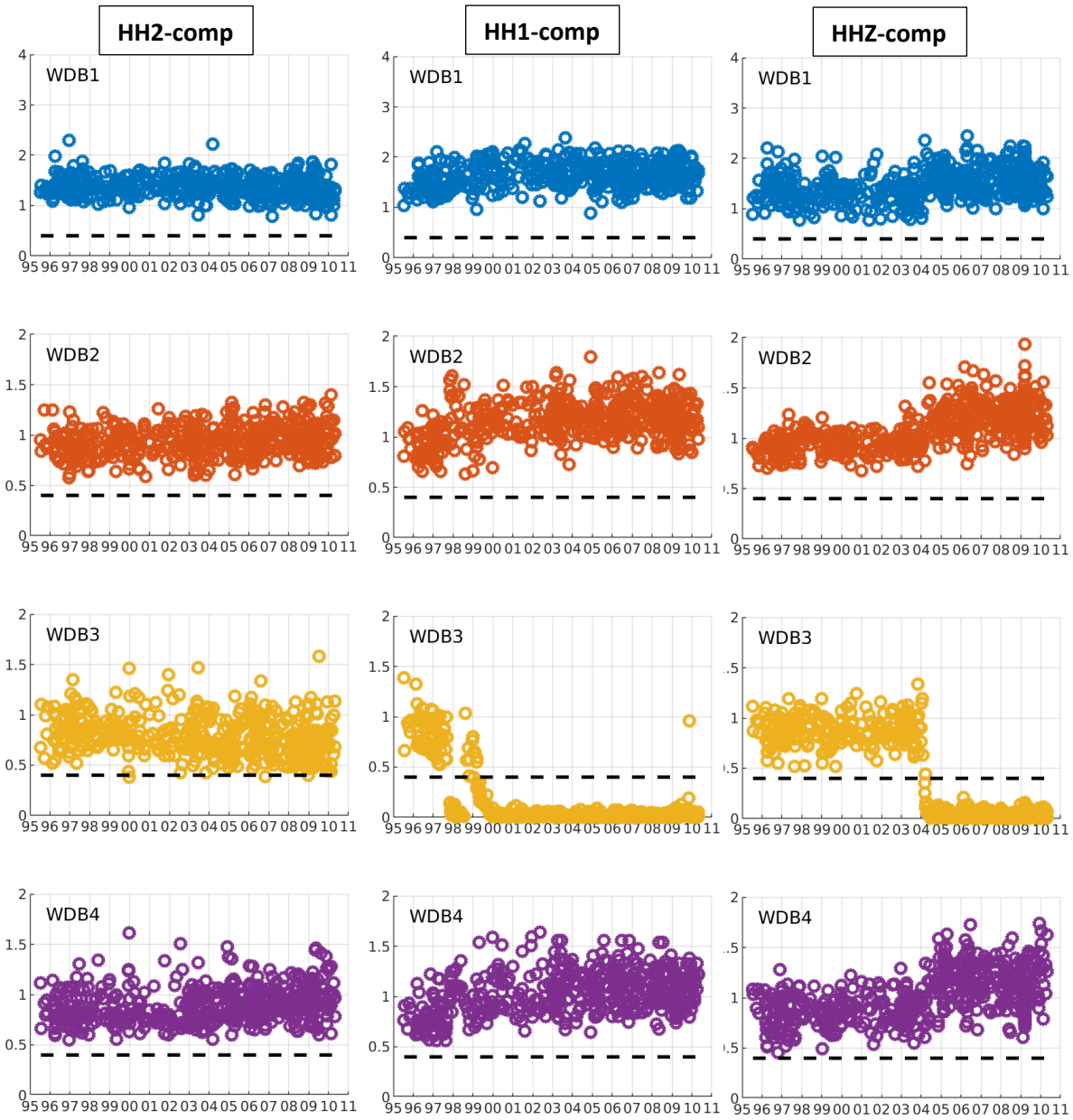

Figure 37. Maximum absolute amplitude values of individual borehole channels for station WDB, normalized with respect to the average maximum absolute amplitude of this channel recorded over all borehole levels.

From the end of 1997 onward, WDB3.HH1 experienced problems. The sensor was revived several times, but this was only temporarily successful. Also in the installation notes (Appendix F) WDB3.HH1 was reported as malfunctioning over time. This channel should not be used for amplitude-sensitive processing.

WDB3.HHZ shows a large decay in amplitude for event 2004-03-07. Likely, the amplifier got broken. This channel is not be used for this event and onwards.

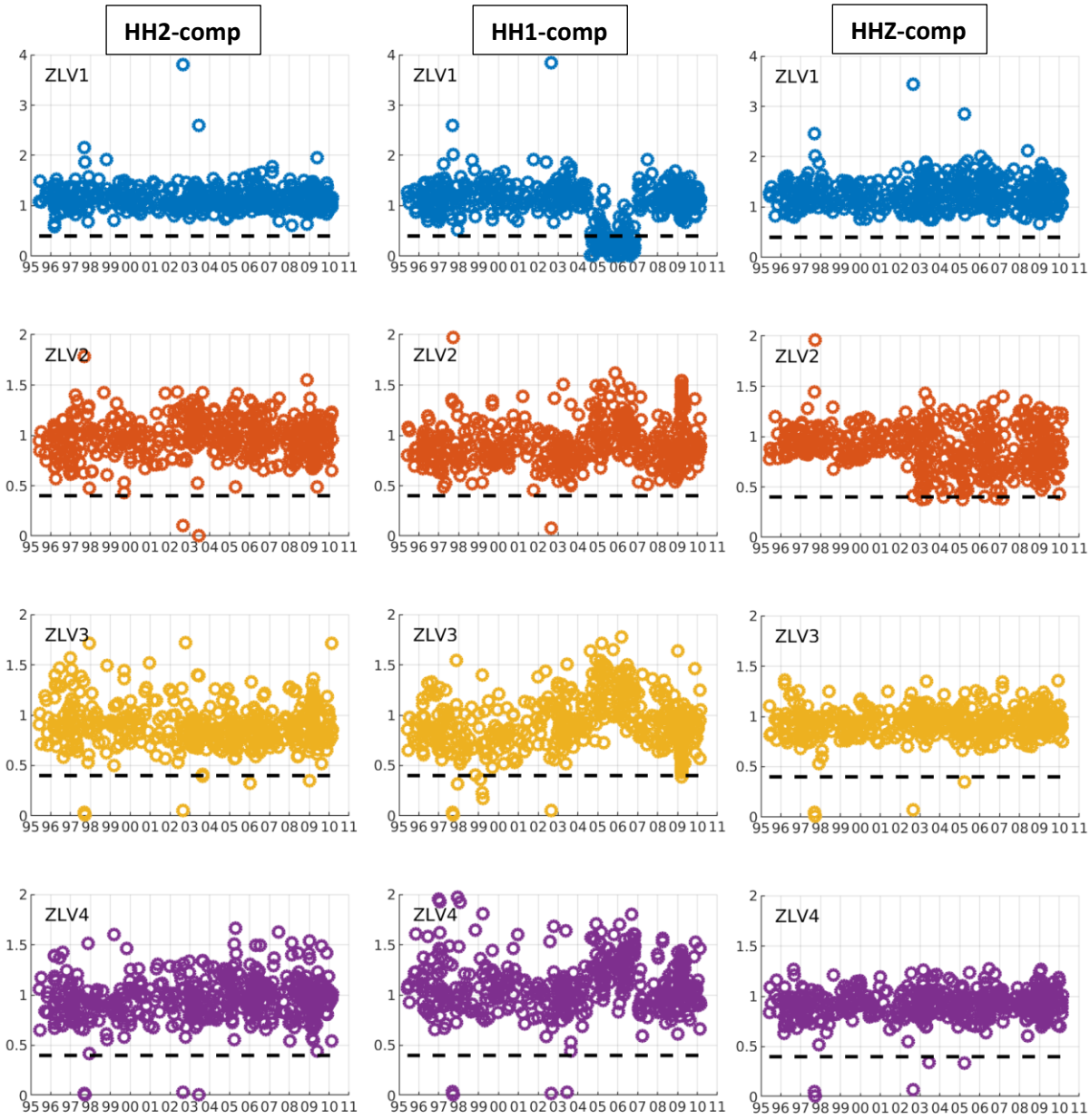

Figure 38. Maximum absolute amplitude values of individual borehole channels for station ZLV, normalized with respect to the average maximum absolute amplitude of this channel recorded over all borehole levels.

ZLV1.HH1 shows low relative amplitudes between halfway 2004 and the end of 2006. ZLV2.HHZ shows a larger variance from the end of 2002 and onwards. Also at ZLV1.HHZ there is concurrently a more subtle increase in variance.

For events 1997-09-13, 1997-09-14, 2002-08-29 and 2003-06-16 there is no good data for some of the channels. The pertaining channels can be identified in the figure. The installation notes (Appendix F) indicate damaged amplifiers at 1997-09-18 for levels 0,3 and 4. In addition damaged amplifiers are reported on 1999-09-22, 2001-08-03, 2002-10-18, 2003-07-10 and 2004-07-29.

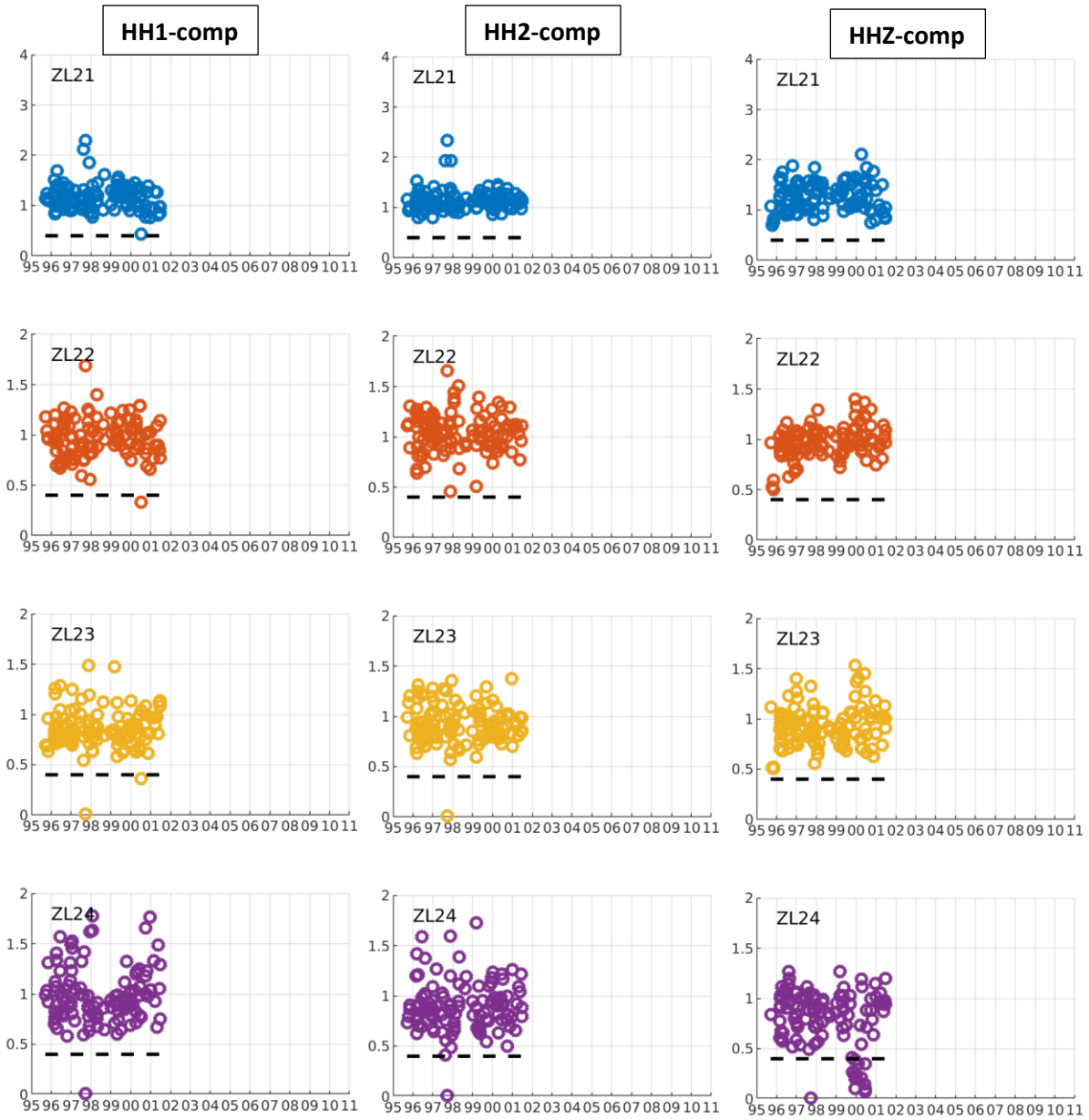

Figure 39. Maximum absolute amplitude values of individual borehole channels for station ZL2, normalized with respect to the average maximum absolute amplitude of this channel recorded over all borehole levels.

For event 1997-09-14 there is defective data on a few channels of ZL23 and ZL24. ZL24.HHZ shows an episode of defective data between the end of 1999 and halfway 2000. There are many reports on damaged amplifiers in this time period (Appendix F). There is no triggered data beyond 2001.

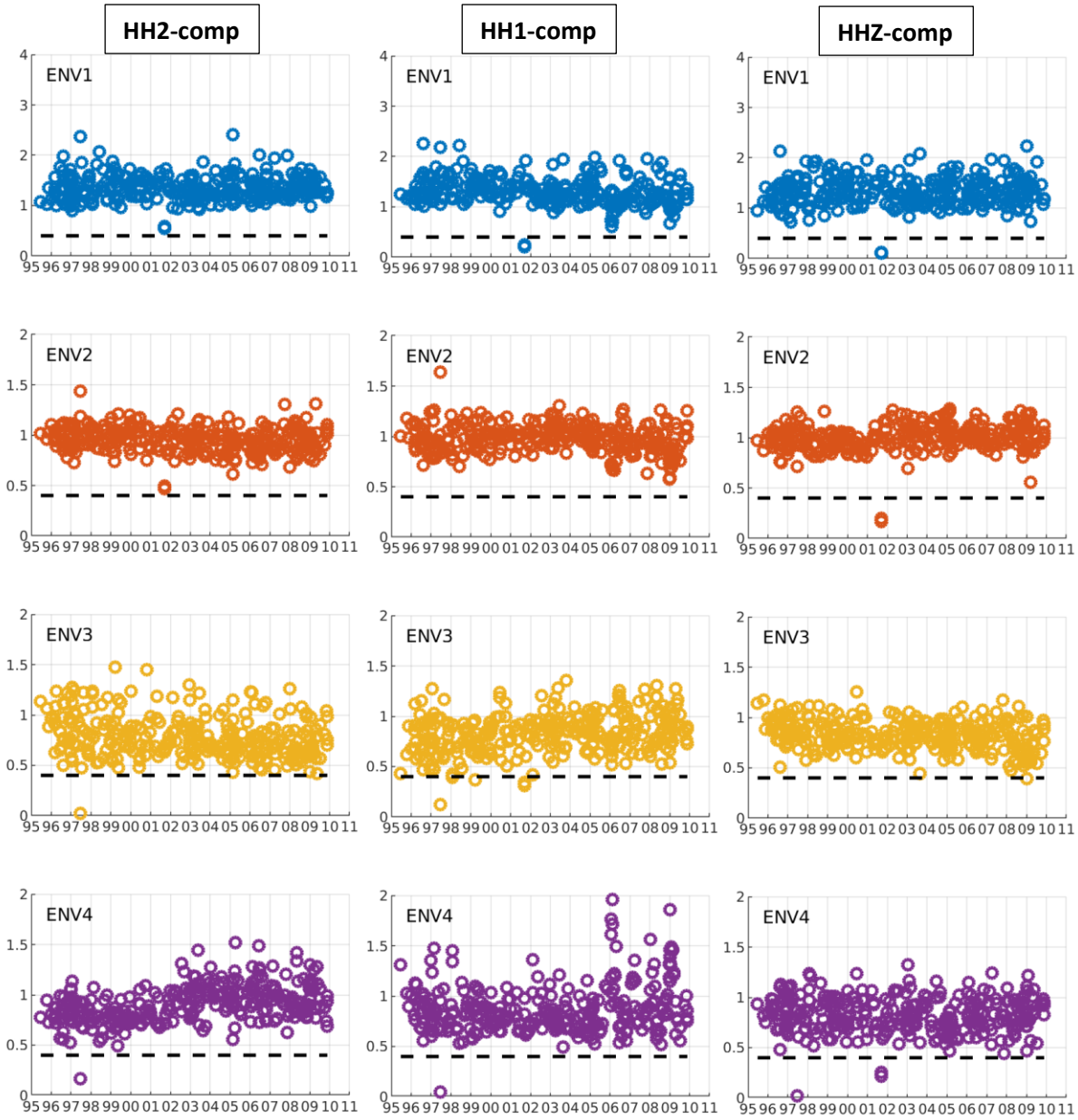

Figure 40. Maximum absolute amplitude values of individual borehole channels for station ENV, normalized with respect to the average maximum absolute amplitude of this channel recorded over all borehole level.

For event 1997-06-20 channels ENV4.HH{1,2,Z} and ENV3.HH{1,2} are broken (see Appendix F). All amplifiers were replaced at 1997-07-10.

For event 2001-09-09 and 2001-09-10 only channels ENV4.HH{1,2} and ENV3.HHZ have good data. This was caused by lightning, all components were found damaged at 2001-08-08 and were replaced at 2001-09-18.

For the third event on 2009-03-17 (at 04:38:27 UTC) channel ENV4.HHZ (likely) has a spurious peak. Moreover, there are events with suspiciously high amplitudes (>1.5) on the horizontal components of ENV2 and ENV4.

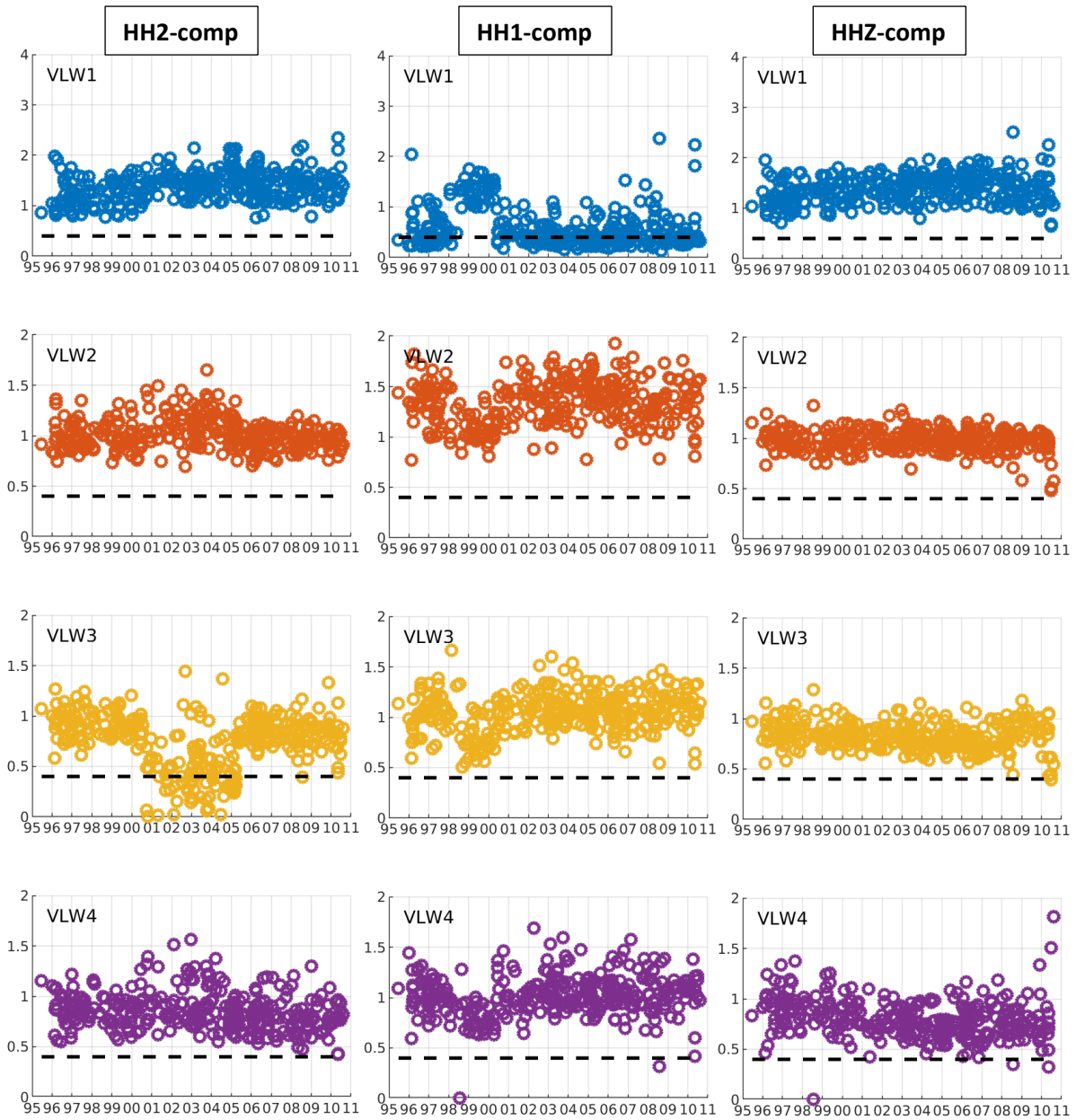

Figure 41. Maximum absolute amplitude values of individual borehole channels for station VLW, normalized with respect to the average maximum absolute amplitude of this channel recorded over all borehole level.

VLW1.HH1 has (for a geophone component close to the surface) too small amplitudes until the beginning of 1998, and again from the beginning of 2000 and onwards. In the installation notes (Appendix F) a problem on component VLW1.HH1 was reported (1996-03-22). The sensor was revived at 1998-07-24. After mid-2000 amplitudes dropped again and the channel should not be used.

For event 1998-07-14 channels VLW4.HH2 and VLW4.HHZ have a broken amplifier, as visible through very low relative amplitudes.

From the beginning of 2000 until halfway 2005 likely VLW3.HH2 has too low amplitudes.

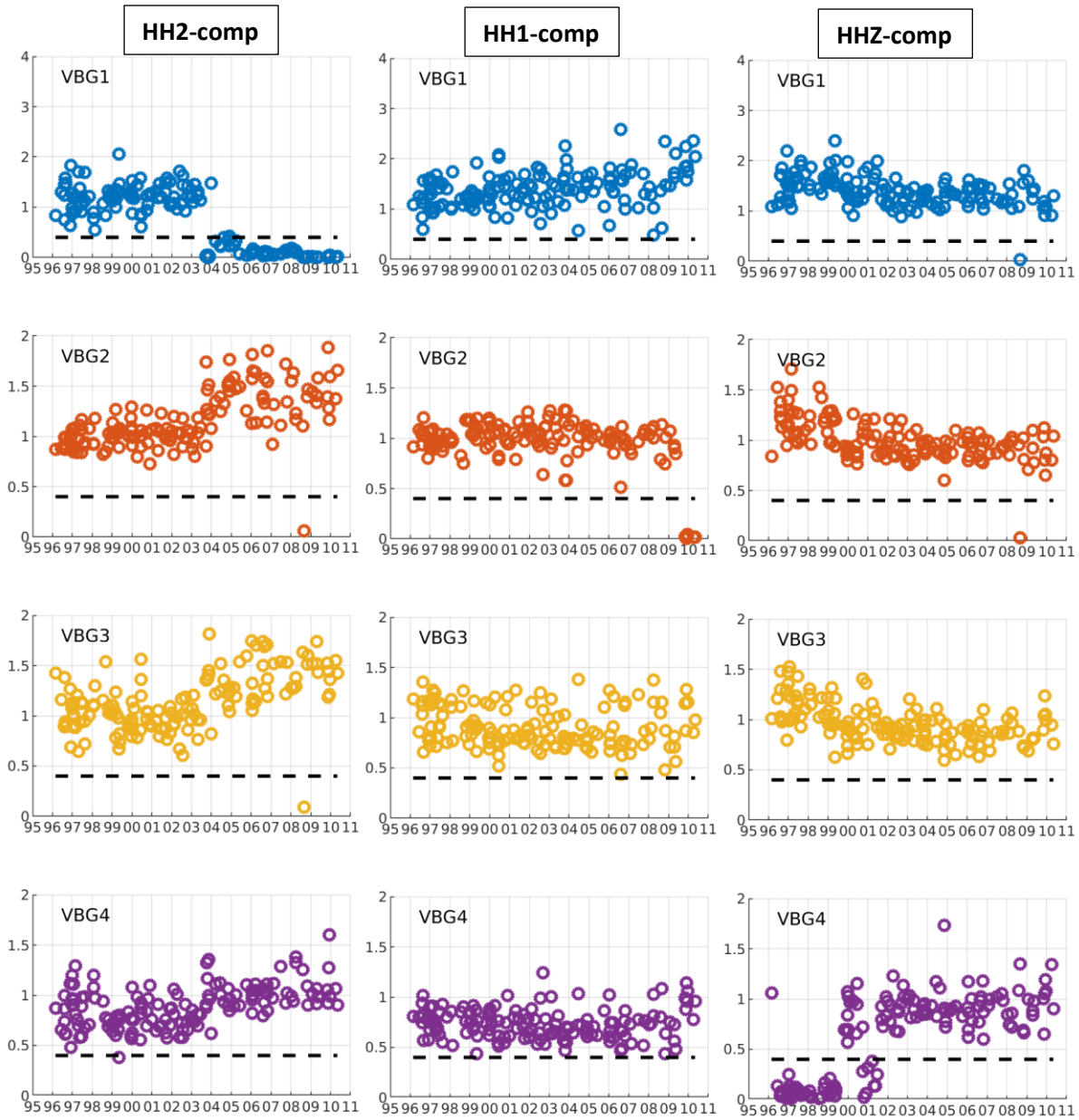

Figure 42. Maximum absolute amplitude values of individual borehole channels for station VBG, normalized with respect to the average maximum absolute amplitude of this channel recorded over all borehole level.

VBG1.HHE shows very low relative amplitudes from halfway 2003 and onwards. VBG2.HH1 shows low relative amplitudes from the end of 2009. Inspection of the records showed a broken VBG2.HH1 component for the period from May 2009 onward.

VBG4.HHZ shows low relative amplitudes from its second recorded event in 1996 until the end of 1999. This is confirmed in the installation notes (Appendix F). There is another episode of low amplitudes for the same component between the end of 2000 and halfway 2001.

For the 2008-08-26 event, VBG4.HH1 has high spurious amplitudes (at 3.79, outside of the scale). The amplitudes at the other depth levels are fine. For the same event, there are spurious amplitudes on VBG3.HHZ and VBG4.HHZ. For event 2004-10-30, VBG4.HHZ has defective data. For 2008-2010 often damaged amplifiers have been reported in the installation notes.

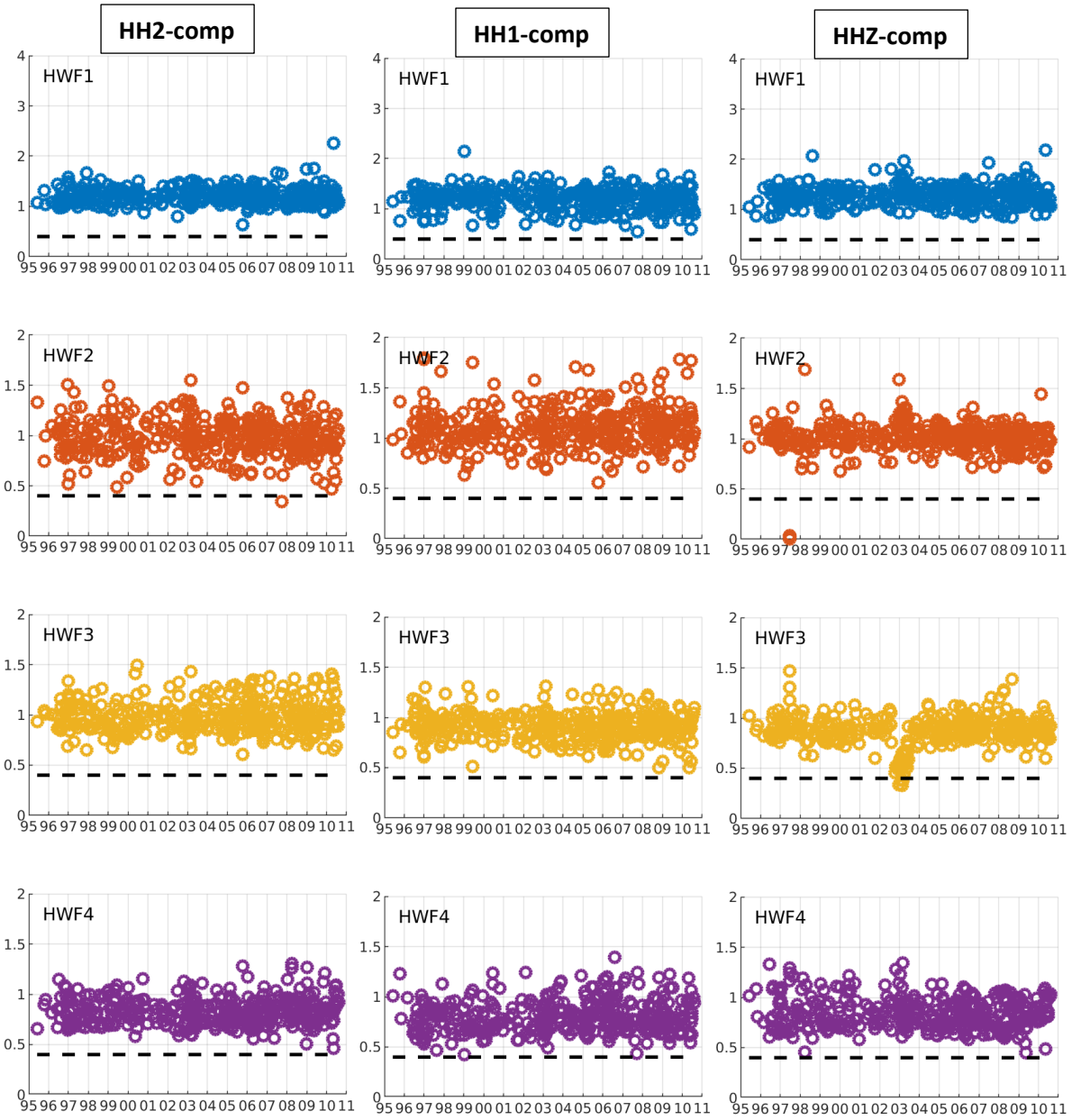

Figure 43. Maximum absolute amplitude values of individual borehole channels for station HWF, normalized with respect to the average maximum absolute amplitude of this channel recorded over all borehole level.

HWF2.HHZ has low relative amplitudes for events 1997-06-20 and 1997-06-21. This is confirmed by a report in the installation notes on a broken HWF2.HHZ component, which is reproduced in Appendix F. This channel was revived on 1997-07-10. Channel HWF3.HHZ shows low relative amplitudes between the end of 2002 and halfway 2003.

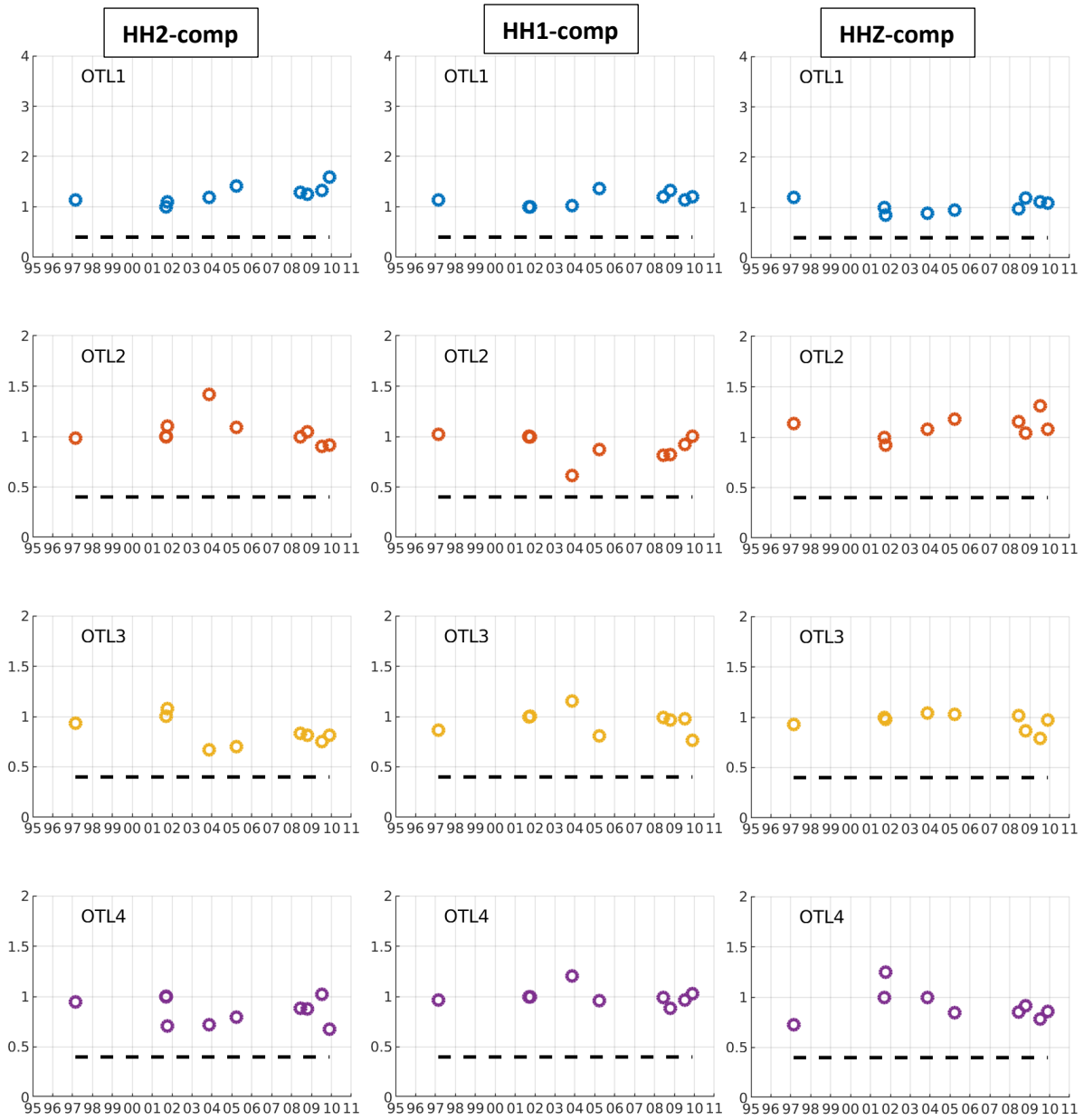

Figure 44. Maximum absolute amplitude values of individual borehole channels for station OTL, normalized with respect to the average maximum absolute amplitude of this channel recorded over all borehole level.

Borehole OTL and the following two boreholes (PPB and WMH) are situated in the northwest of the Netherlands, near the city of Alkmaar. The gas fields in this area produced much less seismicity than in the Groningen area (Figure 2) where all previously discussed boreholes are located.

At borehole OTL there is no sign of channel malfunctioning for any of the channels.

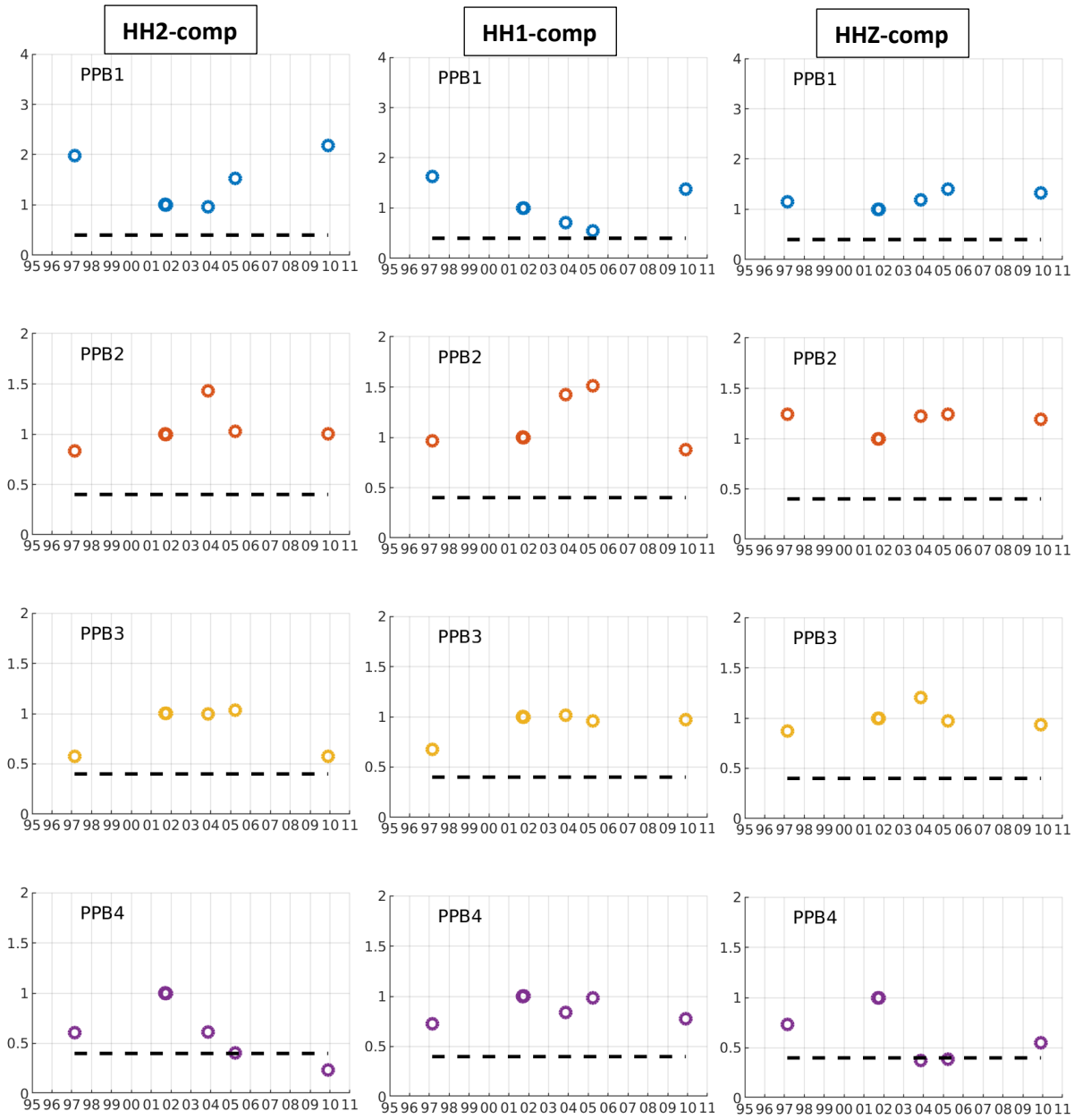

Figure 45. Maximum absolute amplitude values of individual borehole channels for station PPB, normalized with respect to the average maximum absolute amplitude of this channel recorded over all borehole level.

PPB4.HHZ has too low amplitudes for events 2003-11-10 and the second event in the catalog on 2005-03-21 (at 23:21:19 UTC).

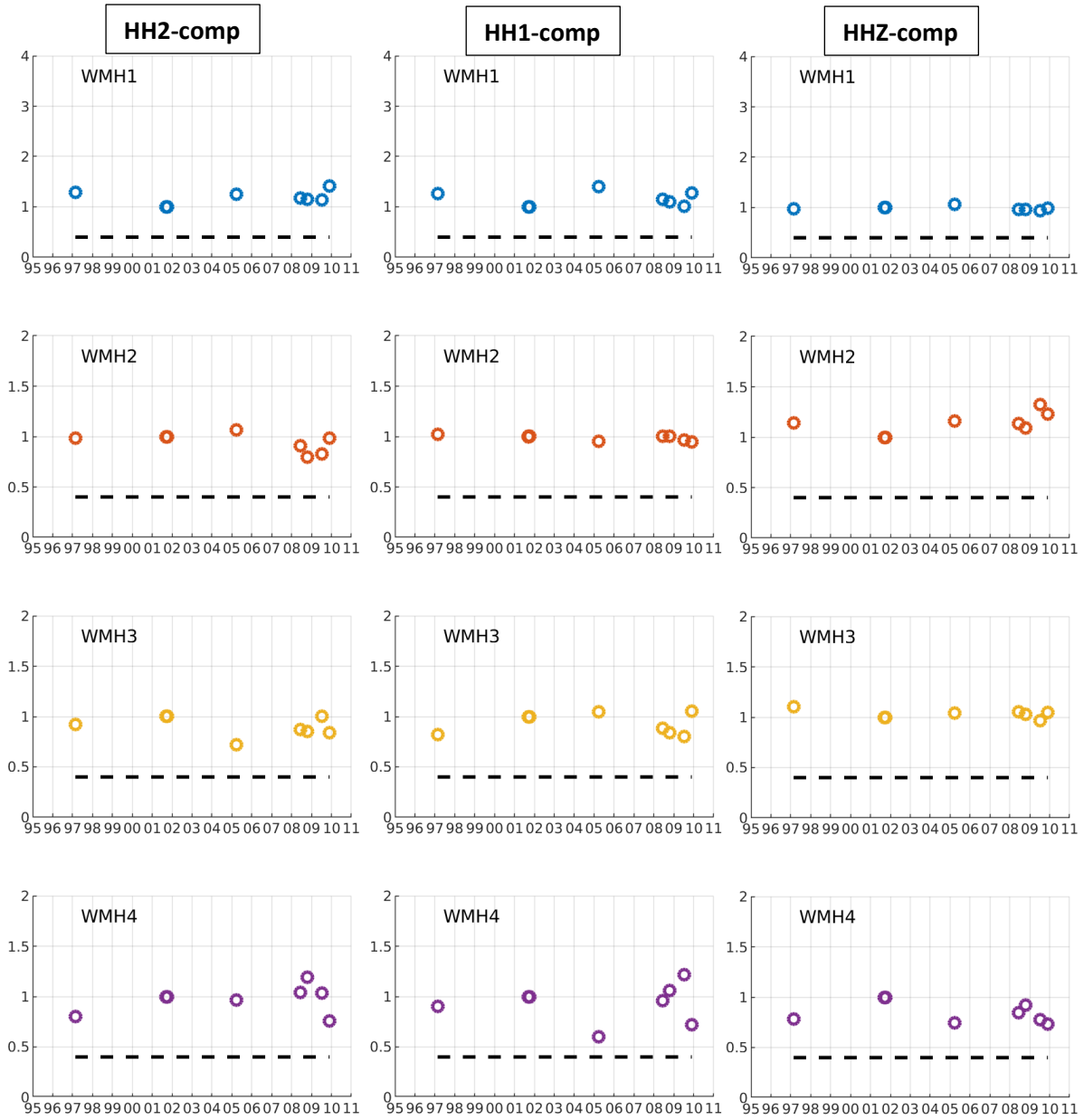

Figure 46. Maximum absolute amplitude values of individual borehole channels for station PPB, normalized with respect to the average maximum absolute amplitude of this channel recorded over all borehole level.

At borehole WMH there is no sign of channel malfunctioning for any of the channels.

An overview of the results from the amplitude analysis described in this chapter is presented in Appendix G in the form of tables and corresponding Figures.

Saturation

In addition to the component degradation, we also looked at the saturation of the components. In Table 12-15 we list the stations and components where we detected a saturation of the waveform records. This does not imply that the records should not be used, but that caution should be taken in case of automatic processing, since for these events somewhere in the waveforms saturation has been detected.

The saturation of the borehole recordings happens for large magnitude earthquakes (M>2.5) and short epicentral distances, but could also occur for lower magnitude events located almost underneath the station.

		HWF0			HWF1			HWF2			HWF3			HWF4	
date	HH1	HH2	HHZ	HH1	HH2	HHZ	HH1	HH2	HHZ	HH1	HH2	HHZ	HH1	HH2	HHZ
2005-10-12	x	x						x							
2006-08-08	x	x													
		VLW0			VLW1			VLW2			VLW3			VLW4	
date	HH1	HH2	HHZ	HH1	HH2	HHZ	HH1	HH2	HHZ	HH1	HH2	HHZ	HH1	HH2	HHZ
1997-02-19				x	x	x	x		x	x	x	x	x	x	x
1998-07-14				x	x	x	x	x		x	x			x	
1999-12-31	x	x	x					x							
2000-10-25	x	x	x	x			x	x						x	
		FSW1			FSW2			FSW3			FSW4			FSW5	
date	HH1	HH2	HHZ	HH1	HH2	HHZ	HH1	HH2	HHZ	HH1	HH2	HHZ	HH1	HH2	HHZ
1998-08-24	x														
2003-10-24	x	x													
2003-11-10		x													
2006-08-08	x	x	x	x	x		x			x	x			x	
2009-04-16	x	x													
		ENM1			ENM2			ENM3			ENM4				
date	HH1	HH2	HHZ	HH1	HH2	HHZ	HH1	HH2	HHZ	HH1	HH2				
2003-11-16								x							
2006-08-08	x	x	x	x	x	x	x	x	x	x	x				
2008-10-30	x		x	x	x		x	x		x	x				
2009-05-08				x											
		ENV1			ENV2			ENV3			ENV4				
date	HH1	HH2	HHZ	HH1	HH2	HHZ	HH1	HH2	HHZ	HH1	HH2	HHZ			
2000-10-25	x				x										
2004-06-21	x	x		x	x		x	x		x	x				
2005-10-12		x													

Table 12. Overview of event/station pairs for which saturation of the recorded signal has been detected. Saturated components are marked with an 'x'. Results for stations HWF, VLW, FSW, ENM and ENV are shown.

		ZLV0			ZLV1			ZLV2			ZLV3			ZLV4	
date	HH1	HH2	HHZ	HH1	HH2	HHZ	HH1	HH2	HHZ	HH1	HH2	HHZ	HH1	HH2	HHZ
1996-06-07			x												
1997-06-21	x	x	x	x	x	x	x	x	x		x	x	x	x	x
2000-09-22	x	x	x	x	x	x	x	x	x	x	x	x	x	x	x
2002-04-14	x	x		x	x		x	x			x		x	x	
2003-10-24		x	x												
2004-06-21	x														
2006-01-10	x														
2006-08-08	x		x					x					x		
2007-02-17			x		x										
2008-01-05	x												x		
2008-04-02	x														
2008-04-22	x				x		x				x		x		
		ZL21			ZL22			ZL23			ZL24				
date	HH1	HH2	HHZ	HH1	HH2	HHZ	HH1	HH2	HHZ	HH1	HH2	HHZ			
1997-06-21	x	x	x	x	x	x		x	x		x	x			
2000-09-22	x	x	x	x	x	x	x	x	x	x	x	x			

Table 13. Overview of event/station pairs for which saturation of the recorded signal has been detected. Saturated components are marked with an 'x'. Results for stations ZLV and ZL2 are shown.

		OTL1			OTL2			OTL3			OTL4				
date	HH1	HH2	HHZ	HH1	HH2	HHZ	HH1	HH2	HHZ	HH1	HH2	HHZ			
2001-09-09	x	x	x	x	x	x	x	x	x	x	x	x			
2001-09-10	x	x	x	x	x	x	x	x	x	x	x	x			
2001-10-10	x	x			x		x			x					
		PPB0			PPB1			PPB2			PPB3			PPB4	
date	HH1	HH2	HHZ	HH1	HH2	HHZ	HH1	HH2	HHZ	HH1	HH2	HHZ	HH1	HH2	HHZ
2001-09-09	x	x	x	x	x	x	x	x	x	x	x	x	x	x	x
2001-09-10	x	x	x	x	x	x	x	x	x	x	x	x	x	x	x
2001-10-10	x	x	x	x	x	x	x	x	x	x	x	x	x	x	x
		WMH1			WMH2			WMH3			WMH4				
date	HH1	HH2	HHZ	HH1	HH2	HHZ	HH1	HH2	HHZ	HH1	HH2	HHZ			
2001-09-09	x	x	x	x	x	x	x	x	x	x	x	x			
2001-09-10	x	x	x	x	x	x	x	x	x	x	x	x			
2001-10-10		x	x	x	x	x	x	x	x	x		x			

Table 14. Overview of event/station pairs for which saturation of the recorded signal has been detected. Saturated components are marked with an 'x'. Results for stations OTL, PPB and WMH are shown.

		WDB0			WDB1			WDB2			WDB3			WDB4	
date	HH1	HH2	HHZ	HH1	HH2	HHZ	HH1	HH2	HHZ	HH1	HH2	HHZ	HH1	HH2	HHZ
2000-06-12	x	x													
2000-06-15	x	x	x												
2002-02-05	x														
2003-04-06			x												
2003-09-27		x													
2003-10-24	x	x	x	x	x	x	x	x	x		x	x	x		x
2003-11-10	x	x	x	x	x	x		x	x		x		x		
2003-11-16	x	x													
2004-01-12	x	x	x		x										
2005-02-18	x														
2005-08-05	x	x													
2005-11-11			x												
2006-01-23	x	x	x												
2006-03-23	x	x													
2006-08-08	x	x	x	x	x	x	x	x	x		x		x	x	x
2007-02-17	x	x	x	x	x	x	x	x	x		x		x	x	x
2007-03-30	x														
2007-04-13	x														
2007-09-30	x	x	x												
2008-01-24	x														
2008-10-30	x	x	x	x	x	x	x	x	x		x		x	x	x
2009-05-08	x	x	x		x		x				x				
2010-03-31				x	x	x			x				x	x	x

Table 15. Overview of event/station pairs for which saturation of the recorded signal has been detected. Saturated components are marked with an 'x'. Results for station WDB are shown.

6. Conclusions

This report contains information on the process of converting historical triggered datasets of the KNMI into a standard modern exchange format. We followed the conventions of the real-time collected data streams at the KNMI, so these datasets can be integrated and made publicly available through the same interfaces, i.e. through a web interface[1] or through webservices[2]. The data are therefore converted from local formats to SEED. Meta-data was evaluated and in case essential information was not yet available, this was added. Especially for the accelerometer dataset the orientation of the sensors was not accurately known and was calculated based on well located events. For both the boreholes and the accelerometers consistency of the polarization of the sensors was investigated and compared to other networks. Two methods were used to investigate waveform amplitude variations. For the boreholes a new and efficient way was found to show malfunctioning of components and possible degradation of the instrumentation over time. For the accelerometers the question was if there is a difference over time in amplitude behavior. This was investigated by evaluating event terms and comparing these with values for the real-time continuous recordings of the upgraded stations after 2014.

[1] http://rdsa.knmi.nl/dataportal/

[2] Using http://rdsa.knmi.nl/fdsnws (see https://www.knmi.nl/kennis-en-datacentrum/dataset/seismische-en-akoestische-data-tools)

Appendix A. XML file example

In this Appendix we show a part of the XML file for borehole station ENM to demonstrate how the response information specified in chapter 3.1 is captured. We show the response for channel HH2 and highlight the different stages: Stage 1 describes the sensor including filters, followed by a description of the datalogger in stage 2.

```
<Channel code="HH2" startDate="1995-04-12T00:00:00" endDate="2010-01-22T00:00:00"
restrictedStatus="open" locationCode="">
    <Latitude>53.4064</Latitude>
    <Longitude>6.4817</Longitude>
    <Elevation>1</Elevation>
    <Depth>50</Depth>
    <Azimuth>212</Azimuth>
    <Dip>0</Dip>
    <SampleRate>120</SampleRate>
    <SampleRateRatio>
     <NumberSamples>120</NumberSamples>
     <NumberSeconds>1</NumberSeconds>
    </SampleRateRatio>
    <StorageFormat>MSEED</StorageFormat>
    <ClockDrift>0</ClockDrift>
    <Sensor resourceId="Sensor#20160317085422.98106.24">
     <Type>SM6</Type>
     <Description>SM6</Description>
     <Model>SM6</Model>
    </Sensor>
    <DataLogger resourceId="Datalogger#20160317085422.980413.19">
     <Description>ENM1.1995.102.HH2</Description>
    </DataLogger>
    <Response>
     <InstrumentSensitivity>
      <Value>429723000</Value>
      <Frequency>10</Frequency>
      <InputUnits>
       <Name>M/S</Name>
      </InputUnits>
      <OutputUnits>
       <Name>COUNTS</Name>
      </OutputUnits>
     </InstrumentSensitivity>
     <Stage number="1">
      <PolesZeros  resourceId="ResponsePAZ#20160317085422.981127.25" name="ENM1.1995.102.HE">
       <InputUnits>
        <Name>M/S</Name>
       </InputUnits>
       <OutputUnits>
        <Name>V</Name>
       </OutputUnits>
       <PzTransferFunctionType>LAPLACE (RADIANS/SECOND)</PzTransferFunctionType>
       <NormalizationFactor>7.981400148e+17</NormalizationFactor>
       <NormalizationFrequency>10</NormalizationFrequency>
       <Pole number="0">
        <Real>-19.99</Real>
        <Imaginary>19.996</Imaginary>
       </Pole>
```

```
        …….. other poles and zeroes …….

      </PolesZeros>
      <StageGain>
        <Value>131141.13</Value>
        <Frequency>10</Frequency>
      </StageGain>
    </Stage>
    <Stage number="2">
      <Coefficients>
        <InputUnits>
          <Name>V</Name>
        </InputUnits>
        <OutputUnits>
          <Name>COUNTS</Name>
        </OutputUnits>
        <CfTransferFunctionType>DIGITAL</CfTransferFunctionType>
      </Coefficients>
      <Decimation>
        <InputSampleRate>120</InputSampleRate>
        <Factor>1</Factor>
        <Offset>0</Offset>
        <Delay>0</Delay>
        <Correction>0</Correction>
      </Decimation>
      <StageGain>
        <Value>3276.8</Value>
        <Frequency>0</Frequency>
      </StageGain>
    </Stage>
  </Response>
</Channel>
```

Appendix B. Polarisation of the Z-component of all borehole levels

In this Appendix we show additional plots of Z-component borehole recordings for teleseismic events, similar to Figure 12.

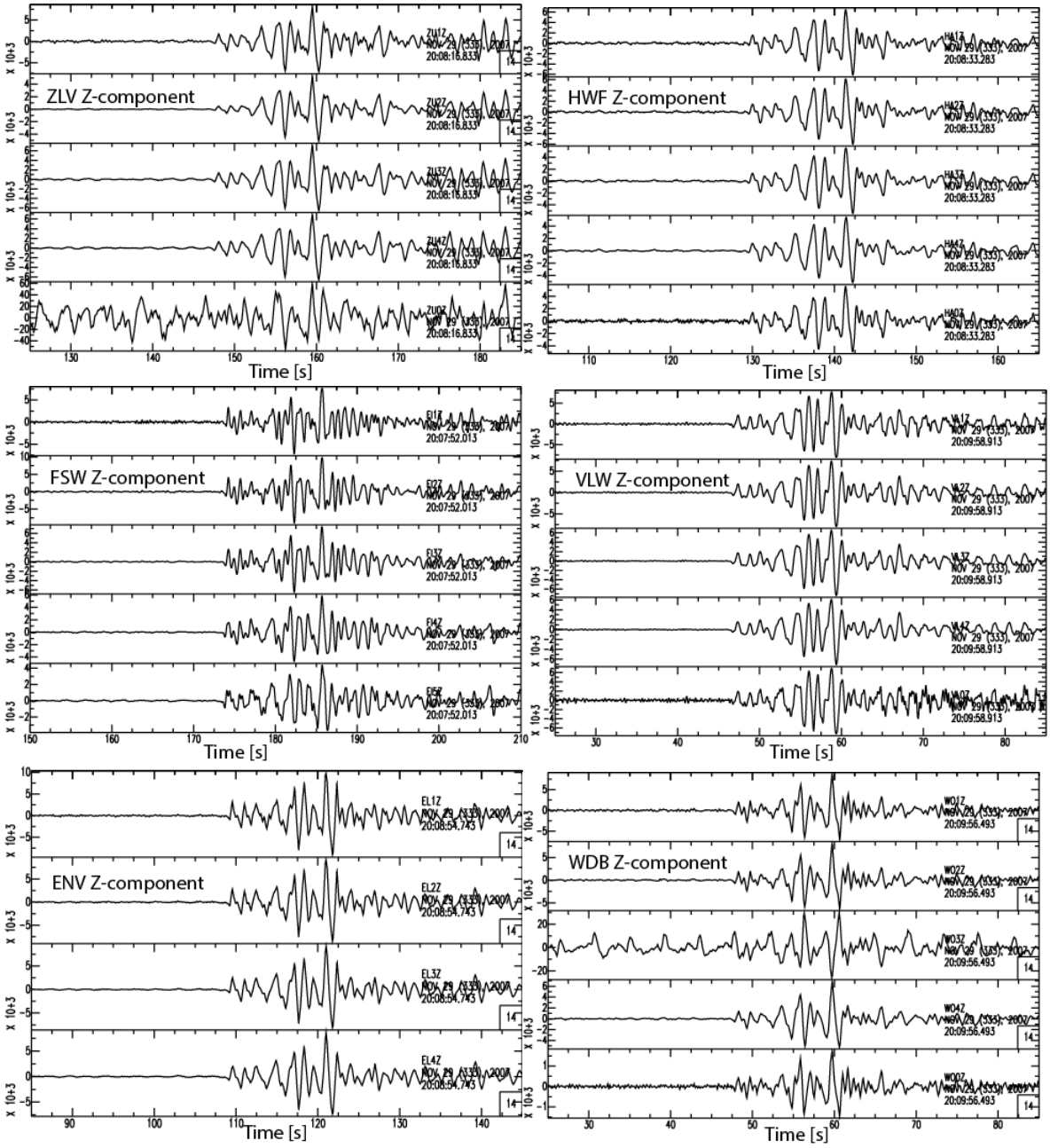

Figure B1. See Figure 12, now for the 156 km deep, 2007-11-29 M7.4 Martinique event.

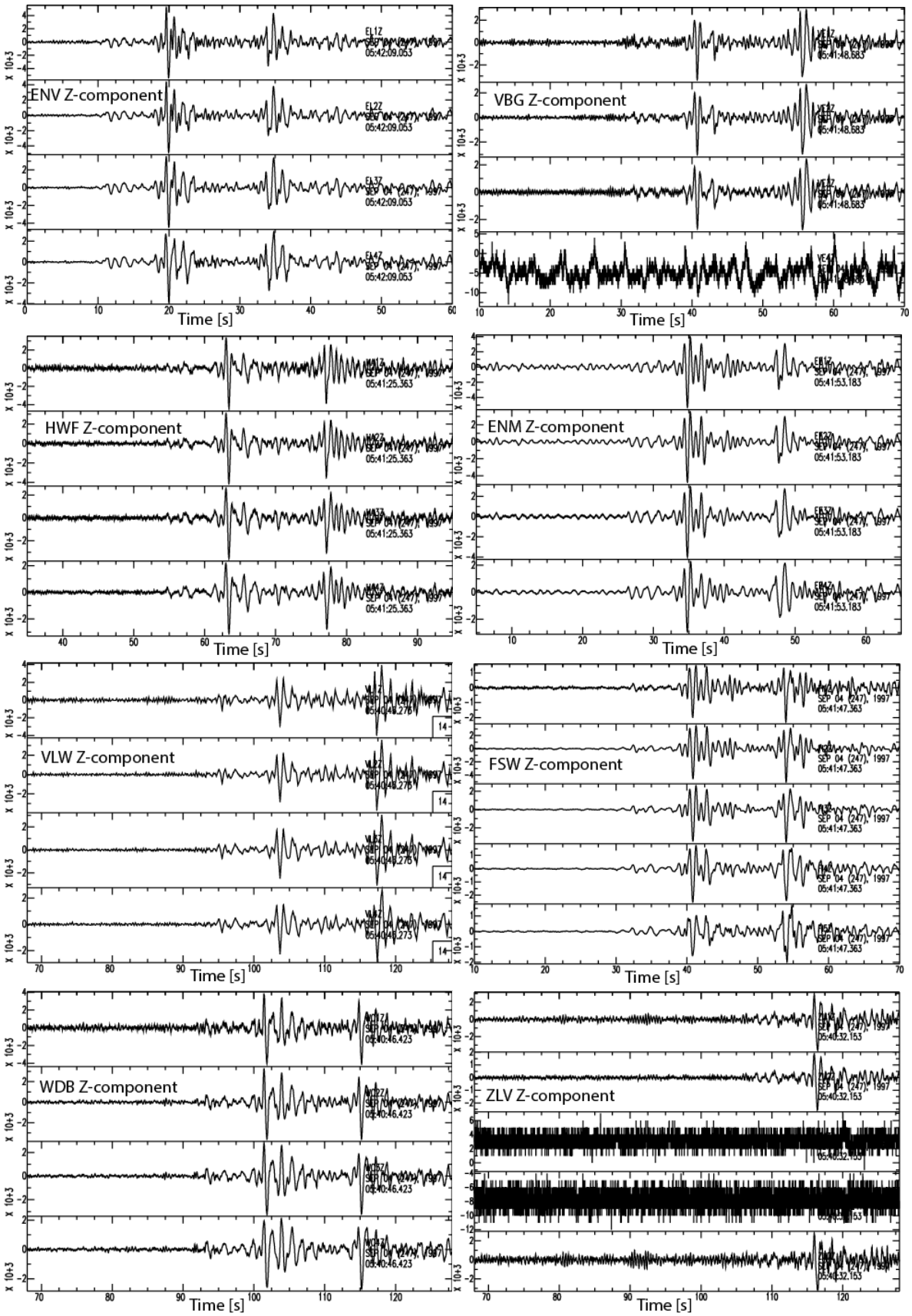
ENV Z-component
VBG Z-component
HWF Z-component
ENM Z-component
VLW Z-component
FSW Z-component
WDB Z-component
ZLV Z-component
Time [s]

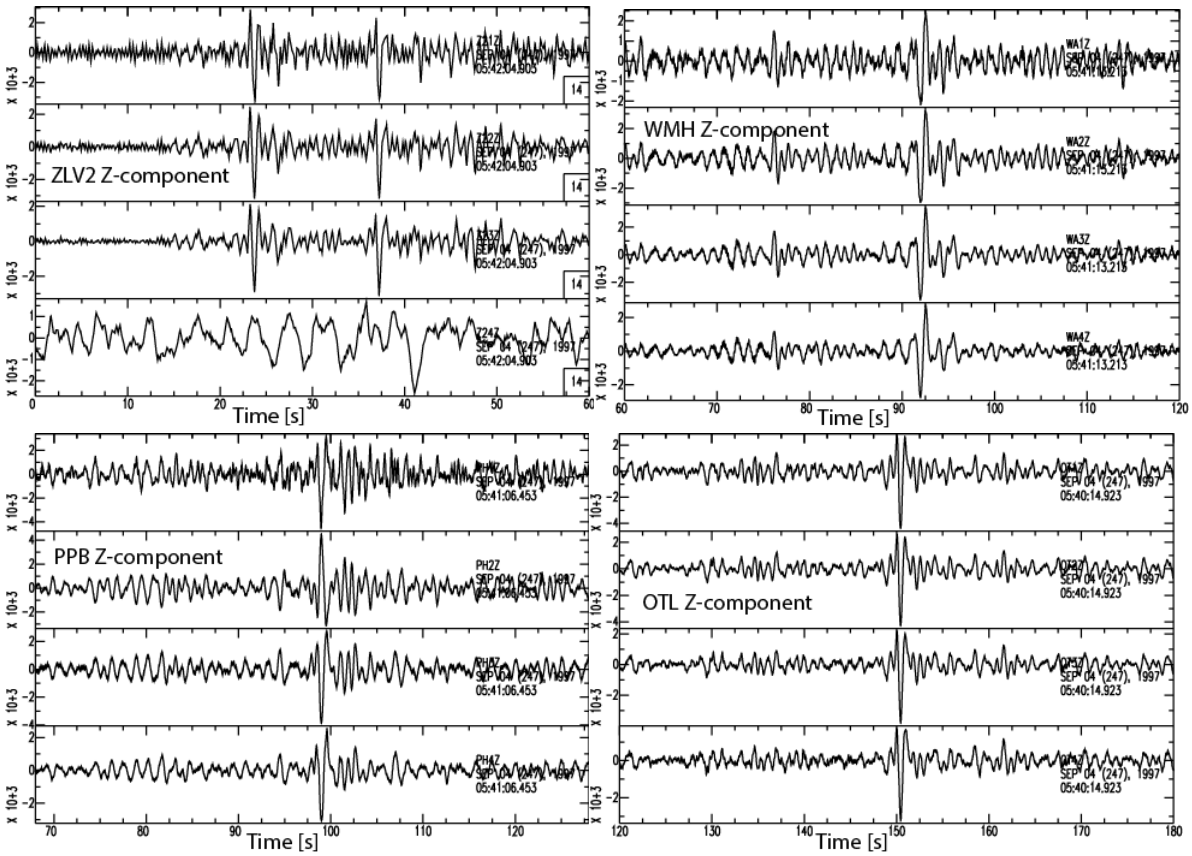

Figure B2. See Figure 12, now for the 625 km deep, 1997-09-04 M6.8 Fiji event.

Appendix C. Overview of borehole station channels after rotation

In this Appendix an overview is given of the rotated channels of each borehole, similar to Figure 23. Channel orientations listed in Table 9 are used for rotation. Figure 23 has not been repeated.

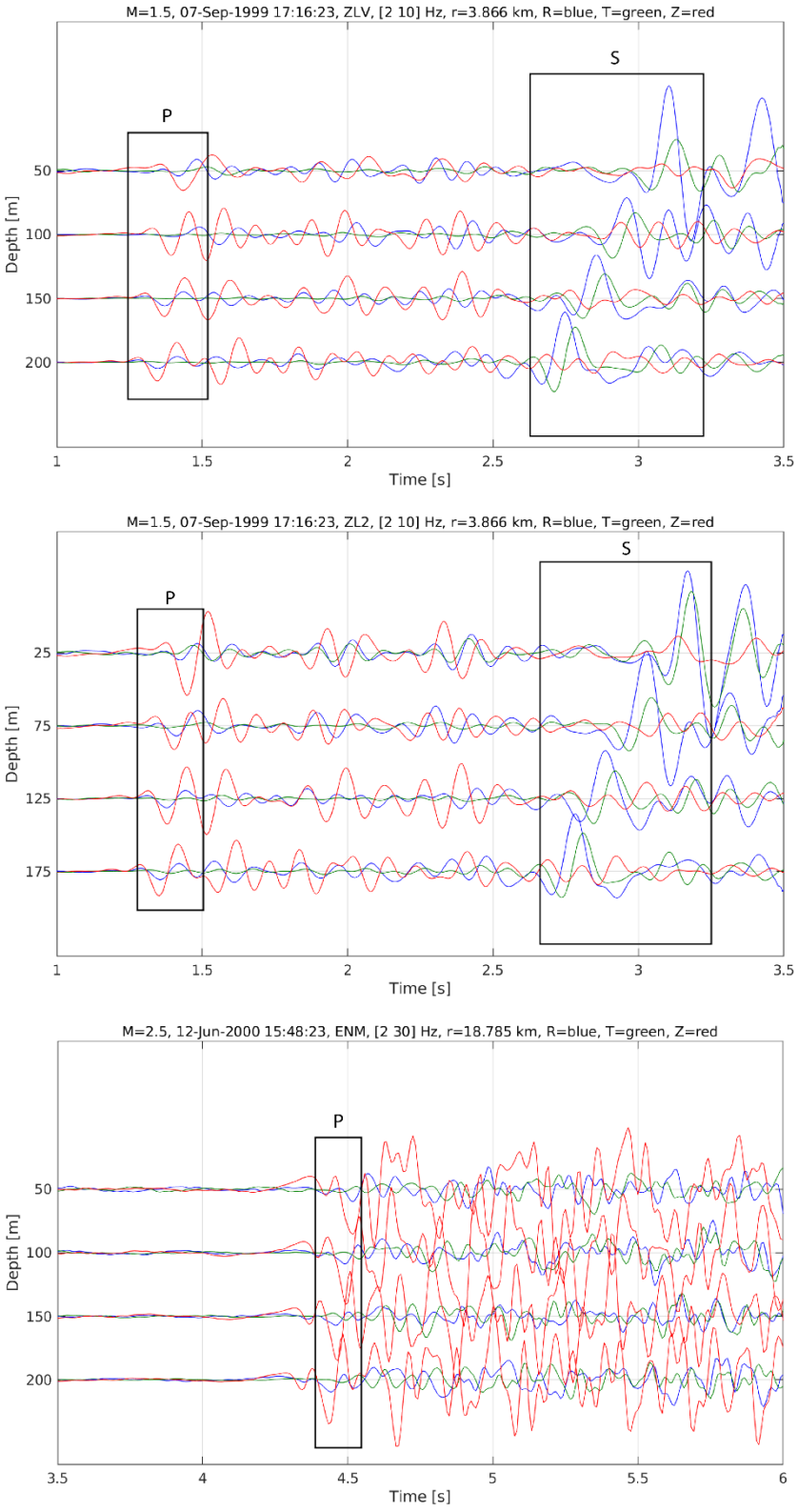

Figure C1. Overview of the vertical (red), radial (blue) and transverse (green) components for borehole stations ZLV, ZL2 and ENM, levels 1-4. The P- and S-onsets are indicated with a box.

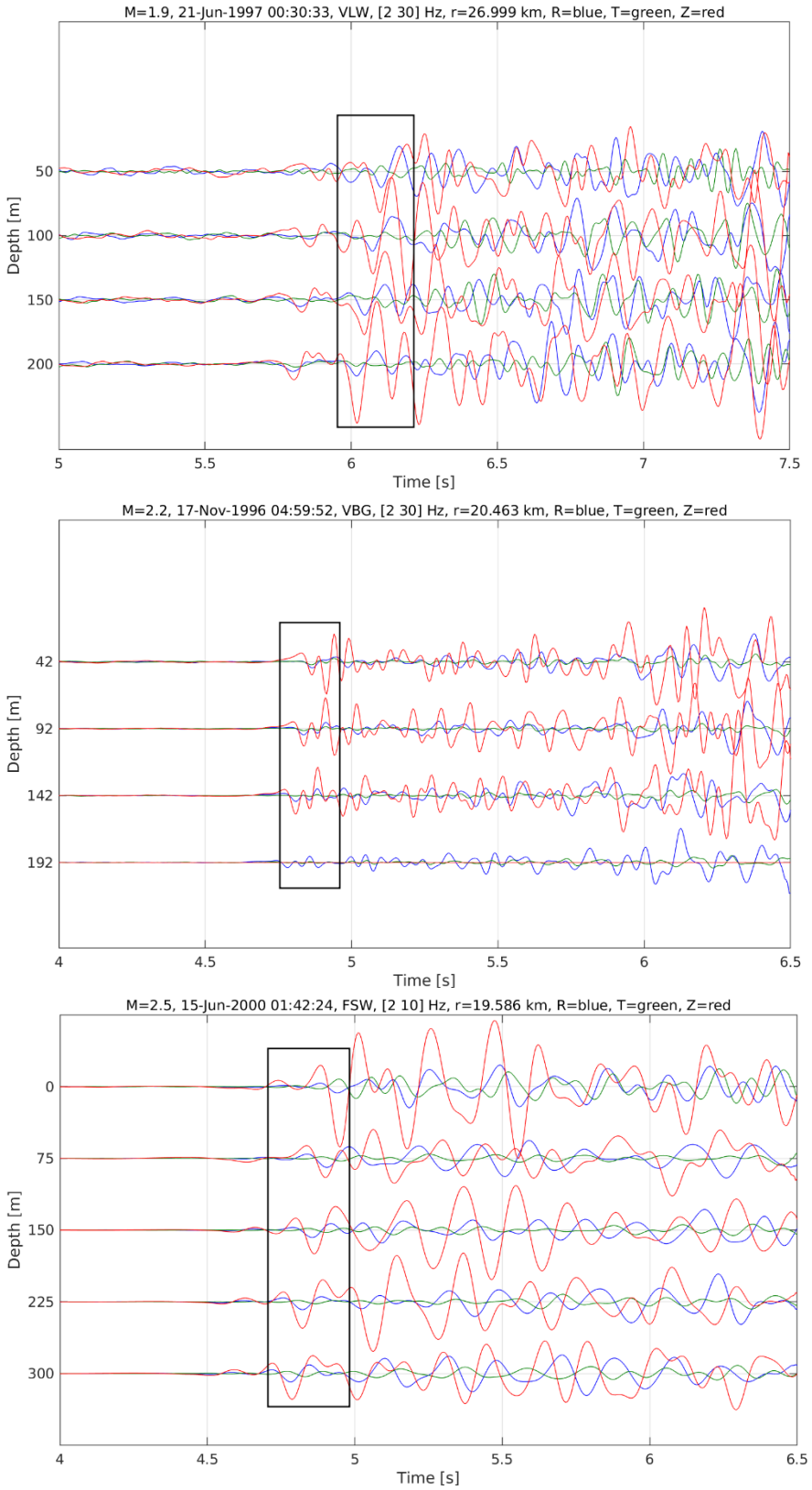

Figure C1 Continued, now for borehole stations VLW, VBG, levels 1-4, and FSW, levels 1-5. All boxes are located around the P-onsets.

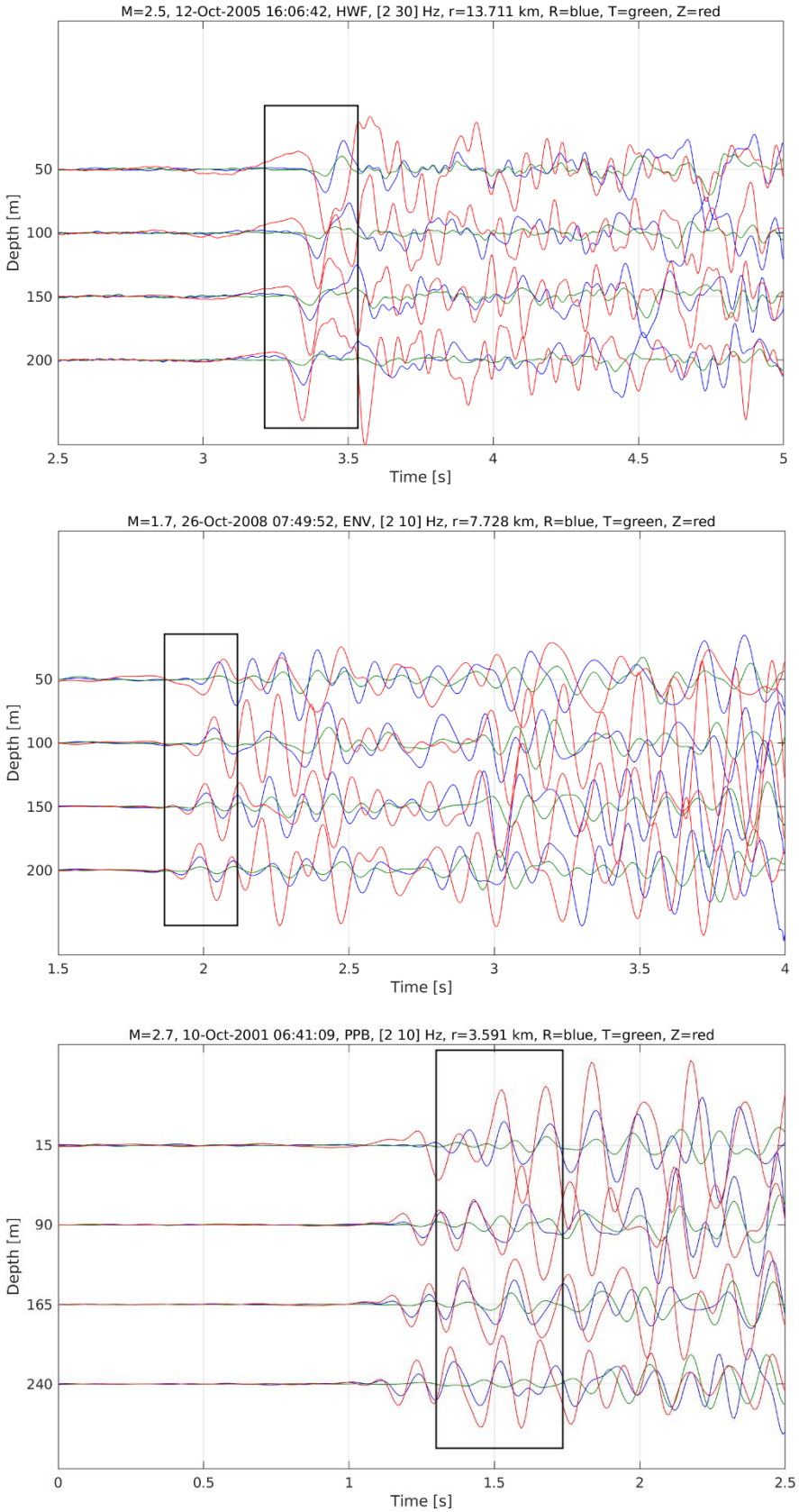

Figure C1 Continued, now for borehole stations HWF, ENV and PPB, levels 1-4.

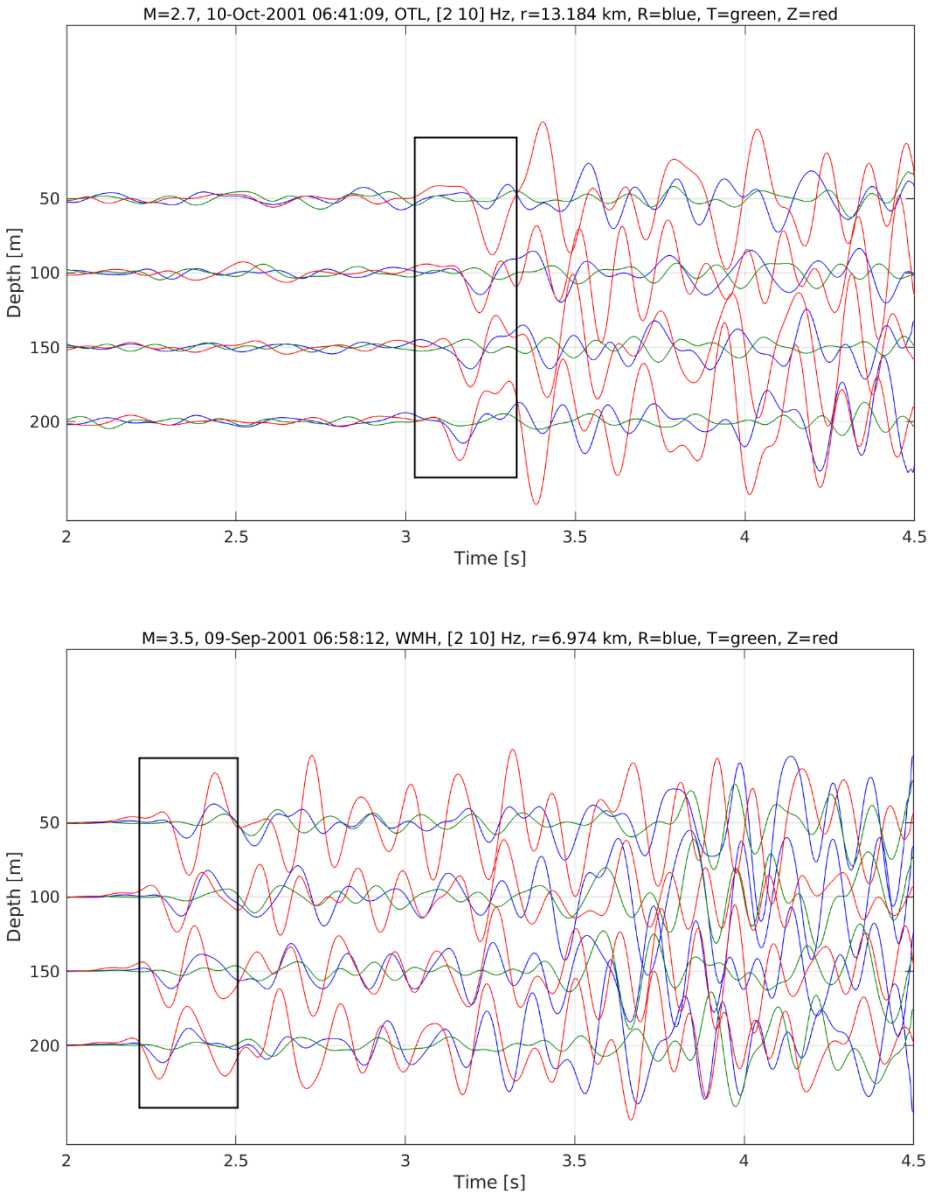

Figure C1 Continued, now for borehole stations OTL and WMH, levels 1-4.

Appendix D. Overview of orientation measures for accelerometer stations

In this Appendix we present the orientation measurements for the accelerometer stations using the automated procedure (Method1) and the manual procedure (Method2). For each station we show in a table the measurements of the orientation of the X (HG1) component (X_axi) and its mean and standard deviation (Std). Inside the tables, we list origin time, Magnitude (M), epicentral distance (Dist). The column labeled "New" is used in cases of manual re-processing and is also used to indicate if the measurement is excluded from the calculation of the mean. Exclusion is based on distance and magnitude criteria, but can also be used in cases where no stable solution could be found.

These measurements form the basis of the values listed in Table 8.

		Method1								Method2					
		M	Dist [km]	X_azi [°]	New	Mean	Std			M	Dist [km]	X_azi [°]	New	Mean	Std
MID1	20081030	3,2	5,3	34		**9**	**26**	MID1	20081030	3,2	5,3	0		**28**	**28**
	20090414	2,6	2,5	343					20090414	2,6	2,4	55			
									20120816	3,6	1,3	20	***x***		
MID3	20030927	2,7	3,4	346		**309**	**21**	MID3	20030927	2,7	3,4	345		**315**	**23**
	20031110	3	4,2	319					20031110	3	4,2	340			
	20031116	2,7	3,8	294					20031116	2,7	3,8	310			
	20060808	3,5	3,3	290					20060808	3,5	3,3	275			
	20081030	3,2	5,2	315					20081030	3,2	5,2	310			
	20090414	2,6	2,4	287					20090414	2,6	2,4	310			
ZAN1	20081030	3,2	4,9	279		**268**	**22**	ZAN1	20060808	3,5	5,5	240			
	20110627	3,2	7,1	237					20081030	3,2	4,9	300		**267**	**25**
	20130904	2,8	2,6	288					20090508	3	1,6	305	***x***		
									20110627	3,2	7	260			
ZAN2	20031110	3	5,7	56				ZAN2	20031110	3	5,6	55			
	20031116	2,7	3,9	43					20031116	2,7	3,8	40		**30**	**24**
	20060808	3,5	4	8		**30**	**18**		20060808	3,5	3,9	-10			
	20081030	3,2	3,3	11					20081030	3,2	3,2	285	***x***		
	20110627	3,2	6,5	34					20090508	3	0,6	25	***x***		
									20110627	3,2	6,4	35			
WSE	20090414	2,6	2	170	350	**20**	**34**	WSE	20081030	3,2	1,1	60	***x***		
	20090508	3	3,6	352					20090414	2,6	2,1	-5			
	20110627	3,2	7	67					20090508	3	3,6	0		**18**	**27**
	20120816	3,6	3,7	195	375				20110627	3,2	6,9	60			
	20130207	3,2	5,6	246	426				20120816	3,6	3,7	25			
	20130209	2,7	3,9	350					20130207	3,2	4,4	40			
									20130209	2,7	4	-15			

Table D1. Overview of orientation measures for the acceleration stations for stations MID1, MID3, ZAN1, ZAN2, WSE. See text above for explanation of the parameters.

		M	Dist [km]	X_azi [°]	New	Mean	Std			M	Dist [km]	X_azi [°]	New	Mean	Std
ROS1	19970116	2,4	1,2	261	x	**353**	**20**	ROS1	19970219	3,4	1,2	354		**352**	**4**
	19970219	3,4	1,2	174	354				19980128	2,7	1,2	350			
	19970620	1,8	2	0	x				19980714	3,3	1,7	355			
	19970818	1,6	1,5	358	x				19991231	2,8	1,3	345			
	19970818	2,1	1,5	376	x				20001025	3,2	1,7	355			
	19980128	2,7	1,2	378											
	19980128	2	1,1	375	x										
	19980714	3,3	1,7	328											
	19990514	1,7	1,6	385	x										
	20010428	2,4	1,7	144	x										
	20020214	2,1	1,3	6	x										
	20031011	1,6	1,7	357	x										
	20060325	2,1	1,3	40	x										
ROS2	19970818	1,6	1,5	350	x	**9**	**42**	ROS2	19980128	2,7	1,4	45		**13**	**24**
	19970818	2,1	1,5	351	x				19980714	3,3	1,4	-12			
	19980128	2,7	1,4	441					19991231	2,8	1,6	26			
	19980128	2	1,5	61	x				20001025	3,2	1,3	-9			
	19980714	3,3	1,4	345											
	19990514	1,7	1,5	314	x										
	19991231	2,8	1,6	347											
	20001025	3,2	1,3	341											
	20010428	2,4	1,4	355	x										
	20020214	2,1	1,4	334	x										
	20031011	1,6	1,7	132	x										
	20060325	2,1	1,5	199	x										
ROS3	19970620	1,8	1,1	310	x	**346**	**4**	ROS3	19980128	2,7	1,8	345		**339**	**5**
	19970818	1,6	1,2	338	x				19980714	3,3	1,1	331			
	19970818	2,1	1,2	160	x 340				19991231	2,8	1,4	338			
	19980128	2,7	1,8	351					20001025	3,2	1,2	343			
	19980714	3,3	1,1	341											
	19990514	1,7	1,1	329	x										
	19991231	2,8	1,4	165	345										
	20001025	3,2	1,2	165	345										
ROS4	19991231	2,8	1,4	103		**65**	**38**	ROS4	19991231	2,8	1,4	80		**73**	**8**
	20001025	3,2	1,2	27					20001025	3,2	1,1	65			
	20010428	2,4	1,1	50	x										
	20060325	2,1	1,6	61	x										
ROS5	20020214	2,1	0,9	331			**331**	ROS5	20020214	2,1	0,9	310		**310**	**30**
						* only dist 0.9 km									
ROS6	20010428	2,4	1,8	322			**322**	ROS6	20010428	2,4	1,8	330		**330**	**30**
						*only 1 measurement									
						and M<2.5									

Table D2. Overview of orientation measures for the acceleration stations for stations ROS1-6. See text above for explanation of the parameters.

		M	Dist [km]	X_azi [°]	New	Mean	Std			M	Dist [km]	X_azi [°]	New	Mean	Std
GARST	20110627	3,2	8,8	337		**351**	**24**	GARST	20110627	3,2	8,7	350		**361**	**14**
	20120816	3,6	4,1	376					20120816	3,6	4	385			
	20130207	2,7	3,2	366					20130207	3,2	3,2	350			
	20130207	3,2	3,9	388					20140213	3	4,7	360			
	20130209	2,7	2,9	324											
	20130904	2,8	4,7	345											
	20140213	3	4,7	322											
KANT	20120816	3,6	2,7	80		**80**	**30**	KANT	20110627	3,2	11,7	10		**20**	**37**
									20120816	3,6	2,5	70			
									20140213	3	8,3	-20			
WIN	20081030	3,2	3,2	42		**358**	**52**	WIN	20081030	100	3,5	370		**322**	**58**
	20090508	3	4,6	-38					20090508	330	5	240			
	20110627	3,2	2,8	23					20110627	130	2,8	400			
	20120816	3,6	7,6	63					20120816	10	7,7	280			
	20130702	3	3,3	29					20140213	50	5,7	320			
	20130904	2,8	3,8	-91											
	20140213	3	5,4	-44											
HKS	20060808	3,5	8,8	333		**354**	**26**	HKS	20140213	130	7,2	400		**3**	**29**
	20120816	3,6	11	354					20110627	135	1,2	405	***x***		
	20130904	2,8	5,9	332					20120816	90	11	360			
	20140213	3	7,2	396					20060808	60	8,7	330			
STDM	20120816	3,6	5,2	54		**54**	**30**	STDM	20120816	150	5,1	60		**60**	**30**
FRB2	20120816	3,6	19,8	39		**39**	**30**	FRB2	20120816	110	19,8	20		**20**	**30**

Table D3. Overview of orientation measures for the acceleration stations for stations GARST, KANT, WIN, HKS, STDM and FRB2. See text above for explanation of the parameters.

Appendix E. Time synchronization for accelerometer stations

In this Appendix we list all events for which a "smr" datafile was available. In the table it is mentioned if the file was time-synchronized or not (sync column).

			time since				time since				time since
event	station	sync	last sync	event	station	sync	last sync	event	station	sync	last sync
19961206_1646	ROS1	no	>3000s	20020214_1701	ROS6	yes		20090414_2105	MID1	yes	
19961228_1816	ROS1	no	>3000s		ROS1	yes			MID3	yes	
19970116_0012	ROS1	yes			ROS2	yes			WSE	no	>3000s
19970219_2153	ROS1	yes			ROS5	yes		20090508_0523	MID1	yes	
19970519_1543	ROS3	yes		20021014_2345	ROS2	yes			ZAN1	yes	
	ROS1	yes		20021224_0257	ROS6	no	>3000s		ZAN2	no	673s
19970620_0045	ROS3	yes			ROS2	yes			WSE	no	>3000s
	ROS1	yes		20030303_2051	MID1	yes		20100503_0926	ZAN1	yes	
19970709_0623	ROS3	yes			MID3	no	983s	20100814_0743	MID1	yes	
19970818_0442	ROS3	yes		20030927_1357	MID3	no	2938s		ZAN2	yes	
	ROS1	yes		20031011_1144	ROS1	yes			WSE	yes	
	ROS2	yes			ROS2	yes		20101115_1142	WSE	yes	
19970818_0517	ROS3	yes		20031110_0022	ZAN2	no	1179s	20110119_1939	MID1	yes	
	ROS1	yes			MID3	yes			MID3	yes	
	ROS2	yes		20031116_2004	ZAN2	no	1692s		WSE	yes	
19980128_2133	ROS3	yes			MID3	yes		20110326_2045	WSE	yes	
	ROS1	yes		20040906_2031	ROS6	yes		20110623_0914	MID1	yes	
	ROS2	yes			ROS1	yes			WSE	yes	
19980128_2234	ROS1	yes			ROS2	yes		20110627_1548	MID1	yes	
	ROS2	yes		20060325_1454	ROS6	yes			ZAN1	yes	
19980714_1212	ROS3	yes			ROS1	yes			ZAN2	yes	
	ROS1	yes			ROS2	yes			WSE	yes	
	ROS2	yes			ROS4	no	>3000s	20110729_2248	WSE	yes	
19990312_1906	ROS1	yes		20060808_0504	ZAN1	yes		20110831_0623	ZAN2	yes	
19990317_2314	ROS1	yes			ZAN2	no	1321s		WSE	yes	
	ROS2	yes			MID3	yes		20110906_2148	WSE	yes	
19990506_1813	ROS3	yes		20060808_0949	MID3	yes		20110925_1259	MID1	yes	
	ROS1	yes		20060826_2241	ZAN2	yes			WSE	yes	
	ROS2	yes		20061023_1338	ZAN2	no	2166s	20111230_0620	MID3	yes	
19990514_1830	ROS3	yes			WSE	no	1027s		WSE	yes	
	ROS1	yes		20070126_0020	ZAN2	no	>3000s	20120815_1917	MID1	yes	
	ROS2	yes			WSE	no	1390s		WSE	yes	
19990515_1928	ROS3	yes		20070514_1219	WSE	yes		20120816_2030	MID1	yes	
	ROS1	yes		20070609_2007	ZAN2	no	>3000s		WSE	yes	
	ROS2	yes		20080518_1323	ZAN2	yes		20130119_2010	WSE	yes	
19991231_1100	ROS3	yes		20081030_0554	MID1	no	>3000s	20130207_2231	WSE	yes	
	ROS1	yes			ZAN1	yes		20130207_2319	WSE	no	1030s
	ROS2	yes			ZAN2	no	930s	20130209_0526	WSE	yes	
	ROS4	yes			MID3	yes		20130702_2303	ZAN1	no	>3000s

20000107_1419	ROS2	yes			WSE	no	>3000s	20130904_0133	ZAN1	no	>3000s
20000327_1023	ROS2	yes		20081107_1640	ZAN2	yes					
20001025_1810	ROS3	yes		20081215_2041	MID1	yes					
	ROS1	yes		20090101_1654	ZAN1	yes					
	ROS2	yes			ZAN2	yes					
	ROS4	yes			WSE	no	>3000s				
	ROS5	yes		20090108_0117	WSE	no	>3000s				
20010428_2300	ROS3	yes		20090109_2016	WSE	no	>3000s				
	ROS1	yes		20090201_0423	ZAN1	yes					
	ROS2	yes			ZAN2	yes					
	ROS4	yes			WSE	no	>3000s				
	ROS5	yes									

Appendix F. Borehole Installation and maintenance issues

In this appendix we list the most relevant parts from installation and maintenance logs concerning the borehole network.

PPB:

- 09-07-1995: vertical, 2nd level: polarity reversed; new amplifiers installed
- 11-01-1996: vertical 2nd level: polarity again reversed
- 15-05-1998: vertical, 2nd level: polarity reversed again (back to old situation)
- 26-11-2010: Upgrade to continuous recording

OTL:

- 11-10-2010: Upgrade to continuous recording

WMH:

- 11-10-2010: Upgrade to continuous recording

ZLV/ZL2:

- 15-02-1996: ZL24 Z-component was repaired. Cable broken.
- 15-02-1996: surface sensors installed at ZLV
- 18-09-1997: pre-amplifiers level 0,3,4 all damaged (ZLV); for ZL2 pre-amps level 3N, 3E and all 4X are damaged.
- 22-09-1999: pre-amp 0N and 2E are damaged (ZLV), pre-amp 4N damaged (ZL2)
- 30-06-2000: 6 pre-amplifiers replaced incl. 3E & 3Z (ZLV); 1 damaged pre-amp at ZL2 (level not specified)
- 03-08-2001: 9 pre-amps damaged at ZLV and ZL2. Only uppermost levels undamaged.
- 21-11-2001: DCF receiver damaged
- 05-04-2002: surface sensors under water.
- 23-08-2002: lowest level pre-amp/filters at 70 Hz, but after 2 hours replaced with original ones..
- 18-09-2002: re-installation 70 Hz anti-alias filter.
- 18-10-2002: ZLV: 9-12 pre-amps damaged; 3 pre-amps 70 Hz damaged. Upper level 28 Hz anti-alias installed.
- 10-07-2003: new pre-amps installed, 5 pre-amps damaged (ZLV); ZL2: pre-amps 70 Hz replaced by 28 Hz.
- 29-07-2004: 6 pre-amplifiers damaged, 5 replaced. Level 1 is still damaged
- 18-05-2010: ZLV connected to continuous recording

VLW:

- 22-03-1996: disturbance on VLW1-N component could not be resolved
- 24-07-1998: pre-amplifier 4N and 4Z replaced. Sensor 1N revived. Surface sensors installed
- 04-04-2005: 5 pre-amplifiers damaged
- 08-08-2008: 9 pre-amplifiers damaged. No spare pre-amplifiers for surface sensors
- 29-10-2008: 2 pre-amplifiers replaced, upgrade to continuous recording

FSW:

- 03-05-1996: new electronics installed (compatible with other boreholes)
- 10-07-1996: problem with 1Z component could not be fixed.

HWF

- 03-05-1996: component 2Z needed repair. Component fixed
- 23-06-1997: component 2Z broken
- 10-07-1997: 2Z repaired
- 24-11-2010: upgrade to continuous recording

VBG:

- 10-07-1996: component 4Z is broken. Could not be repaired.
- 04-07-2001: pre-amplifiers damaged due to lightning
- 05-04-2002: all pre-amplifiers replaced by “lightning proof” ones.
- 11-05-2005: 1st level horizontal component damaged.
- 23-05-2008 2 pre-amplifiers lowest level damaged. Level 1-E not functioning well.
- 06-08-2009: 3 pre-amplifiers lowest level damaged
- 01-09-2010: pre-amplifier 2nd level replaced, new continuous recording installed.

ENV:

- 20-06-1997: 5 amplifiers defect. 1 repaired. Level 1 and 2 did not have pre-amplifiers
- 10-07-1997: all amplifiers replaced
- 08-08-2001: all components were damaged (lightning?).
- 18-09-2001: new components installed, including 12 new pre-amplifiers.
- 12-07-2005: 5 pre-amplifiers replaced
- 18-05-2010: 6 pre-amplifiers replaced, lowest 2 levels (3 and 4)
- 29-10-2010: again 6 pre-amplifiers replaced, levels 3 and 4

WDB:

- 18-09-1997: level 3Z not functioning well.
- 05-12-1997: level 3N not well.
- 24-07-1998: level 3 revived. Surface sensors installed
- 07-11-2000: level 3N not well.
- 12-11-2003: 3N still not well
- 23-03-2006: level 3Z also defect
- 29-04-2010: new continuous recording
- 18-05-2010: pre-amplifiers restarted (were not connected since last visit)

ENM:

- No detailed comments

Appendix G. Overview of component malfunctioning

In this appendix we provide an overview of station malfunctioning for each borehole station. In the tables, we specify for each station the period in which the station is functioning (Amplitude=1) or not (Amplitude=0). In the comments the problem is specified, if possible.

Station **FSW**:

Station	Channel	Start	End	Amplitude	Comment
FSW1	HH1	1992-07-22	2010-04-29	1	
FSW1	HH2	1992-07-22	2010-04-29	1	
FSW1	HHZ	1992-07-22	1996-06-16	1	
FSW1	HHZ	1996-06-17	1996-08-03	0	channel defect
FSW1	HHZ	1996-08-04	2010-04-29	1	
FSW2	HH2	1992-07-22	2010-04-29	1	
FSW2	HHZ	1992-07-22	2010-04-29	1	
FSW3	HH1	1992-07-22	2010-04-29	1	
FSW3	HH2	1992-07-22	2010-04-29	1	
FSW3	HHZ	1992-07-22	2010-04-29	1	
FSW4	HH1	1992-07-22	2010-04-29	1	
FSW4	HH2	1992-07-22	2010-04-29	1	
FSW4	HHZ	1992-07-22	2010-04-29	1	
FSW5	HH1	1992-07-22	2010-04-29	1	
FSW5	HH2	1992-07-22	2010-04-29	1	
FSW5	HHZ	1992-07-22	2000-10-25	1	
FSW5	HHZ	2000-10-26	2002-02-04	0	amplitude too low
FSW5	HHZ	2002-02-05	2010-04-29	1	

Station **ENM**:

Station	Channel	Start	End	Amplitude	Comment
ENM1	HH1	1995-04-12	2010-01-22	1	
ENM1	HH2	1995-04-12	2006-12-31	1	
ENM1	HH2	2007-01-01	2010-01-22	0	high noise and amplitude degradation
ENM1	HHZ	1995-04-12	2010-01-22	1	
ENM2	HH1	1995-04-12	2010-01-22	1	
ENM2	HH2	1995-04-12	2010-01-22	1	
ENM2	HHZ	1995-04-12	2010-01-22	1	
ENM3	HH1	1995-04-12	2010-01-22	1	
ENM3	HH2	1995-04-12	2010-01-22	1	
ENM3	HHZ	1995-04-12	2010-01-22	1	
ENM4	HH1	1995-04-12	2010-01-22	1	
ENM4	HH2	1995-04-12	2010-01-22	1	
ENM4	HHZ	1995-04-12	2010-01-22	1	

Station **VLW:**

Station	Channel	Start	End	Amplitude	Comment
VLW0	HH1	1998-07-24	2010-10-29	1	
VLW0	HH2	1998-07-24	2010-10-29	1	
VLW0	HHZ	1998-07-24	2010-10-29	1	
VLW1	HH1	1995-05-23	1996-03-21	1	
VLW1	HH1	1996-03-22	1998-07-24	0	channel defect
VLW1	HH1	1996-07-24	2000-06-09	1	sensor revived
VLW1	HH1	2000-06-09	2010-10-29	0	channel defect
VLW1	HH2	1995-05-23	2010-10-29	1	
VLW1	HHZ	1995-05-23	2010-10-29	1	
VLW2	HH1	1995-05-23	2010-10-29	1	
VLW2	HH2	1995-05-23	2010-10-29	1	
VLW2	HHZ	1995-05-23	2010-10-29	1	
VLW3	HH1	1995-05-23	2010-10-29	1	
VLW3	HH2	1995-05-23	2000-09-23	1	
VLW3	HH2	2000-09-24	2005-04-04	0	channel defect
VLW3	HH2	2005-04-05	2010-10-29	1	
VLW3	HHZ	1995-05-23	2010-10-29	1	
VLW4	HH1	1995-05-23	2010-10-29	1	
VLW4	HH2	1995-05-23	1998-05-19	1	
VLW4	HH2	1998-05-19	1998-07-23	0	channel defect
VLW4	HH2	1998-07-24	2010-10-29	1	amplifier repaired
VLW4	HHZ	1995-05-23	1998-05-19	1	
VLW4	HHZ	1998-05-19	1998-07-23	0	channel defect
VLW4	HHZ	1998-07-24	2010-10-29	1	amplifier repaired

Station **WDB**:

Station	Channel	Start	End	Amplitude	Comment
WDB0	HH1	1998-07-24	2009-05-24	1	
WDB0	HH1	2009-05-25	2010-04-29	0	channel defect
WDB0	HH2	1998-07-24	2009-05-24	1	
WDB0	HH2	2009-05-25	2010-04-29	0	channel defect
WDB0	HH3	1998-07-24	2009-05-24	1	
WDB0	HH3	2009-05-25	2010-04-29	0	channel defect
WDB1	HH1	1995-04-12	2010-04-29	1	
WDB1	HH2	1995-04-12	2010-04-29	1	
WDB1	HHZ	1995-04-12	2010-04-29	1	
WDB2	HH1	1995-04-12	2010-04-29	1	
WDB2	HH2	1995-04-12	2010-04-29	1	
WDB2	HHZ	1995-04-12	2010-04-29	1	
WDB3	HH1	1995-04-12	1997-10-31	1	
WDB3	HH1	1997-11-01	2010-04-29	0	channel defect
WDB3	HH2	1995-04-12	2010-04-29	1	
WDB3	HHZ	1995-04-12	2004-03-06	1	
WDB3	HHZ	2004-03-07	2010-04-29	0	channel defect
WDB4	HH1	1995-04-12	2010-04-29	1	
WDB4	HH2	1995-04-12	2010-04-29	1	
WDB4	HHZ	1995-04-12	2010-04-29	1	

Station **ENV**:

Station	Channel	Start	End	Amplitude	Comment
ENV1	HH1	1995-06-20	2001-08-07	1	
ENV1	HH1	2001-08-08	2001-09-18	0	channel defect
ENV1	HH1	2001-09-19	2009-12-04	1	
ENV1	HH2	1995-06-20	2001-08-07	1	
ENV1	HH2	2001-08-08	2001-09-18	0	channel defect
ENV1	HH2	2001-09-19	2009-12-04	1	
ENV1	HHZ	1995-06-20	2001-08-07	1	
ENV1	HHZ	2001-08-08	2001-09-18	0	channel defect
ENV1	HHZ	2001-09-19	2009-12-04	1	
ENV2	HH1	1995-06-20	2001-08-07	1	
ENV2	HH1	2001-08-08	2001-09-18	0	channel defect
ENV2	HH1	2001-09-19	2009-12-04	1	
ENV2	HH2	1995-06-20	2001-08-07	1	
ENV2	HH2	2001-08-08	2001-09-18	0	channel defect
ENV2	HH2	2001-09-19	2009-12-04	1	
ENV2	HHZ	1995-06-20	2001-08-07	1	
ENV2	HHZ	2001-08-08	2001-09-18	0	channel defect
ENV2	HHZ	2001-09-19	2009-12-04	1	
ENV3	HH1	1995-06-20	1997-05-18	1	
ENV3	HH1	1997-05-19	1997-07-09	0	channel defect
ENV3	HH1	1997-07-10	2001-08-07	1	
ENV3	HH1	2001-08-08	2001-09-18	1	
ENV3	HH1	2001-09-19	2009-12-04	1	
ENV3	HH2	1995-06-20	1997-05-18	1	
ENV3	HH2	1997-05-19	1997-07-09	0	channel defect
ENV3	HH2	1997-07-10	2001-08-07	1	
ENV3	HH2	2001-08-08	2001-09-18	0	channel defect
ENV3	HH2	2001-09-19	2009-12-04	1	
ENV3	HHZ	1995-06-20	2009-12-04	1	
ENV4	HH1	1995-06-20	1997-05-18	1	
ENV4	HH1	1997-05-19	1997-07-09	0	channel defect
ENV4	HH1	1997-07-10	2001-08-07	1	
ENV4	HH1	2001-08-08	2001-09-18	0	channel defect
ENV4	HH1	2001-09-19	2009-12-04	1	
ENV4	HH2	1995-06-20	1997-05-18	1	
ENV4	HH2	1997-05-19	1997-07-09	0	channel defect
ENV4	HH2	1997-07-10	2001-08-07	1	
ENV4	HH2	2001-08-08	2001-09-18	0	channel defect
ENV4	HH2	2001-09-19	2009-12-04	1	
ENV4	HHZ	1995-06-20	1997-05-18	1	
ENV4	HHZ	1997-05-19	1997-07-09	0	channel defect
ENV4	HHZ	1997-07-10	2001-08-07	1	
ENV4	HHZ	2001-08-08	2001-09-18	0	channel defect
ENV4	HHZ	2001-09-19	2009-12-04	1	

Station **HWF**:

Station	Channel	Start	End	Amplitude	Comment
HWF0	HH1	1998-03-29	2010-11-24	1	
HWF0	HH2	1998-03-29	2010-11-24	1	
HWF0	HHZ	1998-03-29	2010-11-24	1	
HWF1	HH1	1995-06-02	2010-11-24	1	
HWF1	HH2	1995-06-02	2010-11-24	1	
HWF1	HHZ	1995-06-02	2010-11-24	1	
HWF2	HH1	1995-06-02	2010-11-24	1	
HWF2	HH2	1995-06-02	2010-11-24	1	
HWF2	HHZ	1995-06-02	1997-06-07	1	
HWF2	HHZ	1997-06-07	1997-07-10	0	channel defect
HWF2	HHZ	1997-07-10	1997-11-24	1	component repaired
HWF3	HH1	1995-06-02	2010-11-24	1	
HWF3	HH2	1995-06-02	2010-11-24	1	
HWF3	HHZ	1995-06-02	2002-12-01	1	
HWF3	HHZ	2002-12-01	2010-11-24	0	low amplitudes
HWF4	HH1	1995-06-02	2010-11-24	1	
HWF4	HH2	1995-06-02	2010-11-24	1	
HWF4	HHZ	1995-06-02	2010-11-24	1	

Station ZLV

Station	Channel	Start	End	Amplitude	Comment
ZLV0	HH1	1996-02-15	2010-05-18	1	
ZLV0	HH2	1996-02-15	1997-08-22	1	
ZLV0	HH2	1997-08-23	1997-09-18	0	channel defect
ZLV0	HH2	1997-09-19	2005-12-10	1	
ZLV0	HH2	2005-12-11	2010-05-18	0	channel defect
ZLV0	HHZ	1996-02-15	2003-06-07	1	
ZLV0	HHZ	2003-06-08	2003-08-07	0	channel defect
ZLV0	HHZ	2003-08-08	2007-03-10	1	
ZLV0	HHZ	2007-03-11	2008-10-24	0	channel defect
ZLV0	HHZ	2008-10-25	2010-05-18	1	
ZLV1	HH1	1995-04-12	2004-07-28	1	
ZLV1	HH1	2004-07-29	2006-12-01	0	channel defect
ZLV1	HH1	2006-12-02	2010-05-18	1	
ZLV1	HH2	1995-04-12	2010-05-18	1	
ZLV1	HHZ	1995-04-12	2010-05-18	1	
ZLV2	HH1	1995-04-12	2010-05-18	1	
ZLV2	HH2	1995-04-12	2003-06-07	1	
ZLV2	HH2	2003-06-08	2003-08-07	0	channel defect
ZLV2	HH2	2003-08-08	2010-05-18	1	
ZLV2	HHZ	1995-04-12	2003-06-07	1	
ZLV2	HHZ	2003-06-08	2003-08-07	0	channel defect
ZLV2	HHZ	2003-08-08	2010-05-18	1	
ZLV3	HH1	1995-04-12	1997-08-22	1	
ZLV3	HH1	1997-08-23	1997-09-18	0	channel defect
ZLV3	HH1	1997-09-19	2010-05-18	1	
ZLV3	HH2	1995-04-12	1997-08-22	1	
ZLV3	HH2	1997-08-23	1997-09-18	0	channel defect
ZLV3	HH2	1997-09-19	2010-05-18	1	
ZLV3	HHZ	1995-04-12	1997-08-22	1	
ZLV3	HHZ	1997-08-23	1997-09-18	0	channel defect
ZLV3	HHZ	1995-04-12	2010-05-18	1	
ZLV4	HH1	1995-04-12	1997-08-22	1	
ZLV4	HH1	1997-08-23	1997-09-18	0	channel defect
ZLV4	HH1	1997-09-19	2003-06-07	1	
ZLV4	HH1	2003-06-08	2003-08-07	0	channel defect
ZLV4	HH1	2003-08-08	2010-05-18	1	
ZLV4	HH2	1995-04-12	1997-08-22	1	
ZLV4	HH2	1997-08-23	1997-09-18	0	channel defect
ZLV4	HH2	1997-09-19	2003-06-07	1	
ZLV4	HH2	2003-06-08	2003-08-07	0	channel defect
ZLV4	HH2	2003-08-08	2010-05-18	1	
ZLV4	HHZ	1995-04-12	1997-08-22	1	
ZLV4	HHZ	1997-08-23	1997-09-18	0	channel defect
ZLV4	HHZ	1997-09-19	2003-06-07	1	
ZLV4	HHZ	2003-06-08	2003-08-07	0	channel defect
ZLV4	HHZ	2003-08-08	2010-05-18	1	

Station ZL2:

Station	Channel	Start	End	Amplitude	Comment
ZL21	HH1	1995-04-12	2010-05-18	1	
ZL21	HH2	1995-04-12	2010-05-18	1	
ZL21	HHZ	1995-04-12	2010-05-18	1	
ZL22	HH1	1995-04-12	2010-05-18	1	
ZL22	HH2	1995-04-12	2010-05-18	1	
ZL22	HHZ	1995-04-12	2010-05-18	1	
ZL23	HH1	1995-04-12	1997-08-21	1	
ZL23	HH1	1997-08-22	1997-10-31	0	channel defect
ZL23	HH1	1997-11-01	2010-05-18	1	
ZL23	HH2	1995-04-12	1997-08-21	1	
ZL23	HH2	1997-08-22	1997-10-31	0	channel defect
ZL23	HH2	1997-11-01	2010-05-18	1	
ZL23	HHZ	1995-04-12	2010-05-18	1	
ZL24	HH1	1995-04-12	1997-08-21	1	
ZL24	HH1	1997-08-22	1997-10-31	0	channel defect
ZL24	HH1	1997-11-01	2010-05-18	1	
ZL24	HH2	1995-04-12	1997-08-21	1	
ZL24	HH2	1997-08-22	1997-10-31	0	channel defect
ZL24	HH2	1997-11-01	2010-05-18	1	
ZL24	HHZ	1995-04-12	1997-08-21	1	
ZL24	HHZ	1997-08-22	1997-10-31	0	channel defect
ZL24	HHZ	1997-11-01	1999-09-07	1	
ZL24	HHZ	1999-09-08	2000-07-09	0	channel defect
ZL24	HHZ	2000-07-10	2010-05-18	1	

Station VBG:

Station	Channel	Start	End	Amplitude	Comment
VBG1	HH1	1995-04-28	2008-08-05	1	
VBG1	HH1	2008-08-06	2008-10-29	0	spurious signals
VBG1	HH1	2008-10-30	2010-09-01	1	
VBG1	HH2	1995-04-28	2003-06-16	1	
VBG1	HH2	2003-06-17	2010-09-01	0	channel defect
VBG1	HHZ	1995-04-28	2010-09-01	1	
VBG2	HH1	1995-04-28	2008-08-05	1	
VBG2	HH1	2008-08-06	2008-08-29	0	spurious signals
VBG2	HH1	2008-08-30	2009-05-08	1	
VBG2	HH1	2009-05-09	2010-09-01	0	channel defect
VBG2	HH2	1995-04-28	2008-08-05	1	
VBG2	HH2	2008-08-06	2008-10-29	0	spurious signals
VBG2	HH2	2008-10-30	2010-09-01	1	
VBG2	HHZ	1995-04-28	2010-09-01	1	
VBG3	HH1	1995-04-28	2008-08-05	1	
VBG3	HH1	2008-08-06	2008-10-29	0	spurious signals
VBG3	HH1	2008-10-30	2010-09-01	1	
VBG3	HH2	1995-04-28	2008-08-05	1	
VBG3	HH2	2008-08-06	2008-10-29	0	spurious signals
VBG3	HH2	2008-10-30	2010-09-01	1	
VBG3	HHZ	1995-04-28	2008-08-05	1	
VBG3	HHZ	2008-08-06	2008-10-29	0	channel defect
VBG3	HHZ	2008-10-30	2010-09-01	1	
VBG4	HH1	1995-04-28	2008-08-05	1	
VBG4	HH1	2008-08-06	2008-10-29	0	spurious signals
VBG4	HH1	2008-10-30	2010-09-01	1	
VBG4	HH2	1995-04-28	2008-08-05	1	
VBG4	HH2	2008-05-06	2008-10-29	0	channel defect
VBG4	HH2	2008-10-30	2010-09-01	1	
VBG4	HHZ	1995-04-28	1996-05-06	1	
VBG4	HHZ	1996-05-07	1999-05-15	0	channel defect
VBG4	HHZ	1999-05-16	2000-06-15	1	
VBG4	HHZ	2000-06-16	2001-06-21	0	channel defect
VBG4	HHZ	2001-06-22	2008-08-05	1	
VBG4	HHZ	2008-08-06	2008-10-29	0	channel defect
VBG4	HHZ	2008-10-30	2010-09-01	1	

Station OTL:

Station	Channel	Start	End	Amplitude	Comment
OTL1	HH1	1995-04-21	2010-10-11	1	
OTL1	HH2	1995-04-21	2010-10-11	1	
OTL1	HHZ	1995-04-21	2010-10-11	1	
OTL2	HH1	1995-04-21	2010-10-11	1	
OTL2	HH2	1995-04-21	2010-10-11	1	
OTL2	HHZ	1995-04-21	2010-10-11	1	
OTL3	HH1	1995-04-21	2010-10-11	1	
OTL3	HH2	1995-04-21	2010-10-11	1	
OTL3	HHZ	1995-04-21	2010-10-11	1	
OTL4	HH1	1995-04-21	2010-10-11	1	
OTL4	HH2	1995-04-21	2010-10-11	1	
OTL4	HHZ	1995-04-21	2010-10-11	1	

Station WMH:

Station	Channel	Start	End	Amplitude	Comment
WMH1	HH1	1995-04-21	2010-10-11	1	
WMH1	HH2	1995-04-21	2010-10-11	1	
WMH1	HHZ	1995-04-21	2010-10-11	1	
WMH2	HH1	1995-04-21	2010-10-11	1	
WMH2	HH2	1995-04-21	2010-10-11	1	
WMH2	HHZ	1995-04-21	2010-10-11	1	
WMH3	HH1	1995-04-21	2010-10-11	1	
WMH3	HH2	1995-04-21	2010-10-11	1	
WMH3	HHZ	1995-04-21	2010-10-11	1	
WMH4	HH1	1995-04-21	2010-10-11	1	
WMH4	HH2	1995-04-21	2010-10-11	1	
WMH4	HHZ	1995-04-21	2010-10-11	1	

Station PPB:

Station	Channel	Start	End	Amplitude	Comment
PPB0	HH1	1998-05-15	2010-10-16	1	
PPB0	HH2	1998-05-15	2010-10-16	1	
PPB0	HHZ	1998-05-15	2010-10-16	1	
PPB1	HH1	1995-02-10	2010-10-16	1	
PPB1	HH2	1995-02-10	2010-10-16	1	
PPB1	HHZ	1995-02-10	2010-10-16	1	
PPB2	HH1	1995-02-10	2010-10-16	1	
PPB2	HH2	1995-02-10	2010-10-16	1	
PPB2	HHZ	1995-02-10	2010-10-16	1	
PPB3	HH1	1995-02-10	2010-10-16	1	
PPB3	HH2	1995-02-10	2010-10-16	1	
PPB3	HHZ	1995-02-10	2010-10-16	1	
PPB4	HH1	1995-02-10	2010-10-16	1	
PPB4	HH2	1995-02-10	2010-10-16	1	
PPB4	HHZ	1995-02-10	2003-11-09	1	
PPB4	HHZ	2003-11-10	2003-03-22	0	amplitudes too low
PPB4	HHZ	2003-03-23	2010-10-16	1	

References

Beyreuther, M., Barsch, R., Krischer, L., Megies, T., Behr, Y., and Wassermann, J. (2010), ObsPy: A Python Toolbox for Seismology, *Seismological Research Letters*, **81** (3), 530-533.

Bommer, J.J., B. Edwards, P.P. Kruiver, A. Rodriguez-Marek, P.J. Stafford, B. Dost, M. Ntinalexis, E. Ruigrok and J. Spetzler (2019). V6 Ground-Motion Model for the Groningen Field. 19 December, 193 pp.

Chiu, S.C. and C.A. Langston (2011) Waveform inversion for one-dimensional near-surface structure in the new Madrid seismic zone, *Bull. Seism. Soc. Am*. **101**: 93-108.

Diephuis, G. and U. Asmussen (1995) KNMI arrays in Groningen and Drenthe, NAM report

Dost, B. & H.W. Haak (2002) A comprehensive description of the KNMI seismological instrumentation, KNMI Technisch Rapport (TR 245): 60pp.

Dost, B., J. Zednik, J. Havskov, R. Willeman & P. Bormann (2012) Seismic data formats, archival and exchange, in: New Manual of Observatory Practice https://gfzpublic.gfz-potsdam.de/rest/items/item_43216_8/component/file_61044/content

Dost, B. and H.W. Haak (2007) Natural and induced seismicity, in: Wong, Th. E., Batjes, D.A.J & de Jager, J. (eds.): Geology of the Netherlands. Royal Netherlands Academy of Arts and Sciences (Amsterdam): 223-229.

Dost, B., E. Ruigrok and J. Spetzler (2017) Development of seismicity and probabilistic hazard assessment for the Groningen gas field, *Netherlands Journal of Geosciences*, **96**: s235-s245.

Dost, B. and D. Kraaijpoel (2013) The August 16, 2012 earthquake near Huizinge (Groningen), KNMI report, 26pp.

Haak, H.W. (ed. 1993) Summary of the Final report on a multidisciplinary study of the relation between Gasproduction and earthquakes in the northern part of the Netherlands. Royal Netherlands Meteorological Institute, de Bilt, ISBN 90-369-2052-3: 16pp.

Hofman, L. J., Ruigrok, E., Dost, B., & Paulssen, H. (2017). A Shallow Seismic Velocity Model for the Groningen Area in the Netherlands. *Journal of Geophysical Research: Solid Earth*, https://doi.org/10.1002/2017JB014419

Hogenauer, E.B., 1981, An economical class of digital filters for decimation and interpolation, *IEEE transactions on Acoustics, speech and signal processing*, **29(2)**:155-162.

Jepsen, D. C. and B.L.N. Kennett (1990) Three-component analysis of regional seismograms, *Bull. Seism. Soc. Am*. **80**: 2032-2052.

Ktenidou, O.-J., Z. Roumelioti, N. Abrahamson, F. Cotton, K. Pitilakis and F. Hollender (2018) Understanding single-station ground motion variability and uncertainty (sigma): lessons learnt from EUROSEISTEST, *Bull. Earthq. Eng*. **16**: 2311-2336.

Langston, C. (2003) Local earthquake wave propagation through Mississippi embayment sediments, part 1: body-wave phases and local site responses, *Bull. Seism. Soc. Am*. **93:** 2664-2684.

Lee, W.H.K. (Editor),(1989) Toolbox for Seismic Data Acquisition, Processing and Analysis, IASPEI software Library, Volume 1, Seism. Soc. Am., El Cerrito, CA, 283 pp.

Li, Z., S. Ni and P. Sommerville (2014) Resolving shallow shear-wave velocity structure beneath station CBN by waveform modelling of the Mw 5.8 mineral, Virginia, earthquake sequence, *Bull. Seism. Soc. Am.* **104**:944-952.

Ntinalexis, M., J. Bommer, E. Ruigrok, B. Edwards, R. Pinho, B. Dost, A. Correia, J. Uilenreef, P. Stafford, and J. van Elk (2019). Ground-motion networks in the Groningen field: usability and consistency of surface recordings. *Journal of Seismology*, **23(6)**: 1233-1253.

Ringler, A.T. and J.R. Evans (2015) A quick SEED tutorial. Seismological Research Letters, 86: 1717-1725, doi: 10.1785

Romijn, R. (2017) Groningen velocity model 2017 – Groningen full elastic velocity model, NAM report, 12pp.

Ruigrok, E., J. Domingo-Ballesta, G-J. van den Hazel, B. Dost and L. Evers (2019) Groningen explosion database, *First Break* **37**: 3-7.

Ruigrok, E. and B. Dost, 2020, Advice on the computation of peak-ground-velocity confidence regions for events in gas fields other than the Groningen gas field, KNMI Technical Report TR-386.

SodM (2021). Validatie van het seismisch netwerk van het KNMI in Groningen. Eindrapportage Staatstoezicht op de Mijnen, maart 2021.

Royal Netherlands Meteorological Institute

PO Box 201 | NL-3730 AE De Bilt
Netherlands | www.knmi.nl